Elsevier Editorial System(tm) for Lithos
Manuscript Draft

Manuscript Number:

Title: Melt inclusions track melt evolution and degassing of Etnean magmas in the last 15 ka

Article Type: Regular Article

Keywords: Etna, silicate melt inclusions, volatile contents, melt differentiation, degassing

Corresponding Author: Dr. Emanuela Gennaro, Ph.D.

Corresponding Author's Institution: Università di Palermo

First Author: Emanuela Gennaro, Ph.D.

Order of Authors: Emanuela Gennaro, Ph.D.; Giada Iacono-Marziano; Antonio Paonita; Silvio G Rotolo; Caroline Martel; Andrea L Rizzo; Michel Pichavant; Marcello Liotta

Abstract: We present major elements compositions and volatiles contents of olivine-hosted melt inclusions from Etna volcano (Italy), which extend the existing database with the aim of interpreting the chemical variability of Etnean magmas over the last 15 ka. Olivine phenocrysts were selected from the most primitive Fall Stratified (FS) eruptive products of picritic composition (Mg#=67-74, Fo89-91), the Mt. Spagnolo eccentric lavas (Mg#=55-66, Fo88) and among the more recent 2002-2013 eruptive products (Mg#=35-56, Fo68-83). Crystal fractionation and degassing processes were modeled at temperatures of 1050-1300 °C, pressures <500 MPa, and oxygen fugacity between 1 and 2 log units above the Nickel-Nickel Oxide buffer, in order to interpret melt inclusions data.
Melt inclusions show a great variability in major elements chemistry (e.g., 42-56 wt.% SiO_2, 3-15 wt.% CaO, 4-13 wt.% FeO, 2-12 wt.% MgO, 1-6 wt.% K_2O), designating a continuous differentiation trend from FS toward 2013 entrapped melts, which is reproduced by the fractional crystallization of olivine + spinel + clinopyroxene ± plagioclase, in order of appearance.
Volatile contents are also extremely variable, with maxima up to 5.86 wt.% H_2O and 0.59 wt.% CO_2 in FS melt inclusions, and up to 0.42 wt.% S in Mt. Spagnolo inclusions. H_2O and CO_2 contents in the melt inclusions suggest minimum entrapment depths of 12-18 km (below crater level) for FS inclusions and < 10 km for the 2002-2013 trachybasalts.
Petrological arguments coupled to the modelling of fractional crystallization and degassing processes concur to suggest that magmas from Mt. Spagnolo and the recent eruptions may be produced by differentiation from the most primitive volatile-rich FS magma along variable P-T paths, occasionally accompanied by secondary processes as crustal assimilation, mixing, and CO_2 flushing.

Emanuela Gennaro
PhD in Earth and Marine Sciences
PhD in Earth and Univers Sciences
emanuelagennaro@live.it

April 20, 2018

Dear Dr. Nelson Eby,

We wish to submit a new manuscript entitled "*Melt inclusions track melt evolution and degassing of Etnean magmas in the last 15 ka"* for consideration by Lithos.

We confirm that this work is original and has not been published elsewhere nor it is currently under consideration for publication elsewhere. All the authors have seen the manuscript and they agree to its submission to Lithos.

This paper reports on the major elements and volatiles compositions in olivine hosted melt inclusions selected from six typical and historical eruptions of Mount Etna. Among these, there are products investigated for the first time, which increment the existing dataset of melt inclusions from Mount Etna.

This research gives a contribution in the understanding of the chemical variability registered by the recent etnean magmas, currently principally ascribed to the heterogeneity of the mantle source(s). Crystal fractionation and degassing processes are modeled in order to explain the trends described by the compositions and volatile contents of melt inclusions. Our research reveals that under Mt. Etna, the deepest (> 15 km) magma reservoir may contain a volatile content higher than previously thought. This study, in addition, suggests that most of the chemical variability may to be referred to the melt differentiation of a Mg- and volatiles-rich magma, usually accompanied by local/secondary processes as crustal assimilation, mixing and volatile deep flushing.

We trust that your readers in the areas of igneous petrology and geochemistry should be interested to know about the important role of melt inclusions in the understanding the processes occurring before magma eruptions not only in Mt. Etna, but also in other worldwide volcanoes.

Therefore, we think that the argument could be well suited for Lithos.

Kind regards,

Emanuela Gennaro

PhD in Earth and Marine Sciences and Earth and Univers Sciences
University of Palermo-DiSTeM (Italy), Via Archirafi 22, 90123 Palermo, Italy
Institut of Sciences de la Terre d'Orléans (ISTO)/CNRS France, 1A rue de la Férolerie, 45071 Orléans (France)

Melt inclusions track melt evolution and degassing of Etnean magmas in the last 15 ka

Emanuela Gennaro[12]*, Giada Iacono-Marziano[2], Antonio Paonita[3], Silvio G. Rotolo[1,3], Caroline Martel[2], Andrea L. Rizzo[3], Michel Pichavant[2], Marcello Liotta[3]

[1] Dipartimento Scienze della Terra e del Mare (DiSTeM), Università degli Studi di Palermo, Via Archirafi 22, 90123 Palermo, Italy

[2] Institut des Sciences de la Terre d'Orléans (ISTO) UMR CNRS 7327, Université d'Orléans, Campus Géosciences, 1A rue de la Férolerie, 45071 ORLEANS Cedex 2 (France)

[3] Istituto Nazionale di Geofisica e Vulcanologia, Sezione di Palermo, Via Ugo La Malfa 153, 90146 Palermo, Italy

(*corresponding author: emanuelagennaro@live.it)

Abstract

We present major elements compositions and volatiles contents of olivine-hosted melt inclusions from Etna volcano (Italy), which extend the existing database with the aim of interpreting the chemical variability of Etnean magmas over the last 15 ka. Olivine phenocrysts were selected from the most primitive Fall Stratified (FS) eruptive products of picritic composition (Mg#=67-74, Fo_{89-91}), the Mt. Spagnolo eccentric lavas (Mg#=55-66, Fo_{88}) and among the more recent 2002-2013 eruptive products (Mg#=35-56, Fo_{68-83}). Crystal fractionation and degassing processes were

25 modeled at temperatures of 1050-1300 °C, pressures <500 MPa, and oxygen fugacity between 1
26 and 2 log units above the Nickel-Nickel Oxide buffer, in order to interpret melt inclusions data.
27 Melt inclusions show a great variability in major elements chemistry (e.g., 42-56 wt.% SiO_2, 3-15
28 wt.% CaO, 4-13 wt.% FeO, 2-12 wt.% MgO, 1-6 wt.% K_2O), designating a continuous
29 differentiation trend from FS toward 2013 entrapped melts, which is reproduced by the fractional
30 crystallization of olivine + spinel + clinopyroxene ± plagioclase, in order of appearance.
31 Volatile contents are also extremely variable, with maxima up to 5.86 wt.% H_2O and 0.59 wt.%
32 CO_2 in FS melt inclusions, and up to 0.42 wt.% S in Mt. Spagnolo inclusions. H_2O and CO_2
33 contents in the melt inclusions suggest minimum entrapment depths of 12-18 km (below crater
34 level) for FS inclusions and < 10 km for the 2002-2013 trachybasalts.
35 Petrological arguments coupled to the modelling of fractional crystallization and degassing
36 processes concur to suggest that magmas from Mt. Spagnolo and the recent eruptions may be
37 produced by differentiation from the most primitive volatile-rich FS magma along variable P-T
38 paths, occasionally accompanied by secondary processes as crustal assimilation, mixing, and CO_2
39 flushing.

Highlights

Major elements and volatiles compositions in Etnean melt inclusions of the last 15 ky are extremely variable.

The highest volatile contents are found in the deepest and more primitive melt inclusions.

Melt inclusions describe clear trends of progressive degassing and melt differentiation from a picritic hydrous magma to the more evolved ones.

Melt inclusions track melt evolution and degassing of Etnean magmas in the last 15 ka

Emanuela Gennaro[12]*, Giada Iacono-Marziano[2], Antonio Paonita[3], Silvio G. Rotolo[1,3], Caroline Martel[2], Andrea L. Rizzo[3], Michel Pichavant[2], Marcello Liotta[3]

[1] Dipartimento Scienze della Terra e del Mare (DiSTeM), Università degli Studi di Palermo, Via Archirafi 22, 90123 Palermo, Italy

[2] Institut des Sciences de la Terre d'Orléans (ISTO) UMR CNRS 7327, Université d'Orléans, Campus Géosciences, 1A rue de la Férolerie, 45071 ORLEANS Cedex 2 (France)

[3] Istituto Nazionale di Geofisica e Vulcanologia, Sezione di Palermo, Via Ugo La Malfa 153, 90146 Palermo, Italy

(*corresponding author: emanuelagennaro@live.it)

Abstract

We present major elements compositions and volatiles contents of olivine-hosted melt inclusions from Etna volcano (Italy), which extend the existing database with the aim of interpreting the chemical variability of Etnean magmas over the last 15 ka. Olivine phenocrysts were selected from the most primitive Fall Stratified (FS) eruptive products of picritic composition (Mg#=67-74, Fo_{89-91}), the Mt. Spagnolo eccentric lavas (Mg#=55-66, Fo_{88}) and among the more recent 2002-2013 eruptive products (Mg#=35-56, Fo_{68-83}). Crystal fractionation and degassing processes were

modeled at temperatures of 1050-1300 °C, pressures <500 MPa, and oxygen fugacity between 1 and 2 log units above the Nickel-Nickel Oxide buffer, in order to interpret melt inclusions data.

Melt inclusions show a great variability in major elements chemistry (e.g., 42-56 wt.% SiO_2, 3-15 wt.% CaO, 4-13 wt.% FeO, 2-12 wt.% MgO, 1-6 wt.% K_2O), designating a continuous differentiation trend from FS toward 2013 entrapped melts, which is reproduced by the fractional crystallization of olivine + spinel + clinopyroxene ± plagioclase, in order of appearance.

Volatile contents are also extremely variable, with maxima up to 5.86 wt.% H_2O and 0.59 wt.% CO_2 in FS melt inclusions, and up to 0.42 wt.% S in Mt. Spagnolo inclusions. H_2O and CO_2 contents in the melt inclusions suggest minimum entrapment depths of 12-18 km (below crater level) for FS inclusions and < 10 km for the 2002-2013 trachybasalts.

Petrological arguments coupled to the modelling of fractional crystallization and degassing processes concur to suggest that magmas from Mt. Spagnolo and the recent eruptions may be produced by differentiation from the most primitive volatile-rich FS magma along variable P-T paths, occasionally accompanied by secondary processes as crustal assimilation, mixing, and CO_2 flushing.

Keywords:

Etna, silicate melt inclusions, volatile contents, melt differentiation, degassing

1. Introduction

Mount Etna is a persistently active strato-volcano, located in the east sector of Sicily (Italy), seated on the boundary of the colliding African and European plates and close to the Aeolian volcanic arc (e.g., Branca et al., 2011; Clocchiatti et al., 1998). Etna's activity started as a submarine volcano ~500 ka BP and currently consists of lava fountains and paroxysmal activity at the summit

craters, associated with lava flows, effusive to explosive activity from eruptive fissures opened on the upper flanks of the volcano, and huge emissions of volatiles in the atmosphere (e.g. Aiuppa et al., 2008; Allard et al., 2006).

The origin of magmatic activity in the Etna area and its evolution are still matter of debate. Among the different hypotheses we can mention: (i) a hot spot origin (Clocchiatti et al., 1998; Tanguy et al., 1997), (ii) an asymmetric rifting process (Continisio et al., 1997), (iii) a lithospheric 'window' created by the differential rollback of the subduction sectors among the Ionian oceanic domain and the Sicilian continental crust resulting in mantle decompression, partial melting, and the ascent of asthenospheric material from under the neighboring African plate (Doglioni et al., 2001; Gvirtzman and Nur, 1999). During the oldest volcanic stages (~ 220 ka ago), etnean magma recorded the important chemical variation from tholeiitic toward Na-alkaline affinity (Corsaro and Pompilio, 2004a; Tanguy, 1978).

In the last decades, several researchers have observed that the composition of the recent eruptive products (since 1971) has become more enriched in alkalis (K, Rb, Cs) and radiogenic Sr and B elements (e.g., Allard et al., 2006; Armienti et al., 2004; Ferlito and Lanzafame, 2010; Métrich et al., 2004). This enrichment was inferred to result from the interaction between an OIB-type (or OIB-HIMU-type) mantle source with an enriched component (EM1), i.e., a slab-derived mantle component (Schiano et al., 2001), also possibly including δ^{11}B-enriched fluids (Armienti et al., 2004; Tonarini et al., 2001) released from the nearby Ionian slab subducting below the Aeolian Archipelago. Others studies attributed this enrichment to (i) magma contamination during its migration to the surface by assimilation of basement rocks (carbonates, shales, quartzarenites) (e.g., Clocchiatti et al., 1988; Joron and Treuil, 1984; Michaud et al. 1995; Tonarini et al., 1995), (ii) the mixing of a mantle-derived-magmas with a K- and Si-enriched melt (Schiano and Clocchiatti, 1994), (iii) the magma contamination with the uprising supercritical fluids carrying alkali and chlorine, this process being recurrent within Etnean activity (Ferlito and Lanzafame, 2010; Ferlito et al., 2014). Recently, Correale et al. (2014) suggested that the primitive magmas are produced by

different melting degree of a peridotite veined by clinopyroxenite, similar to mantle samples exposed in the close Hyblean plateau. Notwithstanding the numerous studies, several aspects of Etna activity are still not fully understood, including the causes of chemical variations between Etnean magmas and the volatiles contents of the most primitive magmas.

In this paper, we focus on the magmas erupted in the last 15 ka (*Mongibello* volcano, Branca et al., 2011), providing further geochemical and petrological information on magma chemical composition and volatile contents from deep storage to ascent conditions through the study of olivine-hosted melt inclusions (hereafter MIs). Melt inclusions entrapped in olivine crystals have the potential to give information on the chemical composition and volatile contents of magma in its deeper conditions and during magmatic ascent, this information being normally lost by using bulk rock and matrix glass data.

Studied MIs were selected from tephra and lava of six eruptions from central activity (2006, 2008/2009, 2013) and from eccentric or *deep-dyke fed* (DDF, Corsaro et al., 2009) eruptions (Mt. Spagnolo, FS, 2002/2003). All products were characterized for their chemical compositions (major elements) and volatiles contents (H_2O, CO_2, S and Cl). Some of these products are investigated here for the first time (i.e., 2008/2009, 2013 and Mt. Spagnolo for its volatile content). In order to obtain a more reliable dataset and to ensure the internal consistency of this new dataset, all the analyses were performed in the same laboratories with the same analytical conditions and reference materials.

In this work, we attempt to reconcile the different petrological and geochemical features of these mafic magmas, revealed by our new MI data and those of the literature. Differently from previous studies, attributing the origin of magmatic heterogeneity principally to variations of the magmatic source, we ascribe the most of the chemical variability of the *Mongibello* magmas mainly to crystal fractionation and degassing processes within the plumbing system. Heterogeneity of the mantle source would thus assume a minor role, at least as concerns major elements. We also discuss the possible role of other magmatic processes (magma mixing, assimilation of sedimentary host rocks,

deep volatile flushing) that may contribute to the variability in the chemical composition, redox conditions and high volatile content of the most primitive Etnean magmas.

2. Samples and analytical procedures

2.1 Target eruptions and their products

The investigated samples consist of primitive and more evolved lavas and pyroclastic products belonging to the Mongibello period (last 15 ky BP):

- **Monte Spagnolo lavas** (~15-4 ky BP) were produced by a DDF eruption (Corsaro and Métrich, 2016; Kamenetsky and Clocchiatti, 1996). The Monte Spagnolo scoria cone is located about 6 km north-west of the present-day central crater (Fig. 1a). Due to its mineralogical assemblage, principally olivine (Fo_{74-89}) and clinopyroxene, and its radiogenic Sr and unradiogenic Nd compositions, Mt. Spagnolo lava is considered as one of the most primitive magmas erupted in Etnean history (e.g., Armienti et al., 1988; Correale et al., 2014). Mt. Spagnolo melt inclusions in olivine crystals have been already characterized for their chemical compositions (Kamenetsky and Clocchiatti, 1996).
- **FS tephra** (~4 ky BP) were ejected by a DDF high-explosive (sub-Plinian) eruption (Coltelli et al., 2005), and its spread is mostly located in the east and north flanks of the volcano (Fig. 1a), reaching a maximum thickness of 110 cm 7 km away from the summit craters. This eruption were fed by a volatile-rich picro-basalt magma (MgO ~ 13-17.6 wt.%, Ni ~250 ppm, Cr ~900 ppm, from Correale et al., 2014; Corsaro and Métrich, 2016; Kamenetsky et al., 2007; Pompilio et al., 1995), representing the most primitive magma ever erupted at Etna (Pompilio et al., 1995). The high volatile content, the unusual enrichment of large-ion lithophile element (LILE), and the relatively high ^{87}Sr and low ^{143}Nd isotopic composition suggest the possible contribution of crustal fluids in the mantle source zone (e.g., Correale et al., 2014). Melt

inclusions from this eruption have been already characterized for their chemical composition and volatile content (Corsaro and Métrich, 2016; Kamenetsky et al., 2007).

- **2002/2003** tephra were produced by a lateral strombolian eruption along the South rift (Fig. 1a). During this eruptive period, the Northeast rift and summit craters were also active (e.g., Andronico et al., 2005; Spilliaert et al., 2006a). A particular feature of this eruption is the emission of two different magmas: (i) a plagioclase-rich, partially degassed trachybasaltic lava, from the NE rift, and (ii) an undegassed plagioclase-free basaltic lava flows and tephra from the S-rift (Spilliaert et al., 2006a). Melt inclusions from this eruption have been already characterized for chemical composition and volatile content (Collins et al., 2009; Schiavi et al., 2015; Spilliaert et al., 2006). In this study, we focus on the products from the S-rift activity.
- **2006** tephra were produced by a sub-terminal eruption that took place by three new vents opened along the flank of the South East crater (SEC), producing several tephra cones and lava flow (Fig. 1b), and by the summit crater. Melt and fluid inclusions have been already characterized for volatile and trace elements abundance by Collins et al. (2009) and Schiavi et al. (2015). The emitted magma was interpreted as residual of the 2001-2003 eruptive period, and the melt inclusions were inferred to track an episode of CO_2 fluxing from the deep degassing of a primitive magma (Collins et al., 2009).
- **2008/2009** eruption started with the opening of eruptive fissures propagating SE from the summit craters and produced lava flows that expanded in the *Valle del Bove* (Bonaccorso et al., 2011, Fig. 1b). Some intense explosions also occurred in the North East Crater (NEC), producing the tephra (bombs) investigated in this study.
- **2013** eruption (Fig. 1b) consisted of 19 paroxysms occurred at the New South East Crater (NSEC) associated to lava flows from fractures opened mostly along the NSEC cone. The sampled lava flow was associated to the paroxysm occurred on April.

2.2 Methods

Major elements analyses of the finely powdered (< 10 μm) whole rocks (wr) were performed by X-ray fluorescence spectroscopy at the Actlabs Laboratories in Canada, following the internal procedures (Norrish and Hutton, 1969). Analytical uncertainty (1σ) for major elements is < 1 wt.% SiO_2 and Al_2O_3, < 2 wt.% for Fe_2O_3, MgO, CaO, Na_2O and K_2O, <5 wt.% for MnO, TiO_2 and Cr_2O_3 and 5-10 wt.% for P_2O_5.

Cl and S in the whole rocks were determined by INAA (Instrumental Neutron Activation Analysis) and IR (infrared) methods, respectively.

Rock samples and melt inclusions were observed by two scanning electron microscopes (SEM): a Tescan MIRA 3 XMU (BRGM, *Orléans*) and a Zeiss Merlin Compact (ISTO, *Orléans*). Images and semi-quantitative spectra were acquired using 25 keV (Tescan MIRA 3 XMU) and 15 keV (Zeiss Merlin Compact) electron energy.

A Cameca SX FIVE electron microprobe (ISTO, *Orléans*) was used to analyze major elements in glass inclusions and embayments, matrix glasses, olivine phenocrysts and Fe-Ti oxides as well as the S and Cl concentrations in melt inclusions. Acquisitions were carried out using an acceleration voltage of 15 keV, a 6 nA beam current and a peak counting time of 10 s for all the elements, excepting for S (60 s). A focused beam was used for olivine and Fe-Ti oxide crystals, whereas a defocused beam of 2-6 μm size was used for melt inclusions and embayments to reduce Na migration. Natural minerals and oxides were used as standards (Na and Si: albite, K: anorthoclase, Ca: anhydrite, P: apatite, Cl: vanadinite, Mg: MgO, Al: Al_2O_3, Fe: Fe_2O_3, Ti and Mn: $MnTiO_3$). S was calibrated against barite ($BaSO_4$). Analytical uncertainty (1σ) is < 1% for SiO_2, Al_2O_3 and CaO, <3% for FeO, MgO and TiO_2, <5% for MnO, Na_2O and K_2O; < 500 ppm for S and Cl and detection limits are 120-450 ppm and 240-900 ppm, respectively for S and Cl.

H_2O and CO_2 contents were determined by transmission Fourier transform infrared spectroscopy (FTIR) using a Nicolet 760 Magna spectrometer equipped with an IR microscope and

a MCT detector (ISTO, *Orléans*). Doubly-polished glass inclusions were accurately prepared to obtain 18-72 µm thick chips. For each melt inclusions, at least two spectra were acquired to check the homogeneity of dissolved H_2O and CO_2 contents. Absorption spectra were acquired in the range 1000-6000 cm^{-1} with 128/560 scans and a resolution of 4 cm^{-1}, using a Globar internal IR source and a KBr beam-splitter. The concentrations (C) of H_2O and CO_2 dissolved in MIs were calculated from the absorbancies (A) of the 3530 cm^{-1} (total water vibration) and the 1430 cm^{-1} (CO_3^{2-} bending) bands, respectively, using the modified Beer-Lambert law (Stolper, 1982):

$$C = ((MW*A)/(d*l*\varepsilon)*100)$$

where ***MW*** is the molecular weight (in g/mol), ***d*** the melt density (in g/l), ***ε*** the molar absorption coefficient (in $l \cdot mol^{-1} \cdot cm^{-1}$), ***l*** the optic path (i.e. the thickness of the sample, in cm). A molar extinction coefficient (**ε**) of 63 $l \cdot mol^{-1} \cdot cm^{-1}$ was used for the 3530 cm^{-1} band (Dixon et al., 1988), whereas the coefficient for the 1430 cm^{-1} band was calculated for each MI (300-416 $l \cdot mol^{-1} \cdot cm^{-1}$) on the basis of the Na/(Na+Ca) molar ratio of the melt, using the Dixon and Pan (1995) method. The absorbancies of the carbonate doublet were estimated after subtraction of a spectrum of a CO_2-free synthetic glass, with similar composition and H_2O content (Lesne et al., 2011). The melt density for each inclusion was variable in the range (d = 2.68-2.76 $g \cdot cm^{-3}$) and was calculated by using a density of 2.78 $g \cdot cm^{-3}$, for an anhydrous basaltic glass from Etna (Gennaro, 2017), the presence of dissolved water being accounted for with the method proposed by Richet et al. (2000).

H_2O, CO_2, and S contents of melt inclusions were also determined through secondary ion mass spectrometry (SIMS) using the Cameca IMS 1270 and the IMS 1280 HR2 ion microprobes at CRPG, (Nancy, France). Olivine hosted melt inclusions and standard reference glasses were pressed into indium within an aluminum disk, then gold coated and outgassed in the SIMS chamber until a pressure of 10^{-8}-10^{-9} Torr was reached. The acquisition, preceded by a 30 s of pre-sputtering period (needed to erase impurities from the sample surface), was performed using a Cs^+ primary beam of 5 nA, with an impact energy of 20 kV in 12-15 cycles. The secondary beam consisted of both ionized

atoms, commonly used as analytes for volatile determinations (e.g., $^{12}C^-$, $^{32}S^-$), and ionized hydride molecules that create numerous interferences. A mass resolving power (MRP) of 7000 was used for separating these interfering species. In order to check the accuracy on the determined concentrations, glasses with compositions similar to the Etna samples were used as secondary standards. For H_2O and CO_2: basalts N72 from Kamchatka and the KL2-G basalt from Kilauea [0-4.2 wt.% and 0-3172 ppm respectively (Jochum et al., 2006; Shishkina et al., 2010)] were used and, for S the KL2-G, VG-2 and A99 standard glasses (Jarosewich et al., 1979; Witter et al., 2005, 0-1406 ppm). The signals for all volatiles ($^{12}C^-$, $^{16}O^1H^-$, $^{32}S^-$) were gathered in mono-collection mode during the same analysis (acquisition time 12 mn). Concentrations of all volatiles (except H_2O) were calculated by comparing the $^{12}C^-/^{28}Si^-$ vs. SiO_2 (for CO_2) and the $^{32}S^-/^{28}Si^-$ vs. SiO_2 (for S) in the sample and in the reference glass. H_2O was calculated by comparing the OH^-/H^- vs. H_2O in the reference materials with the OH^-/H^- of the sample.

3. Results

3.1 Whole rocks compositions

Major element compositions of the studied lavas and tephra are reported in Table 1 [and plotted in the Total Alkali versus Silica (TAS) diagram (Fig. SI1)]. Our results are generally consistent with those of previous studies (e.g. Correale et al., 2014; Corsaro and Métrich, 2016; Kamenetsky and Clocchiatti, 1996; Kamenetsky et al., 2007; Spilliaert et al., 2006a; Fig. SI1). All the rocks plot within the field defined by historical alkaline lavas (Correale et al., 2014, and references therein), except for FS tephra, which are poorer in alkali and richer in MgO than both the historical alkaline and the oldest tholeiitic lavas (Figs. SI1, 2). The rocks from 2006, 2008/2009 and 2013 eruptions present a trachybasaltic composition, whereas the lavas from Mt. Spagnolo and 2002/2003 eruptions straddle the basaltic-trachybasaltic fields of the TAS diagram (Fig. SI1). FS tephra are picro-basaltic (MgO = 17.9 wt.%); they have the highest CaO/Al_2O_3 ratio (=1.23) and Mg number

225 (Mg# = 77.5), and the lowest alkali content (Na_2O+K_2O < 2 wt.%) among the investigated rocks.
226 Both the MgO content and the CaO/Al_2O_3 ratio decrease from FS, Mt. Spagnolo toward the most
227 recent trachybasaltic compositions (asterisks in Fig. 2). When, considering K_2O as magma
228 differentiation index, the investigated products show a trend of decreasing MgO and of broadly
229 increasing Na_2O, Al_2O_3, FeO_{tot} and TiO_2 from the most primitive FS toward the most recent and
230 differentiated products (not shown). None of the analyzed whole rock composition has a clear Na or
231 K-alkaline affinity, being all transitional between the two series (asterisks in Fig. 3).
232
233 **3.2 Petrography, minerals chemistry, and melt inclusions observations**
234 **Monte Spagnolo**
235 Mt. Spagnolo lavas are poorly-phyric (porphyricity: 10-15 vol.%). They contain phenocrysts of
236 subhedral clinopyroxene (the most abundant mineral phase), followed (in order of abundance) by
237 euhedral to subhedral olivine, plagioclase, with Cr-spinel microphenocrysts. The groundmass is
238 microcrystalline with microlites of plagioclase, clinopyroxene (sometimes skeletal), Ti-magnetite
239 (often dendritic) and olivine (Fig. 4a). Olivine phenocrysts have variable forsterite (Fo) contents:
240 one group is in the range Fo_{70-76} and the other is $Fo_{82-89.}$ Some phenocrysts present reverse zoning,
241 with Fo_{75} cores and Fo_{85} rims (Fig. 4b). Only the most primitive (Fo_{82-89}) phenocrysts, which
242 contain abundant Cr-spinel (Cr_2O_3 = 36-46 wt.%, Table SI1) inclusions, were selected for this
243 study.
244 Melt inclusions within olivine phenocrysts have variable sizes in the range 20 and 140 μm, with
245 spherical to ovoidal shapes; sometimes they contain bubbles and/or small Cr-rich oxide and few
246 daughter minerals (Fig. 4c). Among the studied MIs, 13 have bubble with V_b/V_{MI} between 0.01 and
247 0.16, where V_b is the bubble volume fraction, and V_{MI} the inclusion volume, both estimated
248 assuming a perfect spherical shape for the bubble and the inclusion.
249

FS

Picritic scoria lapilli are highly vesiculated (voids > 50 vol.%) and almost aphyric (phenocrysts ≤ 10 vol.%). The phenocrysts are principally represented by euhedral Fo_{89-91} olivine (up to ~ 5 mm in size), followed by subhedral clinopyroxene and rare Cr-spinel microphenocrysts; these latter are enclosed within olivine phenocrysts but also occur within melt inclusions (Cr_2O_3 = 46-52 wt.%, Table SI1, Fig. 4d). The groundmass is glassy, with sparse microlites of olivine, clinopyroxene, plagioclase and Cr-spinel.

Melt inclusions are abundant in FS primitive olivine; they have spherical and oval shapes with typical scalloped edges (Fig. 4e). They have variable sizes, between 25 and 180 µm, and generally present a typical spherical vapor bubble (V_b/V_{MI} between 0.002 and 0.20).

2002/2003 South

These scoria are vesiculated (voids ~ 30 vol.%), poorly phyric (10-15 vol.% phenocrystals) in agreement with previous studies (Kahl et al., 2015 and references therein). Phenocryst abundances are in the order: clinopyroxene > plagioclase > olivine > Ti-magnetite. Olivine phenocrysts are euhedral to subhedral and have variable Fo contents (between 70 and 83 mol.%). They commonly host melt inclusions and Ti-magnetite microphenocryts (Usp = 21-43 %) (Table SI1, Fig. 4f). The groundmass is microcrystalline with microlites of clinopyroxene, plagioclase, and subordinate olivine and Ti-magnetite.

Melt inclusions in olivine generally have a spherical shape (Fig. 4g), but elongated inclusions (with slightly scalloped edges) were also occasionally observed. They have variable sizes (30-150 µm), sometimes with spherical bubbles (V_b/V_{MI} between 0.002 and 0.125). Several melt inclusions in 2002/2003 trachybasalts have abundant daughter minerals; for this study only crystal-free melt inclusions were selected and analyzed.

2006

These trachybasaltic scoria are vesiculated (voids ~ 30 vol.%) and porphyritic (phenocrysts ~25 vol.%). The phenocrysts consist of plagioclase (the most abundant phase) followed by clinopyroxene and olivine and microphenocrysts of Ti-magnetite, surrounded by a microcrystalline groundmass with plagioclase and clinopyroxene microlites, and less abundant olivine and Ti-magnetite.

Olivine phenocrysts (Fo_{69-81}) host many melt and Ti-magnetite (Usp = 14-40 %, Table SI1) inclusions, and show rare embayments (Fig. 4h). Investigated melt inclusions have variable forms (spherical, oval and elongated, sometimes with slightly scalloped edges, Fig. 4h) and sizes (20-200 µm). Five MIs out of 36 present small vapor bubbles (V_b/V_{MI} = 0.007-0.037) and a few contain Ti-Fe-oxides and small sulfide globules.

2008/2009

Samples collected from this eruption consist of juvenile bombs, highly vesiculated (voids ~ 45 vol.%) and slightly porphyritic (20 vol.% phenocrysts). Phenocrysts consist of plagioclase > clinopyroxene > olivine > Ti-magnetite, while the microcrystalline groundmass include plagioclase, clinopyroxene, and less abundant olivine and Ti-magnetite microlites. The olivine phenocrysts (Fo_{69-81}) host abundant melt and fluid inclusions and Ti-magnetite crystals (Usp = 14-40 %, Table SI1).

Investigated melt inclusions have variable sizes (18-200 µm) and present spherical but also irregular forms. They contain small bubbles (V_b/V_{MI} between 0.001 and 0.05), Ti-Fe-oxides and Cu-Fe sulfides (Fig. 4i).

2013

The 2013 lava is porphyric (20-25 vol.% phenocrystals), with phenocrysts of plagioclase > clinopyroxene > olivine (Fo_{72-80}), and microphenocrysts of Fe-Ti-oxide. The groundmass is microcrystalline with microlites of clinopyroxene, olivine, Ti-magnetite and less abundant plagioclase, apatite and Cu-Fe sulfides (Fig. 4l).

Olivine phenocrysts from this eruption are particularly rich in melt inclusions, whose size is in the range 15-200 µm. MIs have typically spherical to ovoidal shapes, but elongated inclusions are also sometimes observed. They contain bubbles (V_b/V_{MI} between 0.005-0.108, one with 0.325), abundant Cu-Fe-sulfide globules, generally associated with Fe- Ti-oxides (Fig. 4m).

3.3 Major elements composition of melt inclusions, embayments and matrix glasses

The chemical compositions of the studied Etnean melt inclusions have been corrected for post-entrapment crystallization (PEC) of olivine, and their compositions are reported in Table 2, together with the raw compositions of some glass embayments and matrix glasses, and in Figs. 5 and SI1. Several post-entrapment processes were occurred. The most common is the overgrowth of olivine at the melt inclusion interface and its re-equilibration with the host olivine, causing i.e. diffusion of Fe and Mg respectively from the melt and from the crystal, (e.g., Danyushevsky et al., 2000; Danyushevsky et al., 2002; Gaetani and Watson, 2002). In this study, the extent of PEC modifications (i.e., the wt% of olivine to be added to the raw melt inclusion analysis in order to restore the equilibrium $K_D^{ol/melt}$) was calculated assuming olivine-liquid equilibrium and a $K_D^{ol/melt}$ $[(FeO/MgO)_{ol}/(FeO/MgO)_{melt}]$ that range between 0.26 and 0.30, depending on Fe partition. The lowest value of $K_D^{ol/melt}$ is defined for a basaltic melt, considering FeO as FeO_{tot} (Di Carlo et al., 2006), while the highest value (0.30) is calculated only using the ferrous iron (Fe^{2+}). In this latter case, constraints on the redox conditions are required because the Fe_2O_3/FeO ratio in the melt is needed, but not in the first case. Taking into account that redox conditions in Etnean magmas are

poorly constrains, we preferred to calculate $K_D^{ol/melt}$ and PEC using FeO as FeO_{tot} (Di Carlo et al., 2006).

The observed PEC ranges between 0 and 19.5 %, the highest values being for the Mt. Spagnolo and FS melt inclusions (Table 2).

Diffusion of H^+ (protons) may also occur through the host olivine and can lead to H_2O loss or gain in the melt inclusion (e.g., Gaetani et al., 2012). This can alter the chemical composition of the entrapped melts, their volatile contents and their oxygen fugacity (e.g., Bucholz et al., 2013; Danyushevsky and Plechov, 2011; Frezzotti, 2001). We probably identified H^+ loss in Mt. Spagnolo MIs, which most likely experienced the slowest cooling rate among the studied products.

Studied melt inclusions show a great variability in major elements compositions. Silica spans a range between 42 and 56 wt.%, total alkali between 2.2 and 12.7 wt.%, MgO between 1.9 and 12.4 wt.% and CaO between 3.2 and 15 wt.% (Table 2, Figs. 2, 3, 5 and SI1). The melts entrapped in the FS products have the highest MgO and CaO contents and the lowest Al_2O_3 and K_2O contents (Figs. 5b-c-d), suggesting that it represent the most primitive melt in this study.

Compositions of MIs trapped in the MgO-richest olivine (~ Fo_{78-92}) are generally similar to those of their respectively whole rocks (Fig. 2), with the exception of FS rock having MgO content higher than those of MIs (17.9 vs. 12.4 wt.%). This could be due to an accumulation of olivine phenocrysts in FS magma. Differently, the compositions of MIs trapped in MgO-poorer olivines (~ Fo_{68-75}) are more evolved (lower FeO and MgO contents and higher alkali contents) than their respective bulk rocks (Figs. 3, 5).

Using K_2O as a melt differentiation index, clear evolution trends are visible from FS compositions toward MIs of the most recent products (2008-2013), which have the highest Al_2O_3, K_2O and Na_2O, and the lowest MgO and CaO contents (Figs. 5). SiO_2 is generally enriched in MIs from the most differentiated / most recent products. FeO_{tot}, TiO_2 and P_2O_5 show large variations (4.3-12.6 wt.%, 0.7-2.5 wt.%, and 0-1.5 wt.% respectively) and no clear trends appear with K_2O (Figs. 5). As their

348 respective whole rocks, all MIs belong to the alkaline series, except the MIs in FS, which have a
349 basaltic composition (Fig. SI1). The Mt. Spagnolo MIs have a sodic affinity (Na_2O-2 > K_2O), while
350 the most recent products show no clear chemical affinity (Fig. 3).
351 The composition of the studied MIs is consistent with previous results obtained on the same
352 eruptions (e.g., Collins et al., 2009; Corsaro and Métrich, 2016; Kamenetsky and Clocchiatti, 1996;
353 Kamenetsky et al., 2007; Métrich et al., 2004; Spilliaert et al., 2006a, Fig. 2). Our study reveals that
354 the most evolved and Mg-poor melts come from the 2013 olivine-hosted MIs and confirms that the
355 primitive Etnean liquids in the last 15 ky are the FS MIs, being seconded by Mt. Maletto and Mt.
356 Spagnolo (Kamenetsky and Clocchiatti, 1996).

357 Three glass embayments (Table 2, Fig. 3) were also analyzed (two from the 2006 and one from the
358 2002/2003 eruptions). One embayment in the 2006 sample is distinctly more evolved than the melt
359 inclusion hosted in the same olivine (CaO/Al_2O_3 embayment = 0.50 vs. 0.71 in MI; K_2O
360 embayment = 4.35 vs.1.73 wt.% in MI). The other two embayments have compositions similar to
361 the inclusions entrapped in the same olivine. The few matrix glasses analyzed generally show more
362 evolved compositions than their related melt inclusions (Table 2, Fig. 3).
363

364 **3.4 Volatile content of melt inclusions**

365 S contents measured by EMP and SIMS are generally in a good agreement (Fig. SI3). Due to the
366 significantly lower detection limit of SIMS analyses (< 10 ppm S), SIMS values were preferred for
367 MIs with S contents < 300 ppm. For MIs with S > 300 ppm, EMP values were preferred, being the
368 EMP dataset more complete (Table 2). For H_2O and CO_2, only a few inclusions were analyzed with
369 both SIMS and FTIR (3 MIs for H_2O and 1 for CO_2), preventing us to directly compare the two
370 methods (Table 2).
371 MI volatile contents do not correlate with the extent of PEC (Figs. SI2a-b). This, together with the
372 scarcity of Fe-Ti oxides in the investigated MIs and absence of cracks /dislocations in host crystals

all concur for a good preservation of the original dissolved volatiles. However, the episodic presence of vapor bubbles suggests that the measured volatile contents (CO_2 in particular since it is strongly partitioned into the bubble) must be regarded as minimum values for pre-eruptive melts (e.g., Frezzotti, 2001; Robidoux et al. 2017). Most vapor bubbles have V_b/V_{MI} ratios typical of shrinkage bubbles (bubble volumes are 0.2-5 % of the inclusion, from Lowenstern, 1995 and references therein). Some MIs (Mt. Spagnolo, FS, 2002/2003 and 2013) have bubbles with higher inclusion volumes (> 5 %), which could indicate post-entrapment mechanisms such as rapid decompression, thermal shock (resulting in phenocryst fracturing) or depressurization-vesiculation. However, only unfractured phenocrysts have been selected and, so, bubbles with large vapor/melt ratio are assumed to result from the simultaneous entrapment of melt and a separate vapor or fluid phase (Lowenstern, 1995; and references therein). Bubble-bearing MIs do not have systematically lower CO_2 contents than bubble-free ones. In the same way, no systematic relation is observed between the H_2O and CO_2 contents and V_b/V_{MI} (Table 2, Figs. SI2c-d), even if MIs with the highest CO_2 contents (> 4000 ppm) have a low V_b/V_{MI}. In addition, the fact that the H_2O and CO_2 contents are uncorrelated with the inclusion size (Figs. SI2e-f) suggests that diffusive processes did not significantly affect the volatiles in the MIs. However, H_2O loss by H^+ diffusion through the host olivine cannot be excluded, in particular for the Mt. Spagnolo and 2013 lavas, which were slowly cooled, as belong to a lava flow (e.g., Frezzotti, 2001; Gaetani et al., 2012; Lloyd et al., 2013). The small oxide crystals (Fe-Ti oxides and in some case Cr-spinel) that occur both in MIs and host crystals (Figs. 4c, 4d, 4i) are interpreted to preexist to melt entrapment (Table SI1). Crystallization due to post-trapping water loss and/or hydrogen migration is thus excluded (Bucholz et al., 2013; Sobolev et al., 1994).

The H_2O content of the investigated MIs is extremely variable, between 0.01 and 5.9 wt.%, the highest values exceeding the range previously determined for Etnean melts (Fig. 6). The most H_2O-rich melt inclusions are from the FS eruption, and our results (up to 5.9 wt.%) are higher than previous analyses from Kamenetsky et al. (2007; 2.6-3.8 wt%). The 2002/2003 and 2006 MIs

present variable H_2O contents (between 0.1 and 3.2 wt.%), similar to previous data for 2002/2003 (0.3-3.6 wt%, Collins et al. 2009; Spilliaert et al. 2006a) and slightly higher for 2006 (0.1-2 wt%, Collins et al. 2009). Melt inclusions from Mt. Spagnolo and 2013 lavas and 2008/2009 bombs have extremely low H_2O contents (< 0.5 wt.%). These inclusions do not seem to have been affected by secondary processes since their H_2O contents are unrelated to the PEC % (Fig. SI2a) or inclusion size (Fig. SI2e).

CO_2 abundances span from below detection limit up to more than 5500 ppm. The highest values, measured in FS melt inclusions, are significantly higher than those previously estimated by Kamenetsky et al. (2007; 3300 ppm, Fig. 6). The CO_2 contents measured in 2002/2003 and 2006 scoria MIs (119-2470 and 191-1673 ppm, respectively) are in good agreement with previous studies (e.g., Collins et al., 2009; Métrich et al., 2004; Spilliaert et al., 2006a, Fig. 6), and similar to those analyzed in 2008/2009 bombs (87-964 ppm). The CO_2 contents of 2013 and Mt. Spagnolo MIs, measured here for the first time, are also variable and in the range of those of the other eruptions (from below detection limit up to more than 2600 ppm). Bubble-bearing MIs do not show lower CO_2 contents than bubble-free ones, and no systematic relation is observed between the CO_2 content and V_b/V_{MI} (Table 2, Fig. SI2d).

For each inclusion, H_2O-CO_2 contents and major element composition were used to determine melt inclusions entrapment pressures, assuming magma volatile saturation. The solubility model of Iacono Marziano et al. (2012) was used and the calculations performed at temperatures between 1100 and 1200°C (with this model, the temperature effect is negligible). Results give a wide pressures range for FS (76-477 MPa), while, for the other eruptions, results are less dispersed (Fig. 6, Table 2): Mt. Spagnolo (3-154 MPa), 2002/2003 South (11-254 MPa), 2006 (0-153 MPa), 2008/2009 (5-161 MPa), 2013 (0-81 MPa). These pressure estimates are in the same range than those previously reported for the FS, 2002/2003 and 2006 eruptions (Kamenetsky et al., 2007; Collins et al., 2009; Spilliaert et al., 2006a; respectively)], although the volatile content of the most primitive FS magma estimated in this work is significantly higher than those from previous studies.

In addition, the pressure calculations use a solubility model different from previous studies and which has the advantage of being calibrated on a larger range of mafic compositions (Fig. 7 in Iacono-Marziano et al., 2012).

The sulfur content of the investigated melt inclusions is extremely variable and reaches a maximum of 4150 ppm, generally higher than previous measurements (e.g., Collins et al., 2009; Corsaro and Métrich, 2016; Kamenetsky et al., 2007; Metrich and Clocchiatti, 1989; Métrich et al., 2004; Spilliaert et al., 2006a-b; Figs. 7), except one 2006 MI which contain 4500 ppm (Schiavi et al., 2015). Mt. Spagnolo MIs (measured here for the first time) show the highest S concentrations, higher than those analyzed in MIs from FS eruption (< 3473 ppm; this study; Corsaro and Métrich 2016; Kamenetsky et al. 2007). S contents in 2002/2003 South and 2006 MIs are generally lower (128 - 3005 ppm, and 110-3410 ppm respectively) and similar to previous studies (2002/2003: 480-3470 ppm, Spilliaert et al., 2006a; 860-3567 ppm, Schiavi et al., 2015; 2006: 0-1500 ppm, Collins et al., 2009; 158-4593 ppm, Schiavi et al., 2015). The most recent 2008/2009 and 2013 MIs have a maximum of 1100 ppm S. A general trend of decreasing S with increasing K_2O content is observed (Fig. 7a), except for the most primitive FS and the most evolved MIs (K_2O > 2.8 wt.%). In comparison, S shows no clear trends with either H_2O or CO_2 (Figs. 7b-c).

The chlorine content is also highly variable, between 793 and 4670 ppm, the highest values being for the 2002/2003 South MIs. Compared to previous determinations, our data are either higher (Spilliaert et al., 2006) or in the same range (Collins et al., 2009; Corsaro and Métrich, 2016; Kamenetsky et al., 2007; Schiavi et al., 2015). A high variability is commonly observed within the same eruption, without any clear correlation with the K_2O content (Fig. SI4).

The glass embayment in the 2006 olivine phenocryst ("2006-7emb", Fig. 4h) is less water-rich (0.36 wt.% H_2O) than the MI in the same olivine (3.16 wt.% H_2O), suggesting that the embayment equilibrated near the surface (Table 2). The other two embayments ("2006-E2emb" and "2002/3S-24emb") have similar major element compositions and water concentrations, and broadly similar S and Cl contents, than MIs trapped in the same olivine (Table 2). This suggests that MIs and

451 embayments were entrapped almost concurrently at a similar (superficial) depth. S and Cl contents
452 (H_2O and CO_2 were not analyzed) of 2002/2003 matrix glasses are also very similar to MIs (Table
453 2).
454

455 # 4. Modelling and discussion

456 Olivine-hosted melt inclusions of Etnean products erupted in the last 15 ka record important
457 compositional variability (Figs. 2, 3, 5, 6, 7, SI1). The prominent geochemical features emerging
458 from this study are (i) the highly variable volatile contents, with maxima up to 5.86 wt.% H_2O, 0.59
459 wt.% CO_2, 0.42 wt% S, and 0.47 wt.% Cl (Table 2), (ii) the large variability in major element
460 chemistry (e.g. 42.3-56.0 wt.% SiO_2, 4.3-12.6 wt.% FeO, 2-12.4 wt.% MgO), and (iii) the
461 occurrence of systematic magma differentiation trends (Figs. 2, 5). The highest CaO/Al_2O_3 ratios,
462 MgO contents (Fig. 2) and volatiles concentration (maximum 7 wt.%) of MIs trapped in Fo-rich
463 olivines (Fo_{89-91}) suggest that FS is the best candidate to represent the primitive parental melt of
464 Etnean magmas (as already suggested by Kamenetsky et al., 2007). MIs trapped in less Fo-rich
465 olivines (Fo_{88-68}) from the other investigated tephra and lava samples record less primitive melts
466 (Figs. 2, 5).
467

468 ## 4.1 Melt differentiation modelling

469 We have modelled ascent-related crystallization using the MELTS code (Ghiorso and Sack, 1995;
470 Smith and Asimow, 2005) previously used for Etnean magmas (e.g., Kahl et al., 2015; Mollo et al.,
471 2015). The general objective of the simulations was to explore if the compositions of all analyzed
472 MIs can be reproduced starting from primitive melts in FS olivines and, thus, to test if FS MIs
473 represent a suitable parental melt for Etnean magmas in the last 15 ka. In detail, two types of

simulations were carried out and a summary of the different conditions tested is provided in a supplementary table (Table SI2).

4.1.1 Early evolution

Type I simulations were performed to model the early differentiation of the most primitive melts observed in FS tephra. To do so, the average (4 analyses) of two MIs with the highest Mg#, CaO/Al_2O_3 ratio (SiO_2=44 wt.%, Al_2O_3=9 wt.%, FeO_{tot}=8 wt.%, MgO=12 wt.%, CaO=13 wt.%, Na_2O=1.6 wt.%, K_2O=0.9 wt.%) and the highest measured Cr content (Cr_2O_3=0.12 wt.%) was used as starting composition. These most primitive MIs have an average H_2O content of 4 wt.% but, since higher contents (up to 5.86 wt.% H_2O, Table 2, Fig. 6) have been measured in the FS MIs, we used 5 wt.% as the starting melt H_2O content for the MELTS modeling. To reproduce the deepest magmatic conditions, the simulations started from a pressure of 500 MPa (477 is the highest pressure provided by MI, section 3.4 and Fig. 6) and the initial temperature was set at 1300 °C following Armienti et al. (2007; 2012) and considering the temperature of 1325-1356 °C estimated for FS magma by Coltelli et al. (2005). The final conditions were arbitrarily set at 400 MPa and 1200°C (yielding a dP/dT gradient of 1 $MPa°C^{-1}$ for the magma ascent path). An initial fO_2 range between NNO+1 to NNO+2 [in agreement with previous estimates for primitive Etnean magmas: fO_2 ~ NNO+1.8, Kamenetsky and Clocchiati (1996); > NNO+1; Liotta et al. (2012); > NNO+1, Métrich et al. (2009); NNO+1±0.8, Mollo et al. (2015)] was investigated by adjusting the FeO and Fe_2O_3 contents of the starting melt, and the fO_2 (calculated by MELTS) was allowed to vary with progressive crystallization. Results show that, during this P-T evolution, olivine and Cr-spinel (present only in the simulation starting at NNO+2) are the only phases crystallizing from FS melts, and that clinopyroxene is absent. Olivine (Fo_{92}) matches compositions of FS crystals. However, it occurs in very low amounts (<1 wt.%) indicating that most crystallization takes place at T < 1200°C and P < 400 MPa.

4.1.2 Main crystallization stage

The final liquids obtained in type I simulations were used as starting compositions for the type II MELTS models. These started at 1200°C and 400 MPa and used variable dP/dT of 20, 5 and 3 $MPa°C^{-1}$, where dP and dT mean different decrement in T and P for each step of MELTS calculation, i.e., different slopes along the magma ascent path). Different final temperatures (from 1180 to 1068 °C) were explored, following Kahl et al. (2011; 2015) and in agreement with direct field measurements of lava effusion temperatures in the range 980-1080 °C (Calvari et al., 1994), whereas final pressures were fixed at near-surface conditions (Table SI2).

Under these conditions and upon progressively decreasing P and T, crystallization advances in the order olivine, spinel (progressively evolving from Cr-spinel to Ti-magnetite), clinopyroxene and plagioclase (at pressures < 40 MPa and for melt H_2O contents < 2 wt%). The crystallization series in our MELTS models are in general agreement with Mollo et al. (2015), although they used starting melt compositions less primitive than FS. Our calculated mineral assemblages are consistent with key features of Etnean magmas such as the predominance of clinopyroxene and olivine, the presence of plagioclase phenocrysts in the most evolved products and in all groundmasses, the occurrence of Cr-spinel in FS and Mt. Spagnolo MIs and of magnetite in the 2002-2013 MIs. Olivines produced by MELTS range between Fo_{92} and Fo_{60}, covering the entire range of natural products (Fo_{91} in FS to Fo_{68} in the most evolved 2013 lava) although not continuously (Fig. SI5). In MELTS simulations, olivine crystallization is generally inhibited in Ca-rich melts (> 15 wt.% CaO), being replaced by clinopyroxene on the liquidus. However, we observe such Ca-rich MIs in FS and Mt. Spagnolo olivine phenocrysts, indicating that these melts were olivine-saturated. We may speculate that these particular Ca-rich compositions represent microscale melts, due to a dominant role of clinopyroxene dissolution-reaction-mixing (Danyushevsky et al., 2004) as suggested by Pichavant et al. (2009) and Lanzo et al. (2016) for Stromboli and Vulcano.

524 Clinopyroxenes calculated by MELTS have compositions very similar to those found in Mt.
525 Spagnolo lava (Kamenetsky and Clocchiatti, 1996) and in 2001-2012 trachybasalts (En_{33-43}, Fs_{9-18},
526 Wo_{43-50}, Mg# of 54-85, Mollo et al., 2015; Kahl et al., 2015 and references therein; Schiavi et al.,
527 2015), and are close to clinopyroxene inclusions in FS olivine (Kamenetsky et al., 2007). The
528 occurrence of cpx inclusions in FS olivine has yielded Kamenetsky et al. (2007) to suggest its early,
529 deep crystallization in FS magma. Although this proposition is not supported by our MELTS
530 modeling (see type I simulations above), recent studies (e.g., Armienti et al., 2007, 2012;
531 Giacomoni et al., 2016) reveal that clinopyroxene crystallization occurs in Etna basalt and
532 trachybasalts over a large P range (160-1380 MPa). Giacomoni et al. (2016) have suggested that
533 some of these deep clinopyroxene can be xenocrysts, probably derived from crystal mushes
534 (Armienti et al., 2007) and incorporated into the uprising magma.
535
536 ***4.1.3 Melt evolution along the liquid line of descent***
537 All MELTS simulations yielded very similar SiO_2, Al_2O_3, MgO, CaO, Na_2O vs K_2O trends (Figs. 5,
538 8) for residual melts along the liquid line of descent. MI MgO and CaO contents (generally well
539 reproduced) decrease, as does the CaO/Al_2O_3 ratio, while the SiO_2 and alkali contents increase
540 (Figs. 5, 8) as a result of crystallization of olivine + clinopyroxene + spinel + plagioclase.
541 The variability in the H_2O content of inclusions for a given as well as between different
542 eruptions suggests different degassing paths (Fig. 9). For instance, the FS MIs show highly variable
543 H_2O contents at nearly constant K_2O, suggesting near-adiabatic ascent that allowed this highly
544 primitive magma to reach the surface without significant differentiation (Coltelli et al., 1998; 2005).
545 The type II MELTS simulations with a high dP/dT ratio (20 MPa $°C^{-1}$) and a final temperature of
546 1180 °C reproduces well the H_2O degassing trend observed in these MIs (red curves in Fig. 9).
547 Conversely, the Mt. Spagnolo, 2008/2009 and 2013 MIs present very low H_2O contents and
548 variable K_2O (Fig. 9), which may suggest early H_2O degassing, prior to significant crystallization.
549 However, the Mt. Spagnolo MIs are characterized by decoupled volatile abundances, with high CO_2

550 (up to 2670 ppm), S (up to 4150 ppm), and Cl (up to 4100 ppm) and low H_2O (< 0.6 wt.%). This
551 could reflect trapping of an initially volatile-rich melt followed by H_2O loss due to H^+ diffusion in
552 the host olivine during cooling (Gaetani et al., 2012). Alternatively, H_2O could have been stripped
553 from the melt at depth by CO_2 flushing. The former hypothesis appears more realistic due to the
554 slow cooling experienced by the Mt. Spagnolo lava flow. It is also worth reminding that H^+
555 diffusion is particularly effective at high temperatures and low pressures (Gaetani et al., 2012), i.e.,
556 under lava emplacement conditions. Thermobarometric data for Mt. Maletto lavas, similar to the
557 Mt. Spagnolo (Giacomoni et al., 2016; Kamenetsky and Clocchiatti, 1996), reveal a deep
558 intratelluric crystallization episode in those Etnean magmas. Therefore, it is most likely that
559 crystallization of Mt. Spagnolo lavas did not take place only at the near surface conditions implied
560 by the low H_2O contents of MIs. However, because of H_2O loss, the high-pressure
561 crystallization/trapping stage that affected the magmas is not preserved in the Mt. Spagnolo MIs.
562 The 2013 MIs are also from a lava flow and may similarly have suffered post-entrapment H_2O loss.
563 However, their relatively low CO_2 (< 709 ppm) and S contents (<450 ppm) speak for volatile
564 degassing preceding entrapment, as is the case for the 2008/2009 MIs which, nevertheless, come
565 from a strombolian deposit.
566 The 2001 to 2007 MIs show progressive degassing during melt differentiation (i.e. decreasing H_2O
567 contents with increasing K_2O contents Fig. 9), which are well reproduced by the fractional
568 crystallization of the parent FS melt with dP/dT trajectories between 3 and 5 MPa $°C^{-1}$ and final
569 temperatures of 1122 and 1068 °C respectively (blue and green curves in Fig. 9). The water
570 contents of 2008/2009 and 2013 MIs are also generally reproduced by the lowest pressure segments
571 of these two curves, probably following a superficial low-pressure decompression. Fractional
572 crystallization along a dP/dT between 3 and 5 MPa $°C^{-1}$, ending at temperatures of ~1100 °C, can
573 therefore generate most of the H_2O-K_2O trends observed in recent Etnean MIs (2001-2013).
574 Changes in dP/dT and final temperatures within a single eruption could reflect the tapping of
575 individual magma batches with different ascent histories, caused by provenance from different

magma accumulation zones, vertical and lateral changes in the density of basement rocks as well as variable volatile contents and gas fractions (Armienti et al., 2012).

4.1.4 Redox control on melt evolution

The large spread in MI FeO_{tot} (and, to a lesser extent, TiO_2) contents in MIs potentially reflect variations of redox conditions in addition to melt differentiation (e.g., Figs. 5; 10), which in turn control the proportion of spinel crystallization and the FeO_{tot}/MgO ratio of the melt (Pichavant et al., 2002 and reference therein).

For instance, spinel (both Fe-Ti oxide and Cr-spinel) crystallization in Etnean magmas can vary from one eruption to the other and during the same eruption as well. Cr-rich spinel is commonly observed to be included within FS (and Mt. Spagnolo) olivine phenocrysts (Table SI1), consistent with its early appearance from a FS parental liquid in MELTS models, which requires oxidizing conditions. Pichavant et al. (2002) found that melts produced under very oxidizing conditions (ΔNNO > +2.5) have FeO_{tot}/MgO that are constant or decrease with progressive crystallization which indicates preferential partitioning of Fe toward the mineral phases (mainly magnetite) relative to Mg. This behavior is evident in FS and Mt. Spagnolo MIs. In the first ones, the constancy in FeO_{tot}/MgO ratio and FeO_{tot} content, and the decrease of MgO (Figs. 5d-e, 10) could be ascribed to olivine and Cr(Mg)-spinel crystallization, well reproduced by the MELTS models at high initial fO_2 (NNO+2) conditions and with high dP/dT ratio (20 MPa $°C^{-1}$), although calculated phase proportions (<1 for ol and <0.3 wt.% for Cr-spinel) are lower than those found in natural rocks.

Differently from FS, MIs of Mt. Spagnolo (this study and Kamenetsky and Clocchiatti, 1996), Mt. Maletto (Kamenetsky and Clocchiatti, 1996) and Frumento delle Concazze (FdC, Corsaro and Métrich, 2016) eruptions show a different trend, with a stronger decrease of FeO_{tot} and MgO (Figs. 5d-e) and an increase of TiO_2 (Fig. 5g). In addition, Mt. Maletto and Mt. Spagnolo MIs have a FeO_{tot}/MgO ratio constant or decreasing with K_2O, while the FeO_{tot}/MgO ratio of FdC increases

602 slightly during melt evolution (Fig. 10). These behaviors are partially reproduced by a MELTS
603 model with low dP/dT ratio (dP/dT=2 MPa $°C^{-1}$), only when starting from a fO_2 > NNO+3 (black
604 curve in Fig. 10). Such extremely oxidizing redox conditions are needed to let MELTS crystallizing
605 abundant spinel (>1 wt.%), relatively early on the liquidus. However, this curve is not totally
606 coincident with all the MIs of Mt. Spagnolo, because this MELTS model is associated with an
607 important decrease in fO_2 conditions (2 log units) during crystallization. The abundance of Cr-spinel
608 inclusions in Mt. Spagnolo olivine corroborates spinel crystallization as a mechanism to generate
609 the FeO_{tot} and MgO decrease observed in these inclusions (Figs. 5d-e), while a constant high
610 oxygen fugacity seems requested to maintain constant or to slightly decrease the FeO_{tot}/MgO ratio
611 during crystallization. An oxygen fugacity > NNO+3 (to trigger spinel crystallization), seems
612 unrealistically high for Etna basalts, the highest fO_2 estimated for Etna being ~ NNO+1.8
613 (Kamenetsky and Clocchiatti, 1996; Mollo et al. 2015). Yet, high oxygen fugacities are certainly
614 required to account for early spinel crystallization and the high sulfur contents of FS, and
615 particularly Mt. Spagnolo MIs (Jugo, 2009). Indeed, high fO_2 conditions were calculated for FS and
616 Mt. Spagnolo using the olivine-spinel oxybarometer of Ballhaus et al. (1991) and the composition
617 of Cr-spinel inclusions inside MI/ol (Table SI1): oxygen fugacities of respectively ~1.6 and ~2 units
618 log above the buffer NNO were obtained for T between 1170 °C (estimated for Mt. Spagnolo by
619 Kamenetsky and Clocchiatti 1996), and 1300 °C.

620 Green and blue curves in Figs. 5, 10 describe the evolution of a FS magma, associated to
621 important FeO_{tot} and MgO and FeO_{tot}/MgO variations. These variations, in some case, are less
622 important than really shown by the Etnean MIs. On the contrary, the FeO_{tot}/MgO in the residual
623 melt predicted by MELTS models with dP/dT ratios of 3 MPa $°C^{-1}$ (blue curves) are more
624 pronounced than those really calculated for 2001-2013 MIs, suggesting that variations in fO_2 are less
625 significant than those calculated by MELTS.

626 Variable fO_2 conditions, associated to variable Fe-spinel and clinopyroxene crystallization, are
627 necessary to justify the large variability in FeO_{tot} (and TiO_2) contents observed in the MIs from

2001 to 2013 eruptions (Figs. 5d-e-g, 10). On the one hand, no or slight spinel (and clinopyroxene) crystallization is needed to explain FeO_{tot} enrichment in the melt above 11 wt.% (Fig. 5e), while, on the other hand, abundant spinel and clinopyroxene crystallization at temperatures lower than 1070 °C induces FeO_{tot} to decrease in the melt to 8 wt.%. Such a variability in spinel (and clinopyroxene) crystallization is obtained with MELTS simulations by changing the initial oxygen fugacity from NNO+1 to NNO+2, and the dP/dT ratios between 3 and 5 MPa $°C^{-1}$.

Anyway, the lowest FeO_{tot} contents (~ 4 wt.%) of the 2013 MIs is not obtained by the performed MELTS models (Fig. 5e). These MIs show, in Fig. 10, a constant FeO_{tot}/MgO ratio during melt evolution, probably due to abundant magnetite precipitation at constant fO_2.

4.2. Depth of storage and degassing pattern of the erupted magmas

We used the H_2O-CO_2 solubility model of Iacono-Marziano et al. (2012), specifically suited for alkaline mafic melts, to estimate pressures of entrapment (see section 3.4) of melt inclusions (Fig. 6). Bearing in mind that (i) estimated H_2O and CO_2 from MI represent the minimum volatile budget of the trapped melts, and (ii) investigated MIs may also have high S and Cl contents, the estimated pressures have to be regarded as the minimum ones. To convert the entrapment pressures into a (minimum) pre-eruptive magma storage-crystallization depths, we used an average rock density value of 2.65 g cm^{-3}, taking into account the different density of the lithologies in the first 22 km of the Etnean basement: from 2.57 to 2.70 g cm^{-3} (Corsaro and Pompilio, 2004b).

Studied melt inclusions were entrapped at different depths in the Etnean plumbing system down to ~18 km below crater level ("bcl"). The deepest MIs are in the olivine from *FS* eruption, which show the larger range of entrapment pressures (~3-18 km bcl). The inclusions from the other eruptions (Mt. Spagnolo, 2002/2003 South, 2006, 2008/2009 and 2013) were entrapped in a narrower range of pressures (0-254 MPa), indicating shallower depths, generally lower than 7 km bcl (Table 2 and Fig. 6). The minimum entrapment depths are relatively similar to those determined by previous

653 studies (e.g., Collins et al., 2009; Kamenetsky et al., 2007; Spilliaert et al., 2006a), although we
654 used different H_2O-CO_2 solubility model (see 3.4 section).

655 We used the model of Iacono-Marziano et al. (2012) to simulate the degassing of the deepest (~15-
656 18 km bcl), volatile-rich primitive FS magma, with an initial X_{CO_2} of 0.7-0.8 (calculated from the
657 highest H_2O and CO_2 contents in MIs). Considering that the highest CO_2 contents in the FS
658 inclusions are affected by a large error (> 800 ppm), two distinct initial conditions were used to
659 simulate volatile degassing both in closed and open system conditions: 5700 ppm CO_2 - 4 wt.%
660 H_2O (the average H_2O content of MIs FS) - and 5000 ppm CO_2 - 5 wt.% H_2O (the same values used
661 for MELTS fractional crystallization modeling), with the aim of reproducing the large range of
662 H_2O-CO_2 concentrations shown by MIs, by simulating volatile degassing both in closed and open
663 system conditions. In the modeling of a closed system degassing, we varied the excess of fluid
664 phase (i.e. the amount of fluid phase initially coexisting with the magma). The models in closed
665 system conditions with excess of fluid phase between 0 and 20 wt.% define an area in the CO_2-H_2O
666 plot (grey in Fig. 6) that well describes the degassing of the primitive FS melt by reproducing the
667 successive polybaric entrapment of most of FS inclusions. This area (grey in Fig. 6) also encloses
668 some MIs of the 2001-2006 eruptive period (this study; Collins et al., 2009; Métrich et al., 2004;
669 Spilliaert et al., 2006a), suggesting that they may have derived from a volatile-rich, FS-type melt, in
670 terms of H_2O and CO_2 contents.

671 An additional trend (violet area in Fig. 6) describes the degassing of another group of more evolved,
672 partially H_2O and CO_2 degassed MIs entrapped at depth < 250 MPa (mainly from 2002/2003 South
673 and subordinately from 2006 and FS tephra), which are CO_2-richer (probably due to some flushing
674 episode), and/or H_2O poorer than the MIs belonging to the first group. This degassing trend is
675 modeled starting from the average highest volatile contents in the studied MIs from 2002/2003
676 South eruption (H_2O=2.2±0.3 wt.%, CO_2=2180±340 ppm).

A third group of melt inclusions from 2013, 2008/2009 and Mt. Spagnolo eruptions, together with some from 2002/2003 South and 2006 (Collins et al. 2009; Spilliaert et al. 2006a), are H_2O depleted and anomalously enriched in CO_2 (up to 2670 ppm, Fig. 6). The maximum estimated entrapment depth of these MIs is comparable to that estimated for the second group (Fig. 6).

We already mentioned (section 3.4) that Mt. Spagnolo MIs may have suffered post-entrapment H_2O loss and therefore are not well suited to retrieve entrapment depths. However, several other MIs from this study and from the literature clearly suggest the H_2O loss from the melt and the enrichment in CO_2 at a depth of 8-9 km (i.e., passing from the MIs of the first group to those of the second and from those of the second to those of the third; Fig. 6). On the basis of recent decompression experiments of mafic melts, these high CO_2 contents can be explained by CO_2 oversaturation generated by (kinetic) disequilibrium melt degassing during magma ascent (Le Gall and Pichavant, 2016; Pichavant et al., 2013), even if in the case of Mt. Etna the gas discharges of the volcano do not display evidences of degassing far from equilibrium (Paonita et al., 2012).

Alternatively, the need for 20 wt.% excess fluid phase to account for volatile contents in MIs suggests that an extremely high amount of fluid phase could coexist with the magma, in agreement with the massive volatile emissions observed at Mt. Etna (Aiuppa et al., 2008). In particular, the addition of CO_2-rich fluids to the magma has been previously invoked (*'CO_2 fluxing'*; e.g., Collins et al., 2009; Ferlito and Lanzafame, 2010; Spilliaert et al., 2006a; and references therein), with the excess CO_2, deriving either from the degassing of a deep magmatic body, or from the interaction of the magma with sedimentary carbonates (Aiuppa et al., 2017; Chiodini et al., 2011). The latter hypothesis is corroborated by the estimated depth of the magma ponding zone identified in this study, but also by Spilliaert et al., (2006a), at which the CO_2 enrichment mainly occurs: 8-9 km bcl, would be in the Hyblean carbonates (Finetti et al., 2006; Spilliaert et al., 2006a; and references therein).

Differently, FS magma seems to have a deeper accumulation zone at 15-18 km bcl, probably at the boundary between the crystalline basement and the Hyblean carbonates. The depths of these two ponding zones are in relatively good agreement with those estimated by the seismic tomography for the fossil magma chambers (>12 km bcl; e.g. FS eruption), and for the current one (6 km bcl) at Etna (Aloisi et al., 2002).

Instead, no clear evidence exists about the occurrence of Middle to Late Triassic sulfate rocks at the depths of entrapment of FS MIs; however evaporitic rocks, belonging to the Late Messinian Gessoso-Solfifera Formation, widespread in the nearby Caltanissetta Basin (Finetti et al. 2006; Lentini, 1982), may be encountered by Etnean magmas during their ascent to the surface, and contribute to the high S and low SiO_2 contents of Mt. Spagnolo MIs, associated to the particularly high oxygen fugacity (see sections 4.1.4 and 5).

Indeed, the S contents of the melt inclusions characterized in this study are not clearly correlated with their estimated entrapment pressures (Fig. 11a), as observed in Spilliaert et al. (2006b). In particular, several melt inclusions from Mt. Spagnolo, 2002/2003 South and 2006 products, show S contents > 2000 ppm, although they were entrapped at pressure below 150 MPa (Fig. 11a). This suggests that depressurization is not the principal parameter controlling S degassing in the hydrous Etnean magmas, and therefore the S content of MIs.

The redox conditions varying between different eruptions and, to a lesser extent, during the same eruption, seem to play a crucial role in determining S behavior in etnean magmas. The most primitive MIs show early spinel crystallization and high S contents (principally in Mt. Spagnolo), both due to strongly oxidizing redox conditions (section 4.1.4; Jugo, 2009). The more evolved MIs (belonging to the *2001-2013* eruptive period) show variable extents of late spinel crystallization that probably reflects lower and variable fO_2 conditions (Fig. 10). The S content of these inclusions clearly decreases with differentiation (Fig. 7), suggesting that differentiation is a critical process in controlling S degassing, probably by modifying magma redox conditions.

726 Differently from S, Cl seems to be enriched in the melt in the upper part of the plumbing system
727 (the last 100 MPa, Fig. 11b), suggesting an incompatible behavior during melt differentiation,
728 which is however not illustrated by a clear correlation with the K_2O content (Fig. SI4). Coupled
729 processes of degassing and crystallization-driven enrichment could explain these features. We also
730 note that the variable concentration of Cl in Etnean melts has been ascribed to the upward migration
731 of deep Cl-rich fluids (Ferlito et al., 2014; and reference therein), or as a consequence of several
732 interactions and connections between distinct magma pockets within Etna's shallow plumbing
733 system (Corsaro and Metrich, 2016; Kahl et al., 2011). Furthermore, Rizzo et al. (2013) assume the
734 variable isotopic Cl and Cl/K ratio, in rocks and gases of 2008-2011 periods, as representative of a
735 typical depleted mantle magma contaminated by altered oceanic crust.
736 In conclusion, despite the possible different interpretations, volatile contents in MIs strongly
737 suggest important magma degassing during magma evolution and ascent. H_2O, CO_2, and Cl
738 degassing are likely to be mainly driven by magma decompression, while S degassing seems to be
739 related to melt differentiation and redox conditions. This degassing translate into significant gas
740 emissions, which are at present regularly observed at Etna (e.g. Aiuppa et al., 2008; Allard et al.,
741 2006).
742

743 **5. Additional processes contributing to magmas heterogeneity**

744 Even if MELTS fractional crystallization models (section 4.1) seem able to reproduce most of
745 major elements compositions of MIs starting from an H_2O-rich FS parental magma, some chemical
746 features require additional interpretations. On this view, Correale et al. (2014) concluded that the
747 modeling of the whole-rock compositions of Etnean volcanics from the last 15 ka requires pristine
748 melts having significant differences in some major oxides, especially Na_2O, which can be explained
749 by variable melting degrees of a single mantle sources, followed by crystallization. Even if the
750 study of Correale et al. (2014) on whole rocks can be influenced, in the case of FS, by a possible

751 enrichment of olivine crystals, their results apply to MI compositions too. Inspection at Fig. 5f
752 shows, in fact, that Na_2O contents of FS and Mt. Spagnolo MIs do not fit with a single liquid
753 descent line, with FS requiring a pristine melt depleted in Na_2O. According to Correale et al.
754 (2014), this would be due to a large melting degree generating the FS pristine melt.
755 MIs of FS also display SiO_2 contents lower than the less primitive Mt. Spagnolo ones, whereas CaO
756 seems to increase slightly (Figs. 5a-c). These trends can be difficultly explained by the
757 crystallization of olivine and clinopyroxene, MELTS simulations predicting indeed clear SiO_2
758 increase during differentiation, and conversely a continuous decrease of CaO (Figs. 5a-c). The CaO
759 content that increases from FS to Mt. Spagnolo is also incompatible with a higher degree of melting
760 of FS with respect to Mt. Spagnolo, as CaO should increase with melting (Correale et al., 2014).
761 Besides, we already reported (section 3.4) that S content of the MIs of FS is lower than that of Mt
762 Spagnolo. This could therefore suggest the addition of a sulfate component to the magma, i.e. the
763 assimilation of sedimentary sulfates from the host rocks. This assimilation enriches the melt in S
764 and to a lesser extent in CaO, decreases its silica content (Figs. SI6), and strongly oxidizes the
765 magma (Iacono-Marziano et al. 2017). Being this a local process that depends on the physical path
766 followed by each magma upon its ascent, and also from its temperature and ascent rate, sulfate
767 assimilation could therefore account for (i) the changes in the redox conditions (and the resulting
768 different timings and amounts of spinel crystallization) observed between the different eruptions
769 (section 4.1.4, Fig. 10), but also during a single eruption, (ii) the large dispersion in the SiO_2
770 content, of which only the highest SiO_2/K_2O values are reproduced by MELTS (Figs. 5).
771 The occurrence in the Mt. Spagnolo lava of the large compositional range of olivine (Fo_{70-88}), some
772 of which with reverse zoning (section 2.1), could indicate the presence of interactions between two
773 magma batches with different compositions due to dissimilar fractional crystallization-induced melt
774 evolution. Indeed, the occurrence of mixing process in the shallow plumbing system of Mt. Etna has
775 been already reported in previous studies for explaining the compositional variation of products

776 erupted after 1970's (e.g., Corsaro and Pompilio, 2004a; Métrich et al., 2004), as well as, for the
777 Mt. Frumento delle Concazze lava (Corsaro and Métrich, 2016; and references therein).
778
779 Episode of deep mixing between a primitive melt with the one resulting by the incongruent melting
780 (Danyushevsky et al., 2004) of (i) clinopyroxene- or (ii) plagioclase-rich cumulates could be the
781 cause of the (i) high CaO contents of MIs from FS (this study, Corsaro and Métrich, 2016), Mt.
782 Maletto (Kamenetsky and Clocchiatti, 1996), and (ii) of the enrichment of Ba, Sr and Eu observed
783 in MIs of *2001-2006* products by Schiavi et al. (2015).
784 Patterns of trace elements provide further evidences about the occurrence of processes other than
785 simple fractional crystallization. During crystal fractionation of olivine-spinel-clinopyroxene-
786 plagioclase phases from FS magma (this study, Kamenetsky et al., 2007 for trace elements
787 composition), MELTS models show an enrichment of the melt in incompatible trace elements (Figs.
788 SI7). This enrichment is however less important than that observed in natural olivine-hosted MIs
789 (Collins et al., 2009; Kamenetsky et al., 2007; Rose-Koga et al., 2012; Schiavi et al., 2015, Figs.
790 SI7; except for Y, Yb, and Zr). This suggests that the degree of enrichment of the parental melt
791 cannot be the same one for all the eruptions but pristine melts having variable contents of trace
792 elements have to exist. Different degrees of melting of a single source could account for these
793 features, even if the major oxide compositions of the pristine melts could be similar (Correale et al.,
794 2014).
795 The variability of the Rb/Th ratios, moving from a value of 2 in 2002/2003 MIs up to 9.7 in MIs of
796 *FS* and *2001* eruptions estimated by Kamenetsky et al. (2007) and Schiavi et al. (2015), cannot be
797 explained by melting and/or crystallization (Figs. SI7c-d), due to the similar partition coefficients of
798 these two elements. Their different affinity with aqueous fluids addresses to the involvement of a
799 metasomatizing phase. Coupled to the high contents of these elements, which resemble those
800 typical of arc magmatism, these features address to a contribution of a crustal slab-derived
801 component in the mantle source producing Etnean magmas in the last 15 ka (Corsaro and Métrich,

802 2016; Tonarini et al., 2001). Accordingly, the heterogeneous Nd-Sr-Ba elemental contents (28-67,
803 396-1573, 255-817 ppm) and isotopic features ($^{144}Nd/^{143}Nd$: between 0.512836±6 of FS and
804 0.512908±5 of Mt. Spagnolo; $^{87}Sr/^{86}Sr$: 0.703317±6 for Mt. Spagnolo up to 0.703910±6 for FS)
805 were attributed by Correale et al. (2014) to different melting degree of a mantle source (and
806 variably) – metasomatized by crustal fluids, justifying the heterogeneity in the Etnean rocks.
807

808 ## 6. Concluding remarks

809 Olivine hosted melt inclusions were accurately selected from (trachy)-basaltic tephra and lavas
810 formed during Etnean eruptions of the last 15 ka: in particular, from the oldest and most primitive
811 magmas (Mt. Spagnolo basalt and FS picro-basalt) up to more evolved trachybasalts erupted during
812 the paroxysmal event of April 2013, and from 2002/2003 South, 2006 and 2008/2009 eruptions. All
813 the MIs were characterized for their major elements compositions and volatiles contents by electron
814 microprobe, ionic probe, and infrared spectroscopy, using the same conditions to insure an internal
815 consistency in this new dataset. These results were interpreted in terms of the principal magmatic
816 processes, using MELTS code and H_2O-CO_2 solubility models, and integrating literature data.
817 Here the principal remarks from this study:
818

819 – FS tephra entrap, in Mg-rich olivine (Fo_{89-91}), the most undegassed and primitive melt
820 inclusions (Mg#= 67-74) among the investigated products of the last 15 ka. H_2O and CO_2
821 contents (H_2O up to 5.7 wt.%, CO_2 up to more than 5000 ppm), with the highest values
822 indicating high pressure of crystallization (477 MPa, i.e. a depth of entrapment of 18 km
823 bcl), suggest an important volatile source in deepest magmatic system. FS magma
824 experienced a rapid ascent (associated to a high decompression, $dP/dT \geq 20$ MPa $°C^{-1}$) that
825 led to H_2O and CO_2 degassing without substantial melt differentiation and S degassing. The

whole rock composition rather suggests olivine accumulation in the melt. The rapid ascent probably allowed FS primitive magma to reach the surface and to be erupted explosively.

– The most recent trachybasalts of 2001-2013 eruptions host melt inclusions progressively more evolved and degassed, and entrapped in a shallower plumbing system (0-10 km bcl). The composition of MIs of these eruptions indicates that Etnean magmas generally underwent a more gradual decompression ($dP/dT < 5$ MPa °C^{-1}) than in the case of FS eruption, allowing a more important melt differentiation and H_2O-CO_2 degassing in closed system than FS magma.

– The chemical variability observed in the investigated Etnean melt inclusions (e.g., FeO_{tot}: 4.3-12.6 wt.%; CaO: 3.3-15.1 wt.%; MgO: 1.9-12.4 wt.%, K_2O: 0.6-5.6 wt.%) and in the volatiles components (0-7 wt.%) is mainly attributed (on the basis of a petrogenetic modeling using MELTS code) to the effect of melt differentiation of the parental H_2O-rich FS magma, due to fractional crystallization of spinel (Cr-Mg-rich to Ti-magnetite) + olivine + clinopyroxene ± plagioclase in a highly oxidized system (fO_2 between NNO+1 and NNO+2). The MELTS simulations, performed in T-P range of 1300-1050 °C and 500-0.1 MPa, and with variable dP/dT ratio, generally yield to the decrease in MgO, H_2O, CaO/Al_2O_3 ratio, and the increase of alkali (especially K_2O), as outlined in MIs from FS to the most evolved and degassed of 2013. The mineral compositions predicted by MELTS models are generally consistent with those observed in Etnean products.

– Some geochemical features (i.e., large variability in Al_2O_3, Na_2O, CO_2, Cl and trace elements) are not explained by a simple process of magma differentiation, and could suggest the occurrence of other mechanisms, as variable degrees of mantle melting (e.g. *Correale et al., 2014*), or CO_2-Cl-rich fluid flushing (e.g. *Ferlito et al., 2010, 2014*).

– MIs in Mt. Spagnolo olivine phenocrysts (Fo_{82-88}) have primitive features in terms of their major elements (but of lesser entity than FS MIs), but present the highest S contents (4150 ppm), variable CO_2 contents (0-2674 ppm) and low H_2O (< 0.5 wt.%), probably due to a H^+

852 diffusion trough olivine crystals imposed by the slower cooling conditions, thus unreliable
853 to calculate a crystallization pressure. The particular Mt. Spagnolo melt inclusions (partially
854 degassed and less primitive than FS MIs) could be originated through the differentiation of a
855 FS melt under very oxidizing conditions (fO_2 > NNO+2), or alternatively magma mixing
856 episodes between a primitive FS-type melt and an evolved residual magmatic bodies at
857 shallow depth, as inferred by previous studies (e.g. *Corsaro and Métrich, 2016; Kahl et al.,*
858 *2015*). This would also agree with the reverse zoning of olivine crystals. The highest S
859 contents of these MIs and the high oxygen fugacity could alternatively suggest the
860 assimilation of crustal sulfates occurring during magma ascent or ponding.
861

862 **Acknowledgments**

863 *This work is part of the PhD thesis of E. Gennaro, which has been supported by the University of*
864 *Palermo, the MED-SUV project, the "Laboratoire d'Excellence VOLTAIRE" de l'Université*
865 *d'Orléans, and the French agency for research (ANR project #12-JS06-0009-01). We thank I. Di*
866 *Carlo (ISTO, Orléans) for her assistance with the SEM and the EMP methods, E. Deloule and A.*
867 *Gurenko (CRPG, Nancy) for their support during SIMS acquisitions, A. Correale (INGV, Palermo)*
868 *and A. Rosciglione to have provided some Etnean samples.*
869

870 # References
871

872 Aiuppa, A., Giudice, G., Gurrieri, S., Liuzzo, M., Burton, M., Caltabiano, T., McGonigle, A.J.S.,
873 Salerno, G., Shinohara, H., Valenza, M., 2008. Total volatile flux from Mount Etna. Geophys. Res.
874 Lett. 35, L24302. https://doi.org/10.1029/2008GL035871.
875

876 Aiuppa., A., Fischer, T.P., Plank, T., Robidoux, P., Di Napoli, R., 2017. Along-arc, inter-arc and
877 arc-to-arc variations in volcanic gas CO_2/S_T ratios reveal dual source of carbon in arc volcanism.
878 Earth-Science Reviews 168, 24–47.
879
880 Allard, P., Behncke, B., D'Amico, S., Neri, M., Gambino, S., 2006. Mount Etna 1993–2005:
881 Anatomy of an evolving eruptive cycle. Earth-Sci. Rev. 78, 85–114.
882 https://doi.org/10.1016/j.earscirev.2006.04.002.
883
884 Aloisi, M., Cocina, O., Neri, G., Orecchio, B., Privitera, E., (2002). Seismic tomography of the
885 crust underneath the Etna volcano, Sicily. Physics of the Earth and Planetary Interiors 134, 139–
886 155.
887
888 Andronico, D., Branca, S., Calvari, S., Burton, M., Caltabiano, T., Corsaro, R.A., Del Carlo, P.,
889 Garfì, G., Lodato, L., Miraglia, L., others, 2005. A multi-disciplinary study of the 2002–03 Etna
890 eruption: insights into a complex plumbing system. Bull. Volcanol. 67, 314–330.
891
892 Armienti, P., Innocenti, F., Petrini, R., Pompilio, M., Villari, L., 1988. Sub-aphyric alkali basalt
893 from Mt. Etna Inferences Depth Compos. Source Magma Rend Soc It Miner. Pet. 43, 877–891.
894
895 Armienti P., Tonarini S., D'Orazio M., Innocenti F., 2004. Genesis and Evolution of Mt. Etna
896 alkaline lavas: petrological and Sr-Nd-B isotope costraints. Periodico di Mineralogia 73, 29-52.
897

898 Armienti, P., Tonarini, S., Innocenti, F. and D'Orazio, M., 2007. Mount Etna pyroxene as tracer of
899 petrogenetic processes and dynamics of the feeding system. In: Beccaluva, L., Bianchini, G. and
900 Wilson, M. (eds) Cenozoic Volcanism in the Mediterranean Area, Geological Society of America,
901 Special Papers 418, 265-276, doi:10.1130/2007.2418 (13).
902
903 Armienti, P., Perinelli, C., Putirka, K.D., 2012. A New Model to Estimate Deep-level Magma
904 Ascent Rates, with Applications to Mt. Etna (Sicily, Italy). J. Petrol. 54, 795–813.
905 https://doi.org/10.1093/petrology/egs085.
906
907 Ballhaus, C., Berry, C. F., Green, D. H., 1991. High pressure experimental calibration of the
908 olivine-orthopyroxene-spinel oxygen geobarometer: implications for the oxidation state of the upper
909 mantle. Contributions to Mineralogy and Petrology 108, 82-92.
910
911 Bonaccorso, A., Bonforte, A., Calvari, S., Del Negro, C., Di Grazia, G., Ganci, G., Neri, M., Vicari,
912 A., Boschi, E., 2011. The initial phases of the 2008-2009 Mt. Etna eruption: a multi-disciplinary
913 approach for hazard assessment. Journal of Geophysical Research, Vol. 116, B03203, doi:
914 10.1029/2010JB007906.
915
916 Branca, S., Coltelli, M., Groppelli, G., 2011. Geological evolution of a complex basaltic
917 stratovolcano: Mount Etna, Italy. Italian Journal of Geosciences 130, 306-317.
918

919 Bucholz, C.E., Gaetani, G.A., Behn, M.D., Shimizu, N., 2013. Post-entrapment modification of
920 volatiles and oxygen fugacity in olivine-hosted melt inclusions. Earth Planet. Sci. Lett. 374, 145–
921 155. https://doi.org/10.1016/j.epsl.2013.05.033.

922

923 Calvari, S., Coltelli, M., Neri, M., Pompilio, M., Scribano, V., 1994. The 1991-1993 Etna eruption:
924 chronology and lava. Acta Vulcanol. 4, 1–14.

925

926 Cecchetti, A., Marianelli, P., Sbrana, A., 2002. L'eruzione Di Astroni (Caldera Dei Campi Flegrei):
927 Dati Preliminari Dallo Studio Di Inclusioni Silicatiche. Atti Soc. tosc. Sci. nat., Mem., Serie A, 108
928 (2002-2003) pagg. 59-63.

929

930 Chiodini, G., Caliro, S., Aiuppa, A., Avino, R., Granieri, R., Moretti, R., Parello, F., 2011. First
931 13C/12C isotopic characterisation of volcanic plume CO_2 Bullettin of Volcanology, 73:531–542
932 DOI 10.1007/s00445-010-0423-2.

933

934 Clocchiatti, R., Joron, J.L., Treuil, M., 1988. The role of selective alkali contamination in the
935 evolution of recent historical lavas of Mt. Etna. Journal of Volcanology and Geothermal Research
936 34, 241-249.

937

938 Clocchiatti, R., Schiano, P., Ottolini, L., Bottazzi, P., 1998. Earlier alkaline and transitional
939 magmatic pulsation of Mt. Etna volcano. Earth and Planetary Science Letters 163, 399-407.

940

941 Collins, S.J., Pyle, D.M., Maclennan, J., 2009. Melt inclusions track pre-eruption storage and
942 dehydration of magmas at Etna. Geology 37, 571–574. https://doi.org/10.1130/G30040A.1.

943

944 Coltelli, M., Del Carlo, P., Vezzoli, L., 1998. Discovery of a Plinian basaltic eruption of Roman age
945 at Etna volcano, Italy. Geology 26, 1095–1098.

946

947 Coltelli, M., Del Carlo, P., Pompilio, M., Vezzoli, L., 2005. Explosive eruption of a picrite: The
948 3930 BP subplinian eruption of Etna volcano (Italy). Geophys. Res. Lett. 32, L23307.
949 https://doi.org/10.1029/2005GL024271.

950

951 Continisio, R., Ferrucci, F., Gaudiosi, G., Lo Bascio, D., Ventura, G., 1997. Malta Escarpment Mt.
952 Etna: early stages of an asymmetric rifting process? Evidences from geophysical and geological
953 data. Acta Vulcanologica 9, 45-53.

954

955 Correale, A., Paonita, A., Martelli, M., Rizzo, A., Rotolo, S.G., Corsaro, R.A., Di Renzo, V., 2014.
956 A two-component mantle source feeding Mt. Etna magmatism: Insights from the geochemistry of
957 primitive magmas. Lithos 184, 243–258. https://doi.org/10.1016/j.lithos.2013.10.038.

958

959 Corsaro, R.A., and Pompilio, M., 2004a. Dynamics of magmas at Mount Etna. In: Mount Etna:
960 Volcano Laboratory. Geophysical Monograph Series 143, 91-110.

961

962 Corsaro, R.A., Pompilio, M., 2004b. Buoyancy-controlled eruption of magmas at Mt. Etna. Terra
963 Nova 16, 16–22. https://doi.org/10.1046/j.1365-3121.2003.00520.x

964

965 Corsaro, R.A., Métrich, N., Allard, P., Andronico, D., Miraglia, L., Fourmentraux, C., 2009. The
966 1974 flank eruption of Mount Etna: An archetype for deep dike-fed eruptions at basaltic volcanoes
967 and a milestone in Etna's recent history. J. Geophys. Res. Solid Earth 114, B07204.
968 https://doi.org/10.1029/2008JB006013

969

970 Corsaro, R.A., Métrich, N., 2016. Chemical heterogeneity of Mt. Etna magmas in the last 15 ka.
971 Inferences on their mantle sources. Lithos 252, 123–134.
972 https://doi.org/10.1016/j.lithos.2016.02.006

973

974 Coulson, I.M., Stuart, F.M., MacLean, N.J., 2011. Assessing the link between mantle source and
975 sub-volcanic plumbing in the petrology of basalts from the 2001 and 2002/2003 eruptions of Mount
976 Etna, Sicily: Evidence from geochemical and helium isotope data. Lithos, Secular variations in
977 magmatism and tectonic implicationsSpecial session at the 2009 Geological Association of Canada
978 - Mineralogical Association of Canada (GAC-MAC) meeting 123, 254–261.
979 doi:10.1016/j.lithos.2010.11.013

980

981 Danyushevsky, L.V., Della-Pasqua, F.N., Sokolov, S., 2000. Re-equilibration of melt inclusions
982 trapped by magnesian olivine phenocrysts from subduction-related magmas: petrological
983 implications. Contrib. Mineral. Petrol. 138, 68–83. https://doi.org/10.1007/PL00007664

984

985 Danyushevsky, L.V., Sokolov, S., Falloon, T.J., 2002. Melt Inclusions in Olivine Phenocrysts:
986 Using Diffusive Re-equilibration to Determine the Cooling History of a Crystal, with Implications
987 for the Origin of Olivine-phyric Volcanic Rocks. J. Petrol. 43, 1651–1671.
988 https://doi.org/10.1093/petrology/43.9.1651

989

990 Danyushevsky, L. V., R. A. J. Leslie, A. J. Crawford, and P. Durance, 2004. Melt inclusions in
991 primitive olivine phenocrysts: The role of localized reaction processes in the origin of anomalous
992 compositions, J. Petrol., 45, 2531–2553.

993

994 Danyushevsky, L.V., Plechov, P., 2011. Petrolog3: Integrated software for modeling crystallization
995 processes. Geochem. Geophys. Geosystems 12, Q07021. https://doi.org/10.1029/2011GC003516

996

997 Di Carlo, I., Pichavant, M., Rotolo, S.G., Scaillet, B., 2006. Experimental Crystallization of a High-
998 K Arc Basalt: the Golden Pumice, Stromboli Volcano (Italy). J. Petrol. 47, 1317–1343.
999 https://doi.org/10.1093/petrology/egl011

1000

1001 Dixon, J. E., Stolper, E., Delaney, J.R., 1988. Infrared spectroscopic measurements of CO_2 and H_2O
1002 in Juan de Fuca Ridge basaltic glasses. *Earth and Planetary Science letters, 90*, 87-104 87.

1003

1004 Dixon, J. E. and Pan, V., 1995. Determination of the molar absorptivity of dissolved carbonate in
1005 basanitic glass. Am. Mineral. 80, 1339-1342.

1006

1007 Doglioni, C., Innocenti, F., Mariotti, G., 2001. Why Mt. Etna? Terra Nova 13, 25–31.
1008 https://doi.org/10.1046/j.1365-3121.2001.00301.x

1009

1010 Ferlito, C., Lanzafame, G., 2010. The role of supercritical fluids in the potassium enrichment of
1011 magmas at Mount Etna volcano (Italy). Lithos 119, 642–650.

1012

1013 Ferlito, C., Coltorti, M., Lanzafame, G., Giacomoni, P.P., 2014. The volatile flushing triggers
1014 eruptions at open conduit volcanoes: evidence from Mount Etna volcano (Italy). Lithos 184, 447-
1015 455.

1016

1017 Finetti I.R., Lentini F., Carbone S., Del Ben A., Di Stefano A., Forlin E., Guarnieri P., Pipan M.,
1018 Prizzon A., 2006. Geological outline of Sicily and lithospheric tectono-dynamics of its Tyrrhenian
1019 margin from new CROP Seismic data. In CROP Project: deep seismic exploration of the Central
1020 Mediterranean and Italy, Ed. Finetti I.R., 319-376.

1021

1022 Frezzotti, M.-L., 2001. Silicate-melt inclusions in magmatic rocks: applications to petrology. Lithos
1023 55, 273–299. https://doi.org/10.1016/S0024-4937(00)00048-7.

1024

1025 Gaetani, G., A., and Watson, B., E., 2002. Modeling the major-element evolution of olivine-hosted
1026 melt inclusions a Chemical Geology 183, 25-41.

1027

1028 Gaetani, G.A., O'Leary, J.A., Shimizu, N., Bucholz, C.E., Newville, M., 2012. Rapid
1029 reequilibration of H_2O and oxygen fugacity in olivine-hosted melt inclusions. Geology 40, 915–
1030 918. https://doi.org/10.1130/G32992.1.

1031

1032 Gennaro, E. (2017) Sulfur behavior and redox conditions in Etnean hydrous basalts inferred from
1033 melt inclusions and experimental glasses. PhD thesis, Università degli Studi di Palermo, Université
1034 d'Orléans.

1035

1036 Giacomoni, P.P., Coltorti, M., Bryce, J.G., Fahnestock, M.F., Guitreau, M., 2016. Mt. Etna
1037 plumbing system revealed by combined textural, compositional, and thermobarometric studies in
1038 clinopyroxenes. Contrib. Mineral. Petrol. (2016) 171:34. DOI 10.1007/s00410-016-1247-7

1039

1040 Ghiorso, M.S., Sack, R.O., 1995. Chemical mass transfer in magmatic processes IV. A revised and
1041 internally consistent thermodynamic model for the interpolation and extrapolation of liquid-solid
1042 equilibria in magmatic systems at elevated temperatures and pressures. Contrib. Mineral. Petrol.
1043 119, 197–212. https://doi.org/10.1007/BF00307281.

1044

1045 Gvirtzman, Z., Nur, A., 1999. The formation of Mount Etna as the consequence of slab rollback.
1046 Nature 401, 782–785. https://doi.org/10.1038/44555.

1047

1048 Iacono Marziano, G., Morizet, Y., Le Trong, E., Gaillard, F., 2012. New experimental data and
1049 semi-empirical parameterization of H_2O-CO_2 solubility in mafic melts. Geochim. Cosmochim. Acta
1050 97, 1–23. https://doi.org/10.1016/j.gca.2012.08.035.

Iacono-Marziano, G., Ferraina, C., Gaillard, F., Di Carlo, I., Arndt, N.T., 2017. Assimilation of sulfate and carbonaceous rocks: Experimental study, thermodynamic modeling and application to the Noril'sk-Talnakh region (Russia). Ore Geology Reviews, 90, 399-413.

Innocenti, F., Rocchi, S., Trigila, R., 1999. La classificazione delle rocce vulcaniche e subvulcaniche: schema operativo per il progetto CARG. Atti Soc. tosc. Sci. Nat., Mem., Serie A, 106, pagg. 113-124, figg. 17, tabb. 8.

Jarosewich E., Parkes A.S., Wiggins L.B., 1979. Microprobe analyses of four natural glasses and one mineral: an interlaboratory study of precision and accuracy. Smithsonian Contrib Earth Science, 22:53-67.

Jochum K.P., Stoll B., Hervig K., Willbold M., Hofmann A.W., Amini M., Aarburg S., Abouchami W., Hellebrand E., Mocek B., Raczek I., Strake A., Alard O., Bouman C., Becker S., Ducking M., Bratz H., Klemd R., de Bruin D., Canil D., Cornell D., De Hoog C-J., Dalpé C., Danyushevsky L., Eisenhauer A., Gao Y., Snow J., Groschopf N., Gunther D., Latkoczy C., Guillong M., Hauri E.H., Hofer H.E., Lahaye Y., Horz K., Jacob D.E., Kasemann S.A., Kent A.J.R., Ludwig T., Zack T., Mason P.R.D., Meixner A., Rosner M., Misawa K., Nash B.P., Pfander J., Premo W.R., Sun W.D., Tiepolo M., Vannucci R., Vennemann T., Wayne D., Woodhead J.D., 2006. MPI-DING reference glasses for in situ microanalysis: New reference values for element concentrations and isotope ratios. Geochemistry Geophysics Geosystems 7, Q02008, doi:10.1029/2005GC001060.

1074 Joron, J.L., Treuil, M., 1984. Etude geochimique et pétrogenèse des laves de l'Etna. Bulletin of
1075 Volcanology 47, 1125–1144.
1076
1077 Jugo, P.J., 2009. Sulfur content at sulfide saturation in oxidized magmas. Geology 37, 415–418.
1078 https://doi.org/10.1130/G25527A.1.
1079
1080 Kahl, M., Chakraborty, S., Costa, F., Pompilio, M., 2011. Dynamic plumbing system beneath
1081 volcanoes revealed by kinetic modeling, and the connection to monitoring data: An example from
1082 Mt. Etna. Earth Planet. Sci. Lett. 308, 11–22. https://doi.org/10.1016/j.epsl.2011.05.008.
1083
1084 Kahl, M., Chakraborty, S., Pompilio, M., Costa, F., 2015. Constraints on the Nature and Evolution
1085 of the Magma Plumbing System of Mt. Etna Volcano (1991–2008) from a Combined
1086 Thermodynamic and Kinetic Modelling of the Compositional Record of Minerals. J. Petrol. 56,
1087 2025–2068. https://doi.org/10.1093/petrology/egv063.
1088
1089 Kamenetsky, V., Clocchiatti, R., 1996. Primitive magmatism of Mt. Etna: insights from mineralogy
1090 and melt inclusions. Earth Planet. Sci. Lett. 142, 553–572. https://doi.org/10.1016/0012-
1091 821X(96)00115-X.
1092
1093 Kamenetsky, V.S., Pompilio, M., Métrich, N., Sobolev, A.V., Kuzmin, D.V., Thomas, R., 2007.
1094 Arrival of extremely volatile-rich high-Mg magmas changes explosivity of Mount Etna. Geology
1095 35, 255–258. https://doi.org/10.1130/G23163A.1
1096

1097 Lanzo, G., Di Carlo, I., Pichavant, M., Rotolo, S. G., Scaillet, B., 2016. Origin of primitive ultra-
1098 calcic arc melts at crustal conditions - Experimental evidence on the La Sommata basalt, Vulcano,
1099 Aeolian Islands. Journal of Volcanology and Geothermal Research, Elsevier, 321, pp.85-101.
1100
1101 Le Gall, N., Pichavant, M., 2016. Experimental simulation of bubble nucleation and magma ascent
1102 in basaltic systems: Implications for Stromboli volcano. Am. Mineral. 101, 1967–1985.
1103 https://doi.org/10.2138/am-2016-5639.
1104
1105 Lentini, F.,1982. The geology of Mt. Etna basement. Mem. Soc. Geol. It., 23, 7-25.
1106
1107 Lesne, P., Bruno Scaillet, Michel Pichavant, Jean-Michel Bény, 2011. The carbon dioxide solubility
1108 in alkali basalts: an experimental study. Contrib. Mineral. Petrol. 162, 153–168.
1109 https://doi.org/10.1007/s00410-010-0585-0.
1110
1111 Liotta, M., Rizzo, A., Paonita, A., Caracausi, A., Martelli, M., 2012. Sulfur isotopic compositions
1112 of fumarolic and plume gases at Mount Etna (Italy) and inferences on their magmatic source.
1113 Geochem. Geophys. Geosystems 13, Q05015. https://doi.org/10.1029/2012GC004118
1114
1115 Lloyd, A., S., Plank, T., Ruprecht, P., Hauri, E. H., Rose, W., 2013. Volatile loss from melt
1116 inclusions in pyroclasts of differing sizes. Contrib Mineral Petrol 165, 129–153. DOI
1117 10.1007/s00410-012-0800-2.
1118
1119 Metrich, N., Clocchiatti, R., 1989. Melt inclusion investigation of the volatile behaviour in historic
1120 alkali basaltic magmas of Etna. Bull. Volcanol. 51, 185–198. https://doi.org/10.1007/BF01067955.

Metrich, N., Allard, P., Spilliaert, N., Andronico, D., Burton, M., 2004. 2001 flank eruption of the alkali- and volatile-rich primitive basalt responsible for Mount Etna's evolution in the last three decades. Earth Planet. Sci. Lett. 228, 1–17. https://doi.org/10.1016/j.epsl.2004.09.036.

Michaud, V., 1995. Crustal xenoliths in recent hawaiites from Mount Etna, Italy: evidence for alkali exchanges during magma–wall rock interaction. Chemical Geology 122, 21–42.

Mollo, S., Giacomoni, P.P., Coltorti, M., Ferlito, C., Iezzi, G., Scarlato, P., 2015. Reconstruction of magmatic variables governing recent Etnean eruptions: Constraints from mineral chemistry and P–T–fO2–H2O modeling. Lithos 212–215, pp. 311–320.

Norrish, K., Hutton, J.T., 1969. An accurate X-ray spectrographic method for the analysis of a wide range of geological samples. Geochim. Cosmochim. Acta 33, 431–453. https://doi.org/10.1016/0016-7037(69)90126-4.

Paonita, A., Caracausi, A., Iacono-Marziano, G., Martelli, M., Rizzo, A., 2012. Geochemical evidence for mixing between fluids exsolved at different depths in the magmatic system of Mt Etna (Italy). Geochim. Cosmochim. Acta 84, 380–394. https://doi.org/10.1016/j.gca.2012.01.028.

1143 Pichavant, M., Martel, C., Bourdier, J.L., and Scaillet, B., 2002. Physical conditions, structure, and
1144 dynamicsof a zoned magma chamber: Mount Pele´e (Martinique, Lesser Antilles Arc). Journal of
1145 Geophysical Research, Vol. 107, No. B5, 2093, 10.1029/2001jb000315.

1146

1147 Pichavant, M., Di Carlo, I., Le Gac, Y., Rotolo, S. G., Scaillet, B., 2009. Experimental Constraints
1148 on the Deep Magma Feeding System at Stromboli Volcano, Italy. Journal of Petrology, Volume 50,
1149 Number 4 Pages 601-624 2009 Doi:10.1093/Petrology/Egp014.

1150

1151 Pichavant, M., Di Carlo, I., Rotolo, S., Scaillet, B., Burgisser, A., Le Gall, N., Martel, C., 2013.
1152 Generation of CO2-rich melts during basalt magma ascent and degassing.

1153

1154 Pompilio M, Coltelli M, Del Carlo P, Vezzoli L, 1995. How do basaltic magmas, feeding explosive
1155 eruptions, rise and differentiate at Mt. Etna? Period. Mineral.

1156

1157 Richet, P., Whittington, A., Holtz, F., Behrens, H., Ohlhorst, S., Wilke, M., 2000. Water and the
1158 density of silicate glasses. Contributions to Mineralogy and Petrology 138(4): 337-347.

1159

1160 Rizzo, A.L., Caracausi, A., Liotta, M., Paonita, A., Barnes, J.D., Corsaro, R.A., Martelli, M., 2013.
1161 Chlorine isotope composition of volcanic gases and rocks at Mount Etna (Italy) and inferences on
1162 the local mantle source. Earth Planet. Sci. Lett. 371–372, 134–142.
1163 https://doi.org/10.1016/j.epsl.2013.04.004

1164

1165 Robidoux, P., Aiuppa, A., Rotolo, S.G., Rizzo, A.L., Hauri, E.H., Frezzotti, M.L., 2017. Volatile
1166 contents of mafic-to-intermediate magmas at San Cristóbal volcano in Nicaragua. Lithos 272–273,
1167 pp. 147–163

1168

1169 Rose-Koga, E.F., Koga, K.T., Schiano, P., Le Voyer, M., Shimizu, N., Whitehouse, M.J.,
1170 Clocchiatti, R., 2012. Mantle source heterogeneity for South Tyrrhenian magmas revealed by Pb
1171 isotopes and halogen contents of olivine-hosted melt inclusions. Chem. Geol. 334, 266–279.
1172 https://doi.org/10.1016/j.chemgeo.2012.10.033

1173

1174 Schiano, P., Clocchiatti, R., 1994. Worldwide occurrence of silica-rich melts in sub-continental and
1175 sub-oceanic mantle minerals. Nature 368, 621–624. https://doi.org/10.1038/368621a0.

1176

1177 Schiano, P., Crocchiati, R., Ottolini, L., Busà, T., 2001. Transition of Mount Etna lavas from a
1178 mantle-plume to an island-arc magmatic source. Nature 412, 900-904.

1179

1180 Schiavi, F., Rosciglione, A., Kitagawa, H., Kobayashi, K., Nakamura, E., Nuccio, P.M., Ottolini,
1181 L., Paonita, A., Vannucci, R., 2015. Geochemical heterogeneities in magma beneath Mount Etna
1182 recorded by 2001-2006 melt inclusions. Geochem. Geophys. Geosystems 16, 2109–2126.
1183 https://doi.org/10.1002/2015GC005786

1184

1185 Shishkina, T.A., Botcharnikov, R.E., Holtz, F., Almeev, R.R., Portnyagin, M.V., 2010. Solubility of
1186 H_2O- and CO_2 -bearing fluids in tholeiitic basalts at pressures up to 500MPa. Chemical Geology
1187 277, 115-125.

Smith, P.M., Asimow, P.D., 2005. Adiabat_1ph: A new public front-end to the MELTS, pMELTS, and pHMELTS models. Geochem. Geophys. Geosystems 6, Q02004. https://doi.org/10.1029/2004GC000816.

Sobolev, A.V., Danyushevsky, L.V., 1994. Petrology and geochemistry of bonitites from the north termination of the Tonga Trench: constraints on the generation conditions of primary high-Ca boninite magmas. J. Petrol. 35, 1183– 1211.

Spilliaert, N., Allard, P., Métrich, N., Sobolev, A.V., 2006a. Melt inclusion record of the conditions of ascent, degassing, and extrusion of volatile-rich alkali basalt during the powerful 2002 flank eruption of Mount Etna (Italy). J. Geophys. Res. Solid Earth 111, B04203. https://doi.org/10.1029/2005JB003934.

Spilliaert, N., Metrich, N. and Allard, P., 2006b. S-Cl-F degassing pattern of water-rich alkali basalt: modelling and relationship with eruption styles on Mount Etna volcano. Earth and Planetary Science Letters 248, 772-786.

Stolper, E., 1982. Water in silicate glasses: an infrared spectroscopic study Contributions to Mineralogy and Petrology 81, 1-17.

1209 Tanguy, J.C., 1978. Tholeitic basalt magmatism of Mount Etna and its relations with the alkaline
1210 series. Contributions to Mineralogy and Petrology 66, 51–67.
1211
1212 Tanguy, J.-C., Condomines, M., Kieffer, G., 1997. Evolution of the Mount Etna magma:
1213 Constraints on the present feeding system and eruptive mechanism. J. Volcanol. Geotherm. Res. 75,
1214 221–250. https://doi.org/10.1016/S0377-0273(96)00065-0.
1215
1216 Tonarini, S., Armenti, P., D'Orazio, M., Innocenti, F., Pompilio, M., Petrini, R., 1995. Geochemical
1217 and isotopic monitoring of Mt. Etna 1989–1993 eruptive activity: bearing on the shallow feeding
1218 system. Journal of Volcanology and Geothermal Research 64, 95–115.
1219
1220 Tonarini, S., Armienti, P., D'Orazio, M., Innocenti, F., 2001. Subduction-like fluids in the genesis
1221 of the Mt. Etna magmas: evidence from boron isotopes and fluid mobile elements. Earth and
1222 Planetary Science Letters 5989, 1–13.
1223
1224
1225 Von Aulock, F.W., Kennedy, B.M., Schipper, C.I., Castro, J.M., Martin, D.E., Oze, C., Watkins,
1226 J.M., Wallace, P.J., Puskar, L., Bégué, F., Nichols, A.R.L., Tuffen, H., 2014. Advances in Fourier
1227 transform infrared spectroscopy of natural glasses: From sample preparation to data analysis. Lithos
1228 206-207, 52-64.
1229

1230 Witter, J.B. Kress, V. C., and Newhall, C. G., 2005. Volcán Popocatépetl,, Mexico. Petrology,
1231 Magma Mixing, and Immediate Sources of Volatiles for the 1994 Present Eruption. Journal of
1232 Petrology, 11, 2337-2366.

1233

Figures captions

Fig. 1 - a) Etna map (modified form Coulson et al., 2011), with the small inset illustrating the geodynamic contest of Etnean area (from Ferlito et al., 2014) and b) DEM (Digital Elevation Model) detail of the summit area, showing the sampling sites.

Fig. 2 - CaO/Al_2O_3 versus MgO contents of whole rock analyses (wr, more evident in the small picture), melt inclusions (MI) PEC corrected, together with literature MI data (Collins et al., 2009; Corsaro and Métrich, 2016; Kamenetsky and Clocchiatti, 1996; Kamenetsky et al., 2007; Métrich et al., 2001; Schiavi et al., 2015; Spilliaert et al., 2006a).

Fig. 3 - K_2O/Na_2O versus K_2O plot, showing the distribution of the studied Etnean glass inclusions (MI, corrected for post-entrapment crystallization) and whole rock analyses (wr), straddling the sodic / potassic affinity limit (after Innocenti et al., 1999), except the sub-alkaline FS products (also improperly reported).

Fig. 4 - BSE images of: a) skeletal clinopyroxene (cpx) and dendritic Ti-magnetite (Ti-mg) microlites in the groundmass, b) a reversely zoned olivine phenocrysts (core=Fo_{75}, rim=Fo_{85}), hosting melt inclusions and Fe-Ti oxide minerals, and c) a melt inclusion containing Cr-spinel at the olivine rim, a bubble and few daughter crystals of Monte Spagnolo lava. d) An olivine phenocryst (Fo_{91}) in FS juvenile tephra, hosting Cr-spinel and a melt inclusion; (e) a typical rounded melt inclusion with scalloped edges and a spherical vapor bubble, in FS. f) Olivine phenocryst in 2002/2003 scoria, entrapping a melt inclusion and Fe-Ti-oxides; g) transmitted light optical image

of a spherical double-polished melt inclusion from 2002/2003 South eruption. h) Transmitted light image of an olivine hosting elongated melt inclusions and a glass embayment, and surrounded by matrix glass from 2006 eruption; i) BSE image of a 2008/2009 olivine hosted MI with a sulfide globule and a vapor bubble associated to an oxide. l) Cu-Fe sulfide and apatite microlites in the microcrystalline groundmass, and m) olivine hosted melt inclusion with irregular shape and with Cu-sulfide and Ti-magnetite phases in 2013 lava, taken by BSE technique.

Fig. 5 - Major element composition of the studied melt inclusions (MIs), using K_2O as a differentiation index. All MIs data are corrected for *post-entrapment crystallization (PEC)* and normalized to 100%.
Colored curves describe the evolution of the major elements in Etnean magma calculated by MELTS code (Ghiorso and Sack, 1995; Smith and Asimow, 2005). MELTS simulations, in the T-P range 1068-1300 °C and 0.1-500 MPa, are obtained for two different initial redox conditions (NNO+1<fO_2<NNO+2) and with an initial H_2O contents of 5wt.% (see text and table SI2 for details). Yellow curves describe the deep evolution of a primitive FS melt with a dP/dT =1 MPa $°C^{-1}$, while the red curves delineate the MELTS model with a dP/dT =20 MPa $°C^{-1}$. Green curves indicate dP/dT = 5 MPa $°C^{-1}$ while light blue curves dP/dT = 3 MPa $°C^{-1}$. The simulations starting from a fO_2 of NNO+2 are described by continues curves, while those from NNO+1 with dashed curves.

Fig. 6 - CO_2 and H_2O contents of investigated melt inclusions (estimated by SIMS and FTIR). Isobars curves are calculated at 1200 °C using the model of Iacono-Marziano et al. (2012), and an average composition of the studied melt inclusions. The depths ("below crater levels") are calculated from the density of the sedimentary basement of Mt. Etna (Corsaro and Pompilio, 2004b). For comparison, data from previous studies are also reported (Collins et al., 2009;

1282 Kamenetsky et al., 2007; Metrich et al., 2004; Spilliaert et al., 2006a). The grey area is obtained
1283 simulating the degassing of the two groups of FS inclusions having the highest H_2O and CO_2
1284 contents, using closed system condition and different initial excess of fluid phase (between 0 and 20
1285 %). The violet area is obtained simulating the degassing of 2002/2003 MIs with H_2O and CO_2
1286 contents of 2 wt.% and 2500 ppm, respectively. The error bars represent the highest standard
1287 deviations obtained for the volatile-richest inclusions.

1288

1289 **Fig. 7** – S content in Etnean melt inclusions as a function of K_2O content (considered as a
1290 differentiation index). In the investigated samples, S decrease from the Mt. Spagnolo MIs (4150
1291 ppm) toward the evolved and degassed MIs, following the increase of K_2O in the melt. No
1292 systematic relation is observed between S and H_2O or CO_2 contents (b and c, respectively). Error
1293 bars for S, H_2O and CO_2 contents are reported in the smaller pictures (a-b).

1294

1295

1296 **Fig. 8** - CaO/Al_2O_3 versus K_2O plot for Etnean melt inclusions (this study and from literature,
1297 symbols as in Fig. 2). The MELTS simulations describing the melt differentiation of H_2O-rich FS
1298 magma (5wt.% H_2O) are also shown. (For details about conditions models and color curves, see
1299 text, Table SI2 and caption of Fig. 5). All resulting liquid lines of descent are generally in almost
1300 complete overlap.

1301

1302 **Fig. 9** – H_2O versus K_2O contents of the studied melt inclusions. Literature data are also presented
1303 for FS and 2001-2007 eruptions (Collins et al., 2009; Kamenetsky et al., 2007; Metrich et al., 2004;
1304 Schiavi et al., 2015; Spilliaert et al., 2006).

Only the II type MELTS models are presented (starting from T-P of 1200 °C-400 MPa), describing H_2O and K_2O evolution of a primitive FS melt with 5 wt.% H_2O and two different initial fO_2 conditions (NNO+1: dashed curves, NNO+2: solid curves). For details, see text and table SI2. The red curves describe a rapid decompression with a dP/dT of 20 MPa $°C^{-1}$ while the green and blue curves melt differentiation with a dP/dT of 5 and 3 MPa $°C^{-1}$ respectively.

Fig. 10 - FeO_{tot} / MgO vs. K_2O contents measured in Etnean melt inclusions (this study, Collins et al., 2009; Corsaro and Métrich, 2016; Kamenetsky and Clocchiatti, 1996; Kamenetsky et al., 2007; Metrich et al., 2004; Schiavi et al., 2015; Spilliaert et al., 2006) and the differentiation paths calculated by MELTS (see text and Table SI2, caption of Fig. 5 for details). All data are normalized to 100% anhydrous. For the MIs symbols see the caption of Figs. 2 and 5. For a clearer understanding, data literature symbols were replaced by colored delimitated area. The black curve illustrates a MELTS test at very high initial fO_2 (> NNO+3), in order to reproduce early spinel crystallization to imitate MIs of Mt. Spagnolo, Mt. Maletto and Frumento delle Concazze (see text for explanation). Some of MELTS models (with dP/dT of 20 and 5 MPa $°C^{-1}$) show the increase of FeO_{tot}/MgO during fractional crystallization, similarly to that described by the evolution from FS + Mt. Spagnolo toward 2002-2013 magmas, suggesting variations in redox condition during melt evolution. Among those MIs, FS, Mt Spagnolo and 2013 are indeed characterized by a constant FeO_{tot}/MgO ratio during evolution, ascribed to intense spinel crystallization at constant fO_2 conditions (very high for FS and Mt. Spagnolo, more reduced for 2013 magma, crystallizing magnetite).

Fig. 11 – Pressure-related evolution of S (a) and Cl (b) in melt inclusions from the studied eruptions. Entrapment pressures are inferred from the dissolved H_2O and CO_2 contents using the

model of Iacono-Marziano et al. (2012). Data for 2002/2003 South eruptions of Spilliaert et al. (2006a) are also reported.

Table 1 - Whole rock compositions

	Mt. Spagnolo lava	FS scoria	2002/2003 South scoria	2006 scoria	2008/2009 bomb	2013 lava
SiO_2	48.37	46.46	46.93	48.02	47.50	48.29
TiO_2	1.54	0.84	1.86	1.75	1.70	1.75
Al_2O_3	15.09	9.35	16.11	17.25	17.30	17.62
Fe_2O_3	10.42	10.29	12.20	11.18	10.80	11.02
MnO	0.17	0.17	0.20	0.19	0.18	0.19
MgO	7.31	17.90	6.12	4.96	4.90	4.69
CaO	11.69	11.46	11.58	10.10	10.00	9.88
Na_2O	3.45	1.25	2.98	3.74	3.80	3.74
K_2O	1.40	0.59	1.90	2.18	2.10	2.22
P_2O_5	0.63	0.22	0.52	0.62	0.60	0.61
Cr_2O_3	0.04	0.19	0.02	b.d.l.	b.d.l.	0.03
LOI	0.06	1.86	-0.37	-0.29	0.24	-0.43
Total	100.2	100.6	100.0	99.7	99.1	99.6
Cl	0.16	0.08	0.12	0.11	0.077	0.12
S	0.01	b.d.l.	0.01	0.01	0.01	b.d.l.
Mg#	58.16	77.51	49.85	46.78	47.34	45.75
CaO/Al_2O_3	0.77	1.23	0.72	0.59	0.58	0.56

Major elements, chlorine, and sulfur contents of the studied rocks (expressed in wt.%).

LOI = loss on ignition; Mg# = 100 x $Mg/(Mg+Fe_{tot})$; b.d.l. = below detection limit.

Table 2 - Compositions of melt inclusions, embayments and matrix glasses

sample name	Fo	SiO_2	TiO_2	Al_2O_3	FeO	MnO	MgO	CaO	Na_2O	K_2O	Cr_2O_3	NiO	P_2O_5	tot	Mg#	CaO/ Al_2O_3	PEC %	H_2O (SIMS) wt.%	H_2O (FTIR) wt. %	CO_2 (SIMS) ppm	CO_2 (FTIR) ppm	S (EMP) ppm	S (SIMS) ppm	Cl ppm	P (MPa)	Depth (km)	V_B/V_{MI}
Spa-1a	87.8	42.01 (±0.92)	1.59 (±0.06)	18.40 (±0.40)	7.94(± 0.50)	0.17 (±0.04)	8.29 (±0.19)	8.28 (±0.58)	5.51 (±0.40)	1.96 (±0.06)	n.d.	n.d.	0.88 (±0.20)	95.03	65.05	0.45	14.4	0.24		185 (±9)		**3539** (±141)	3190 (±118)	4104 (±331)	12.5	0.48	0.011
Spa -1b	87.8	43.10	1.75	14.38	6.64	0.24	6.93	13.15	4.07	1.46	n.d.	n.d.	0.58	92.30	65.04	0.91	13.8	0.10 (±0.01)				3140		3090			0.06
Spa-3	82.3	47.56 (±0.56)	1.45 (±0.12)	16.37 (±0.16)	7.54 (±0.80)	b.d.l.	5.10 (±0.31)	10.21 (±1.03)	4.64 (±0.06)	2.16 (±0.04)	n.d.	n.d.	0.55	95.58	54.66	0.62	8.3	0.05 (±0.01)		410 (±17)		**1935** (±35)	1466 (±281)	2370 (±14)	39.5	1.52	0.05
Spa-3n	82.3	46.93 (±0.04)	1.51 (±0.15)	15.90 (±0.01)	9.41 (±0.75)	0.17 (±0.08)	6.39 (±0.20)	9.37 (±0.13)	4.24 (±0.02)	1.92 (±0.06)	n.d.	n.d.	0.60 (±0.12)	96.44	54.76	0.59	11.0		0.16 (±0.07)		b.d.l.	1515 (±49)		1820 (±156)	5.9 [a]	0.23	0.16
Spa -4n	86.9	45.30 (±1.34)	1.52 (±0.16)	16.81 (±0.40)	6.86 (±0.04)	0.08 (±0.07)	6.60 (±0.15)	12.59 (±0.08)	4.58 (±0.04)	1.43 (±0.08)	n.d.	n.d.	0.49 (±0.02)	96.26	63.17	0.75	12.3	0.21				2745 (±176)		2840 (±254)			
Spa-5	86.1	44.09 (±0.04)	1.45 (±0.10)	15.24 (±0.25)	8.65 (±0.45)	0.20 (±0.16)	7.88 (±0.27)	14.46 (±0.25)	3.60 (±0.12)	1.27 (±0.09)	n.d.	n.d.	0.64	97.48	61.89	0.95	14.8	0.16 (±0.01)				**3160** (±446)	3533 (±283)	2907 (±229)			0.01
Spa-5n	86.2	45.38 (±0.29)	1.59 (±0.03)	15.99 (±0.44)	7.51 (±0.63)	0.12 (±0.09)	7.30 (±0.83)	13.36 (±0.37)	4.53 (±0.09)	1.28 (±0.10)	n.d.	n.d.	0.53 (±0.09)	97.59	63.41	0.84	10.7	0.28				3410 (±240)		3405 (±63)			0.15
Spa-6	85.7	44.00	1.62	16.64	6.86	0.08	5.99	13.83	4.29	1.47	0.03	0.01	0.8	95.61	60.88	0.83	11.2	0.19		267 (±30)		2750 (±176)		2970 (±254)	21.4	0.83	0.04
Spa-7	85.3	50.19 (±0.17)	1.89 (±0.18)	17.91 (±0.05)	6.23 (±0.32)	0.14 (±0.04)	5.26 (±0.20)	10.96 (±0.37)	4.29 (±0.16)	1.89 (±0.06)	n.d.	n.d.	0.65 (±0.10)	99.41	60.08	0.61	9.7	0		626 (±162)		857 (±320)		1523 (±370)	76.9	2.96	0.03
Spa-7n	87.5	51.33 (±0.17)	1.33 (±0.12)	16.92 (±0.02)	5.13 (±0.24)	0.08 (±0.03)	5.24 (±0.03)	9.95 (±0.05)	5.54 (±0.06)	2.17 (±0.24)	n.d.	n.d.	0.36 (±0.16)	98.05	64.55	0.59	8.6	0.11		1279 (±16)		3410 (±240)		3405 (±63)	109.3	4.21	0.04
Spa-9	85.7	44.04 (±0.49)	1.75 (±0.04)	16.64 (±0.37)	7.14 (±0.36)	0.09 (±0.02)	6.03 (±0.09)	13.50 (±0.42)	4.08 (±0.17)	1.49 (±0.03)	0.058 (±0.03)	b.d.l.	0.69 (±0.02)	95.51	60.09	0.81	11.7					2985 (±219)		2985 (±276)			0.04
Spa-11	85.0	44.57	1.76	17.07	7.17	0.13	5.93	12.6	4.2	1.62	n.d.	n.d.	0.95	96.00	59.58	0.74	11.3					2710		2760			
Spa- D	86.8	46.22	1.72	13.51	7.76	0.19	7.41	7.74	5.85	3.10	n.d.	n.d.	0.79	94.29	62.99	0.57	15.1		0.07 (±0.01)		b.d.l.	310		1980	2.9 [a]	0.11	
Spa- L	86.5	44.05	1.57	19.07	6.72	0.23	6.27	6.41	5.38	2.91	n.d.	n.d.	1.51	94.12	62.45	0.34	11.9		0.1		b.d.l.	1830		2090	3.5 [a]	0.13	
Spa- O1	84.1	46.49	1.89	13.79	9.54	0.11	7.37	8.70	5.31	2.20	n.d.	n.d.	0.67	96.07	57.93	0.63	16.6		0.12		b.d.l.	280		2700	3.9 [a]	0.15	0.02
Spa-T1	87.4	43.34 (±0.20)	1.51 (±0.07)	14.22 (±0.37)	7.98 (±0.07)	0.21 (±0.05)	8.09 (±0.07)	14.20 (±0.07)	3.97 (±0.06)	0.87 (±0.13)	n.d.	n.d.	0.58 (±0.03)	94.97	64.38	1.00	13.2	0.26		2336 (±63)		**3570** (±14)	3886 (±75)	3785 (±21)	153.9	5.9	0.02
Spa-T2	87.4	45.07	1.55	14.42	7.37	0.01	7.50	14.84	4.70	1.01	n.d.	n.d.	0.62	97.09	64.46	1.03	11.3	0.26		2674 (±76)		3770		3140	143.8	5.54	0.01

Spa-T3	87.4	44.63	1.41	14.21	7.55	0.18	7.65	15.08	4.34	1.04	n.d.	n.d.	0.61	96.70	64.36	1.06	12.3	0.24		2107 (±48)		**4150**	3906 (±58)	3850	119.6	4.60	
Spa-T4	87.4	44.78 (±0.95)	1.69 (±0.13)	14.63 (±0.06)	8.65 (±0.46)	b.d.l.	8.77 (±0.22)	13.04 (±0.43)	4.29 (±0.29)	1.20 (±0.05)	n.d.	n.d.	0.33 (±0.21)	97.43	64.38	0.89	15.6	0.24		1025 (±27)		**2863** (±231)	3000 (±66)	3220 (±139)	74.9	2.89	
Spa-U1	88.2	48.02 (±0.38)	2.13 (±0.14)	15.57 (±0.52)	6.55 (±0.40)	b.d.l.	7.14 (±0.13)	5.93 (±1.05)	5.65 (±0.59)	2.51 (±0.09)	n.d.	n.d.	0.75 (±0.02)	94.37	66.02	0.38	15.5	0.12		583 (±29)		b.d.l.	**184 (±4)**	2655 (±304)	44.9	1.73	
Spa-U2	88.2	47.93	2.18	15.65	6.55	0.12	7.14	5.93	5.65	2.51	n.d.	n.d.	0.75	94.41	66.02	0.38	15.5	0.15		635 (±21)		b.d.l.	**258 (±6)**	2570	48.6	1.87	
Spa-U3	88.2	47.65 (±0.45)	2.10 (±0.17)	14.47 (±0.33)	7.58 (±0.34)	b.d.l.	8.26 (±0.02)	7.34 (±0.13)	4.91 (±0.78)	3.06 (±0.03)	n.d.	n.d.	0.73 (±0.02)	96.24	66.01	0.51	18.6					b.d.l.		3163 (±476)			
Spa-U4	88.3	47.92	1.90	14.94	7.23	0.16	7.89	8.30	5.45	2.35	n.d.	n.d.	0.71	96.85	66.05	0.56	16.7					b.d.l.		3040			
FS-00	89.5	48.99 (±0.32)	0.85 (±0.17)	10.23 (±0.10)	8.62 (±0.43)	0.09 (±0.05)	10.76 (±0.12)	13.16 (±0.19)	1.89 (±0.09)	0.82 (±0.07)	0.09 (±0.01)	0.05 (±0.01)	n.d.	95.55	68.99	1.29	4.0	**3.70 (±0.05)**	3.11	882 (±72)	b.d.l.	**1100** (±179)	1281 (±36)	1633 (±151)	157.9	6.08	0.2
FS-01	89.5	47.29 (±0.37)	0.99 (±0.11)	9.89 (±0.47)	8.59 (±0.36)	0.21 (±0.07)	10.66 (±0.84)	13.13 (±0.28)	1.50 (±0.07)	0.91 (±0.11)	0.06 (±0.01)	0.04 (±0.01)	n.d.	93.27	68.87	1.33	12.6	1.39 (±0.31)				2178 (±222)		1767 (±206)			0.08
FS-03b	89.4	46.69 (±0.38)	1.08 (±0.07)	9.16 (±0.18)	8.46 (±0.20	0.19 (±0.11)	10.37 (±0.35)	13.66 (±0.21)	1.58 (±0.06)	0.71 (±0.07)	0.09 (±0.01)	0.02 (±0.01)	n.d.	92.01	68.60	1.49	12.0	3.10 (±0.41)				1625 (±263)		975 (±96)			
FS-03c	89.5	47.19 (±0.32)	1.16 (±0.07)	9.54 (±0.33)	8.55 (±0.23)	0.16 (±0.07)	10.48 (±0.51)	13.40 (±0.37)	1.70 (±0.04)	0.75 (±0.06)	0.07 (±0.01)	0.05 (±0.01)	n.d.	93.05	68.60	1.40	8.2	4.72 (±0.07)		4635 (±434)		**1533** (±225)	1461 (±158)	783 (±172)	406.3	15.64	0.006
FS-05	89.2	46.58 (±0.37)	1.19 (±0.18)	8.91 (±0.30)	9.17 (±0.38)	b.d.l.	10.99 (±0.84)	12.64 (±0.21)	1.55 (±0.03)	1.17 (±0.07)	0.06 (±0.01)	0.05 (±0.01)	n.d.	92.31	68.12	1.42	14.7	4.88 (±0.02)		4903 (±575)		**1120** (±110)	1133	1500 (±71)	396.6	15.27	0,00
FS-06b	90.1	47.10 (±0.26)	0.93 (±0.14)	9.59 (±0.08)	8.61 (±0.38)	0.14 (±0.08)	11.45 (±0.53)	13.14 (±0.37)	1.63 (±0.07)	0.87 (±0.06)	0.06 (±0.01)	0.03 (±0.01)	n.d.	93.55	70.33	1.37	6.9	3.36		3294 (±283)		**1600** (±82)	1510 (±28)	1329 (±125)	322.1	12.4	0,00
FS-06c	90.1	46.35 (±0.12)	0.86 (±0.04)	9.19 (±0.05)	8.62 (±0.39)	0.17 (±0.09)	11.47 (±0.60)	13.68 (±0.34)	1.61 (±0.09)	0.74 (±0.06)	b.d.l.	b.d.l.	n.d.	92.74	70.34	1.49	14.7	2.62 (±0.03)		1599 (±71)		2650 (±154)		1450 (±71)	179.6	6.91	0.06
FS-06n	90.1	46.02	0.83	9.77	8.85	0.22	12.38	12.21	1.43	0.83	0.047 (±0.01)	0.302 (±0.01)	0.22 (±0.10)	93.11	71.38	1.25	16.2	1.74 (±0.05)		1560 (±43)		**1300**	1026 (±11)	1120	200.5	7.72	0.02
FS-07	89.7	47.85 (±0.19)	0.94 (±0.06)	9.31 (±0.06)	8.54 (±0.48)	0.13 (±0.07)	10.32 (±0.18)	13.71 (±0.26)	1.44 (±0.08)	0.89 (±0.08)	0.07 (±0.01)	0.02 (±0.01)	n.d.	93.22	68.30	1.47	10.0	3.85 (±0.08)		34 (±3)		**2180** (±164)	2118	1640 (±152)	457.5	17.62	0.05
FS-08b	89.0	47.30 (±0.26)	1.18 (±0.06)	9.96 (±0.21)	8.70 (±0.25)	0.12 (±0.07)	10.29 (±0.53)	12.38 (±0.32)	1.88 (±0.07)	1.04 (±0.05)	0.07 (±0.01)	0.02 (±0.01)	n.d.	92.94	67.83	1.24	8.4	4.18 (±0.10)		5564 (±814)		**1689** (±169)	2006 (±42)	1189 (±127)	477.3	18.38	0.02
FS-08c	89.2	46.49 (±0.37)	1.09 (±0.04)	9.30 (±0.11)	8.64 (±0.22)	0.16 (±0.11)	10.44 (±0.19)	12.92 (±0.38)	1.71 (±0.09)	1.01 (±0.08)	0.08 (±0.01)	0.02 (±0.01)	n.d.	91.86	68.29	1.39	13.3	5.57 (±0.08)		3706 (±372)		**1700** (±141)	1660 (±58)	1050 (±173)	341.5	13.15	0.06
FS-09 n	90.7	46.07 (±0.26)	1.02 (±0.07)	9.93 (±0.05)	7.82 (±0.15)	0.15 (±0.08)	11.16 (±0.31)	13.36 (±0.48)	1.61 (±0.08)	0.88 (±0.03)	b.d.l.	b.d.l.	0.30 (±0.20)	92.3	71.78	1.35	5.5		1.59	n.d.	1116	2390 (±332)		2033 (±152)	144.8	5.57	0.03

FS-09	90.0	47.61 (±0.01)	1.10 (±0.03)	9.77 (±0.25)	8.02 (±0.12)	0.21 (±0.05)	10.53 (±0.24)	14.74 (±0.44)	1.71 (±0.05)	0.90 (±0.03)	0.09 (±0.01)	0.05 (±0.01)	n.d.	94.73	70.06	1.51	14.8	3.88 (±0.06)		5694 (±493)		2600 (±141)		1900 (±283)	426.2	16.41	
FS-10b	90.3	46.28 (±0.42)	0.89 (±0.06)	9.65 (±0.21)	8.75 (±0.21)	0.17 (±0.11)	11.81 (±0.67)	12.97 (±0.33)	1.54 (±0.05)	0.78 (±0.09)	0.07 (±0.01)	0.04	n.d.	92.95	70.64	1.34	10.5	5.66 (±0.02)		3170 (±96)		**1575** (±226)	1504 (±50)	1342 (±178)	318.8	12.28	0.03
FS-10c	90.5	44.93 (±0.30)	1.20 (±0.10)	9.88 (±0.51)	8.23 (±0.25)	0.13 (±0.09)	11.42 (±0.78)	13.23 (±0.19)	1.63 (±0.12)	0.58 (±0.08)	0.08 (±0.01)	0.02 (±0.01)	n.d.	91.33	71.21	1.34	19.5	1.84 (±0.23)		1977 (±356)		1400 (±63)		1150 (±55)	223.1	8.59	0.02
FS-11	90.0	47.30 (±0.25)	1.02 (±0.12)	10.20 (±0.15)	8.79 (±0.39)	0.16 (±0.08)	11.50 (±0.26)	11.45 (±0.19)	1.89 (±0.07)	1.13 (±0.06)	b.d.l.	b.d.l.	n.d.	93.44	69.99	1.12	9.5	4.47 (±0.05)		1112 (±143)		**1164** (±186)	1216 (±32)	891 (±114)	186.1	7.17	0.17
FS-12a	89.2	44.87 (±0.40)	0.95 (±0.07)	10.39 (±0.24)	10.26 (±0.24)	0.21 (±0.06)	12.36 (±0.03)	13.34 (±0.11)	1.96 (±0.04)	0.79 (±0.05)	n.d.	n.d.	0.25 (±0.03)	95.38	68.23	1.28	13.8	0.99 (±0.01)		1089 (±30)		**1683** (±130)	1710 (±36)	1310 (±160)	108.8	4.19	0,00
FS-12b	89.2	46.39 (±0.83)	0.87 (±0.07)	10.25 (±0.43)	8.90 (±0.13)	0.23 (±0.10)	10.72 (±0.22)	12.80 (±0.08)	1.49 (±0.17)	0.86 (±0.02)	n.d.	n.d.	0.23 (±0.05)	92.74	68.22	1.25	10.8	3.83 (±0.05)		n.d.		**1805** (±131)	2378 (±150)	1360 (±300)			0.07
FS-13b	89.6	46.46 (±0.43)	1.00 (±0.12)	9.39 (±0.48)	8.69 (±0.30)	0.19 (±0.08)	10.95 (±0.81)	13.74 (±0.21)	1.56 (±0.13)	0.72 (±0.13)	b.d.l.	0.04 (±0.01)	n.d.	92.74	69.19	1.46	15.7	3.89 (±0.33)		5872 (±885)		**2386** (±291)	1874 (±202)	1857 (±79)	452.6	17.43	0.02
FS-13c	89.7	46.38 (±0.33)	0.93 (±0.06)	9.29 (±0.32)	8.77 (±0.43)	0.16 (±0.10)	11.04 (±0.30)	13.85 (±0.13)	1.57 (±0.05)	0.63 (±0.05)	0.08 (±0.01)	0.05 (±0.01)	n.d.	92.75	69.17	1.49	14.9	2.86 (±0.31)		2300 (±402)		2433 (±115)		1933 (±115)	237.2	9.13	0.03
FS-14	89.3	46.6 (±0.15)	1.05 (±0.08)	9.16 (±0.20)	8.93 (±0.23)	b.d.l.	10.89 (±0.34)	12.96 (±0.15)	1.65 (±0.08)	1.03 (±0.05)	n.d.	0.05 (±0.01)	n.d.	92.32	68.49	1.41	9.8	1.51 (±0.27)		1796 (±424)		2100 (±292)		1600 (±158)	209.6	8.07	0.06
FS-21	90.2	44.06 (±0.33)	0.92 (±0.11)	9.82 (±0.27)	8.33 (±0.65)	0.17 (±0.02)	11.14 (±0.69)	13.72 (±0.56)	1.39 (±0.06)	1.02 (±0.03)	0.075 (±0.01)	b.d.l.	0.31 (±0.18)	90.96	70.45	1.40	6.3	5.86 (±0.03)		3808 (±165)		**3473** (±90)	3723 (±111)	3217 (±420)	305.0	11.75	0.03
FS-24	88.6	44.70	1.51	9.44	9.26	0.19	10.52	12.27	1.74	0.81	n.d.	n.d.	0.08	90.52	66.94	1.30	9.7		3.51 (±0.04)		580 (±83)	2420		1700	113.9	4.39	0.14
FS-25	90.6	45.27 (±0.01)	0.78 (±0.06)	9.07 (±0.07)	8.74 (±0.57)	0.23 (±0.12)	12.21 (±0.19)	13.01 (±0.17)	1.58 (±0.02)	0.63 (±0.06)	n.d.	b.d.l.	0.38 (±0.13)	91.90	71.35	1.43	10.5		3.65 (±0.10)		1720 (±186)	2463 (±175)		2380 (±66)	189.2	7.28	0.17
FS-26	90.0	45.47 (±0.60)	1.15 (±0.09)	9.10 (±0.60)	7.92 (±0.47)	b.d.l.	10.38 (±0.70)	13.49 (±0.16)	1.73 (±0.16)	0.71 (±0.60)	n.d.	0.114 (±0.01)	0.63 (±0.02)	90.85	70.03	1.48	16.3	3.73 (±0.03)		2111 (±96)		**3223** (±220)	2640 (±73)	2145 (±231)	230.6	8.88	0.06
FS-28a	90.4	44.31 (±0.54)	0.88 (±0.14)	9.32 (±0.17)	8.42 (±0.09)	b.d.l.	11.49 (±0.22)	13.36 (±0.22)	1.56 (±0.05)	0.65 (±0.01)	0.047 (±0.01)	b.d.l.	0.49 (±0.17)	90.63	70.87	1.43	7.2		4.41 (±0.02)		1567 (±138)	2570 (±226)		2365 (±134)	183.7	7.07	0.05
FS-28b	90.4	45.96 (±0.19)	0.86 (±0.03)	9.46 (±0.05)	8.12 (±0.20)	b.d.l.	11.07 (±0.01)	14.01 (±0.16)	1.58 (±0.07)	0.78 (±0.02)	0.102 (±0.05)	b.d.l.	0.16 (±0.03)	92.22	70.85	1.48	7.9		2.48		1396	1710 (±198)		1285 (±346)	161.5	6.22	0.15
FS-B	90.5	43.97 (±0.39)	0.86 (±0.01)	9.20 (±0.08)	8.08 (±0.10)	0.10 (±0.01)	11.27 (±0.36)	13.28 (±0.30)	1.43 (±0.33)	0.87 (±0.01)	0.06 (±0.04)	b.d.l.	0.16 (±0.10)	89.43	71.32	1.44	5.4		4.65		2853	2235 (±190)		1800 (±98)	261.3	10.06	0.03
FS-D	90.6	44.66 (±0.25)	1.08 (±0.08)	10.26 (±0.22)	7.91 (±0.21)	0.13 (±0.06)	11.12 (±0.07)	12.55 (±0.01)	1.86 (±0.02)	0.84 (±0.01)	0.12 (±0.08)	b.d.l.	0.41 (±0.03)	90.94	71.48	1.22	3.9		4.28		2687	2235 (±205)		1570 (±42)	270.2	10.4	0.03
FS-Xa	89.9	44.09 (±0.56)	0.99 (±0.11)	10.28 (±0.27)	7.76 (±0.17)	0.17 (±0.04)	10.10 (±0.67)	13.80 (±0.25)	1.74 (±0.11)	1.09 (±0.11)	0.028 (±0.01)	b.d.l.	0.25 (±0.07)	90.30	69.88	1.34	4.5		4.50 (±0.15)		2482 (±123)	2190 (±160)		1410 (±216)	239.7	9.23	0.09
FS-Z	91.0	43.7 (±0.39)	1.11 (±0.06)	8.80 (±0.11)	8.21 (±0.58)	0.10 (±0.01)	12.15 (±0.05)	12.47 (±0.01)	1.75 (±0.07)	0.87 (±0.02)	0.04 (±0.06)	b.d.l.	0.35 (±0.12)	89.55	72.51	1.42	8.3		3.56		2645	2310 (±212)		1965 (±430)	230.7	8.88	0.13

2002/3S-1	75.2	46.95 (±0.87)	1.25 (±0.14)	16.90 (±0.23)	10.67 (±0.35)	0.35 (±0.12)	4.72 (±0.08)	7.08 (±0.10)	4.34 (±0.17)	1.96 (±0.10)	b.d.l.	b.d.l.	0.8	95.02	44.09	0.42	1.7	1.97 (±0.14)		2470 (±618)		**1513** (±61)	2025 (±27)	2383 (±223)	238.7	9.19	
2002/3S-3	75.7	45.53 (±0.20)	1.50 (±0.07)	16.30 (±0.08)	10.29 (±0.51)	0.19 (±0.13)	4.95 (±0.10)	10.69 (±0.27)	3.18 (±0.07)	2.03 (±0.10)	n.d.	n.d.	0.44	95.1	46.16	0.66	0	2.12 (±0.05)		2262 (±527)		**1964** (±187)	1268 (±26)	1382 (±143)	254.3	9.79	0.04
2002/3S-5	81.8	42.83 (±0.95)	1.97 (±0.02)	15.10 (±0.16)	10.24 (±0.09)	0.12 (±0.01)	6.71 (±0.02)	12.27 (±0.01)	2.69 (±0.21)	1.68 (±0.06)	n.d.	n.d.	0.34 (±0.03)	93.95	53.88	0.81	10.1	2.80 (±0.07)				2885 (±247)		1330 (±354)			0.02
2002/3S-6	77.8	48.68 (±0.17)	1.59 (±0.07)	15.55 (±0.34)	9.32 (±0.47)	0.23 (±0.16)	4.75 (±0.16)	6.49 (±0.07)	4.02 (±0.17)	2.12 (±0.11)	n.d.	n.d.	0.69	93.44	47.6	0.42	1.6	2.16 (±0.04)		1810 (±201)		**603** (±97)	435 (±17)	2343 (±129)	225.0	8.66	0.01
2002/3S-7	75.0	44.87 (±0.38)	1.84 (±0.05)	15.88 (±0.09)	11.12 (±0.13)	0.22 (±0.12)	4.85 (±0.12)	6.71 (±0.03)	4.06 (±0.12)	4.74 (±0.03)	n.d.	n.d.	0.78	95.07	43.74	0.42	6.9					860 (±141)		4670 (±890)			0.06
2002/3S-9	75.4	50.49 (±1.79)	1.93 (±0.28)	17.39 (±0.76)	8.15 (±1.14)	0.09 (±0.07)	3.65 (±0.59)	7.59 (±0.68)	4.01 (±0.24)	2.82 (±0.27)	n.d.	n.d.	0.98	97.1	44.39	0.44	0.2					855 (±35)		3170 (±269)			
2002/3S-10	73.9	50.09 (±0.69)	1.56 (±0.06)	15.79 (±0.13)	10.21 (±0.24)	0.20 (±0.13)	4.22 (±0.15)	6.06 (±0.10)	4.32 (±0.07)	2.35 (±0.11)	n.d.	n.d.	0.70	95.5	42.42	0.38	1.2	2.14 (±0.03)		2122 (±182)		**878** (±100)	777 (±21)	2208 (±216)	238.8	9.19	
2002/3S-11b	82.9	42.94	2.11	17.15	8.56	0.25	6.06	13.17	3.32	2.27	n.d.	n.d.	0.50	96.33	55.79	0.77	8.2					1190		1700			0.09
2002/3S-13	82.7	42.92 (±0.80)	1.74 (±0.01)	15.53 (±0.09)	9.69	0.16 (±0.07)	6.74 (±0.08)	11.65	2.86 (±0.07)	1.98 (±0.09)	n.d.	n.d.	0.37	93.64	55.35	0.75	6.2			1520 (±195)		2445 (±49)		1505 (±35)			0.05
2002/3S-16a	73.7	46.48 (±1.39)	1.56 (±0.11)	15.26 (±0.50)	11.54 (±0.57)	b.d.l.	4.38 (±0.01)	7.82 (±0.21)	5.39 (±0.22)	1.69 (±0.06)	n.d.	n.d.	1.04 (±0.18)	95.19	40.35	0.51	1.9					1260 (±98)		3250 (±74)			0.04
2002/3S-16b	73.7	45.46	1.61	14.45	11.72	0.22	4.85	6.43	6.56	2.03	n.d.	n.d.	0.72	94.04	42.44	0.44	0					1300		2970			0.08
2002/3S-23	82.6	43.92 (±0.60)	1.57 (±0.15)	15.50 (±0.20)	9.79 (±0.38)	0.10 (±0.14)	6.78 (±0.04)	10.70 (±0.03)	3.57 (±0.03)	1.96 (±0.02)	n.d.	n.d.	0.35 (±0.18)	94.24	55.25	0.69	3.7	2.33 (±0.01)		963 (±16)		**3005** (±50)	3068 (±12)	1545 (±177)	122.9	4.73	0.03
2002/3S-24	80.3	44.72 (±0.23)	1.62 (±0.14)	15.00 (±0.03)	11.83 (±0.25)	0.19 (±0.03)	7.01 (±0.11)	8.09 (±0.11)	4.12 (±0.11)	2.74 (±0.04)	n.d.	n.d.	0.54 (±0.03)	95.86	51.37	0.54	9.8	0.3		119 (±3)		**620** (±28)	896 (±15)	1995 (±49)	11.3	0.43	
2002/3S-26	72.6	48.34 (±0.86)	1.91 (±0.02)	15.28 (±0.44)	9.37 (±0.128)	b.d.l.	3.61 (±0.06)	6.24 (±0.20)	4.91 (±0.22)	3.51 (±0.19)	b.d.l.	n.d.	0.83 (±0.10)	94.13	40.72	0.41	1.7		0.36 (±0.02)		b.d.l.	225 (±78)		1560 (±184)	6.9	0.27	0.04
2002/3S-29a	69.6	51.92	1.01	14.5	10.20	0.25	3.87	5.88	4.93	2.94	n.d.	n.d.	0.80	96.3	40.35	0.41	2.3	1.00		348 (±10)		b.d.l.	**237** (±2)	2830	50	1.93	0.01
2002/3S-29b	69.6	50.47 (±0.10)	1.20 (±0.01)	13.56 (±0.03)	11.64 (±0.05)	b.d.l.	4.13 (±0.11)	5.40 (±0.07)	5.39 (±0.19)	3.21 (±0.01)	n.d.	n.d.	0.79 (±0.01)	95.91	38.74	0.40	2.6	0.13		236 (±5)		490 (±113)		2020 (±14)	20.1	0.77	
2002/3S-31	69.8	49.43	1.09	17.05	8.40	0.18	2.83	9.44	5.4	2.01	n.d.	n.d.	0.70	96.53	37.52	0.55	5.3	0.70 (±0.01)				**700**	513 (±37)	1500			0.13
2002/3S-32	72.9	46.31 (±1.52)	1.88 (±0.18)	14.07 (±0.25)	9.21 (±0.53)	b.d.l.	3.75 (±0.08)	6.37 (±0.20)	4.24 (±0.30)	2.83 (±0.05)	b.d.l.	0.22 (±0.03)	0.82 (±0.11)	89.59	42.06	0.45	0		1.30		b.d.l.	128 (±92)		2043 (±161)	27.4 [a]	1.05	
2002/3S-33a	80.7	43.00	1.71	15.69	9.15	0.21	5.58	11.11	3.47	2.08	n.d.	n.d.	0.59	92.59	52.09	0.71	2.1		1.33		353	2687		1697	52.4	2.02	0.02

		(±0.20)	(±0.10)	(±0.11)	(±0.45)	(±0.06)	(±0.11)	(±0.18)	(±0.08)	(±0.07)			(±0.07)									(±172)		(±155)			
2002/3S-33b	80.7	42.71 (±0.27)	1.56 (±0.07)	15.45 (±0.33)	10.30 (±0.46)	b.d.l.	6.27 (±0.16)	11.22 (±0.19)	3.27 (±0.11)	1.97 (±0.06)	n.d.	n.d.	0.55 (±0.14)	93.3	52.04	0.73	5.3		2.0 (±0.14)		181	2643 (±207)		2380 (±104)	54.1	2.08	0.05
2002/3S-24 emb	80.3	46.68 (±0.50)	2.19 (±0.15)	14.91 (±0.60)	10.84 (±0.30)	0.22 (±0.03)	3.45 (±0.20)	7.90 (±0.07)	4.72 (±0.11)	3.46 (±0.19)	n.d.	n.d.	0.63 (±0.15)	95	36.2	0.53		0.17		n.d.		**620** (±367)	595 (±8)	2410 (±70)	0.5 [a]	0	
2002/3S-6 gm		43.40 (±2.68)	1.96 (±0.11)	13.84 (±0.32)	10.47 (±0.41)	b.d.l.	3.17 (±0.24)	6.98 (±0.43)	3.85 (±0.30)	3.31 (±0.08)	n.d.	n.d.	0.78 (±0.24)	87.86	35.05	0.50						b.d.l.		b.d.l.			
2002/3S-10 gm		48.51 (±0.80)	1.99 (±0.02)	16.14 (±0.29)	10.33 (±0.59)	0.27 (±0.11)	3.28 (±0.10)	7.79 (±0.10)	3.78 (±0.05)	3.48 (±0.18)	n.d.	n.d.	0.95 (±0.05)	96.52	36.14	0.48						b.d.l.		b.d.l.			
2002/3S-13 gm		50.88 (±0.57)	2.00 (±0.08)	16.29 (±0.11)	10.77 (±0.11)	0.13 (±0.12)	3.21 (±0.15)	7.78 (±0.05)	3.72 (±0.12)	3.62 (±0.15)	n.d.	n.d.	0.81 (±0.14)	99.21	34.7	0.48						b.d.l.		b.d.l.			
2002/3S-23 gm		49.49	2.12	14.61	11.78	0.21	2.92	7.02	4.96	3.70	n.d.	n.d.	0.91	97.73	30.66	0.48						b.d.l.		2100			
2002/3S-32 gm		47.24 (±2.14)	1.88 (±0.21)	15.32 (±0.54)	9.97 (±0.60)	0.27 (±0.09)	3.60 (±0.10)	7.95 (±0.13)	4.65 (±0.05)	3.15 (±0.09)	n.d.	n.d.	0.76	95.09	39.25	0.52								1330			
2006-1 a	69.6	49.57 (±0.17)	1.37 (±0.21)	16.00 (±0.13)	11.07 (±0.24)	0.23 (±0.10)	3.70 (±0.04)	6.81 (±0.09)	3.84 (±0.73)	2.61 (±0.14)	n.d.	n.d.	0.70 (±0.12)	95.90	37.34	0.43	0.8					310 (±210)		2930 (±250)			
2006-1 b	70.4	49.03 (±0.46)	1.54 (±0.08)	15.73 (±0.23)	11.14 (±0.05)	0.21 (±0.04)	3.85 (±0.02)	6.95 (±0.11)	3.73 (±0.84)	2.55 (±0.11)	n.d.	n.d.	0.66 (±0.07)	95.39	38.12	0.44	1.2					910 (±100)		3320 (±180)			
2006-4	70.5	49.42 (±0.01)	1.60 (±0.08)	15.66 (±0.06)	10.20 (±0.04)	b.d.l.	3.67 (±0.03)	7.75 (±0.08)	4.66	2.26 (±0.01)	n.d.	n.d.	0.83 (±0.28)	96.98	39.08	0.49	0		0.92 (±0.02)		470	380 (±28)		2390 (±226)	62.4	2.4	
2006-7	81.1	42.25 (±0.31)	1.33 (±0.26)	15.71 (±0.08)	10.53 (±0.11)	0.09 (±0.08)	6.58 (±0.01)	11.10 (±0.14)	2.93 (±0.07)	1.73 (±0.10)	n.d.	n.d.	0.37 (±0.10)	92.62	52.69	0.71	3.4	**3.16 (±0.14)**	2.19 (±0.08)	**678 (±77)**	1193 (±151)	**2573** (±159)	2664 (±101)	1493 (±400)	130.6	5.03	0.01
2006-12	78.8	45.02 (±0.08)	1.76 (±0.15)	16.79 (±0.02)	10.11 (±0.22)	0.16 (±0.03)	5.13 (±0.02)	10.70 (±0.30)	3.24 (±0.10)	2.07 (±0.12)	n.d.	n.d.	0.57 (±0.11)	95.55	47.49	0.64	0.6	2.60 (±0.11)		598 (±75)		**2683**	3475 (±179)	1693	126.3	4.86	0.01
2006-B3a	77.2	46.75 (±0.21)	1.52 (±0.06)	16.03 (±0.10)	10.44 (±0.24)	0.07 (±0.05)	5.14 (±0.15)	8.52 (±0.18)	4.08 (±0.72)	1.66 (±0.03)	n.d.	n.d.	0.57 (±0.09)	94.78	46.74	0.53	1.7	**2.38 (±0.08)**	1.82	**450** (±49)	b.d.l.	**1903** (±127)	2384 (±116)	1910 (±284)	106.9	4.12	
2006-B3b	77.2	46.86 (±0.29)	1.70 (±0.17)	15.78 (±0.18)	9.93 (±0.30)	0.24 (±0.13)	4.89 (±0.18)	8.45 (±0.06)	3.61 (±0.94)	1.62 (±0.05)	n.d.	n.d.	0.52 (±0.11)	93.60	46.75	0.54	0.7	2.66 (±0.11)		618 (±78)		1800 (±67)		1984 (±123)	145.5	5.6	
2006-B5a	80.2	44.46 (±0.44)	1.52 (±0.04)	15.61 (±0.29)	10.64 (±0.22)	0.09 (±0.04)	6.30 (±0.09)	10.43 (±0.08)	3.73 (±0.07)	2.09	0.52	n.d.	0.52 (±0.06)	95.39	51.35	0.67	4.2	1.32 (±0.18)		1673 (±275)		**2570**	2515 (±436)	1437	153.2	5.9	0.02
2006-B5c	80.2	49.40 (±0.32)	1.78 (±0.15)	14.44 (±0.11)	10.21 (±0.16)	0.26 (±0.16)	6.05 (±0.07)	7.37 (±0.14)	3.98 (±1.16)	3.27 (±0.15)	n.d.	n.d.	0.66	97.42	51.37	0.51	7.8	0.34		192 (±28)		b.d.l.	**161** (±7)	1913 (±156)	22.4	0.86	
2006-B5d	80.2	45.01 (±0.40)	1.67 (±0.22)	15.19 (±0.18)	11.70 (±0.46)	0.31 (±0.07)	6.93 (±0.02)	8.59 (±0.07)	4.54 (±0.30)	2.62 (±0.06)	0.07 (±0.05)	n.d.	0.55 (±0.10)	97.11	51.36	0.57	9.2	0.80				**720** (±104)	1288 (±48)	1827 (±263)			0.01

2006-B5n	80.2	43.60	1.58	17.03	10.26	0.05	6.08	11.22	3.83	2.23	n.d.	n.d.	0.55	96.43	51.37	0.66	4.1					**3410**		3405			0.04
2006-B6	76.2	46.71 (±0.41)	1.48 (±0.18)	17.15 (±0.18)	9.56 (±0.24)	0.10 (±0.04)	4.46 (±0.05)	8.93 (±0.10)	5.11 (±0.18)	2.98 (±0.11)	n.d.	n.d.	0.52 (±0.10)	97.00	45.4	0.52	1.2	0.81 (±0.02)		554 (±59)		**773** (±114)	1166 (±47)	1750 (±213)	48.9	1,88	
2006-B8a	75.4	49.40 (±0.08)	1.71 (±0.08)	15.81 (±0.17)	9.82 (±0.34)	0.18 (±0.06)	4.39 (±0.32)	6.01 (±0.11)	4.15 (±0.11)	2.81 (±0.10)	n.d.	n.d.	0.58 (±0.05)	94.86	44.35	0.38	0.7	2.32 (±0.07)		441 (±43)		**907** (±58)	1455 (±68)	1967 (±55)	112.9	4.35	
2006-B8b	75.4	48.83 (±0.34)	1.56 (±0.06)	14.64 (±0.52)	9.82 (±0.13)	0.21 (±0.01)	4.37 (±0.01)	8.45 (±0.11)	3.88 (±0.10)	2.07	n.d.	n.d.	0.86 (±0.19)	94.70	44.23	0.58	0	2.05 (±0.07)		817 (±73)		**905** (±276)	1622 (±65)	1780 (±226)	140.1	5.39	
2006-C7a	70.2	51.15 (±0.10)	1.51 (±0.15)	15.01 (±0.21)	9.96 (±0.34)	b.d.l.	3.71 (±0.07)	6.83 (±0.07)	4.9 (±0.15)	2.48 (±0.05)	n.d.	n.d.	0.60 (±0.11)	96.22	39.89	0.46	0					b.d.l.		1730 (±57)			
2006-C7b	70.2	49.73 (±0.51)	1.92 (±0.17)	14.54 (±0.10)	9.80 (±0.35)	0.26 (±0.15)	3.75 (±0.08)	7.37 (±0.17)	4.66 (±0.09)	2.26 (±0.03)	n.d.	n.d.	0.75 (±0.05)	95.04	40.54	0.51	0					**300** (±226)		1995 (±120)			
2006-C8	73.6	48.68 (±0.32)	1.96 (±0.07)	16.24 (±0.27)	10.97 (±0.04)	0.14 (±0.11)	4.46 (±0.13)	6.24 (±0.02)	4.96 (±0.71)	2.63 (±0.06)	n.d.	n.d.	0.87 (±0.13)	97.15	42.02	0.38	3.4					**663** (±280)		2780 (±427)			
2006-C11	72.0	49.65 (±0.37)	1.77 (±0.16)	15.12 (±0.29)	10.04 (±0.56)	b.d.l.	3.96 (±0.04)	7.33 (±0.19)	4.47 (±1.14)	2.52 (±0.05)	n.d.	n.d.	0.67 (±0.07)	95.73	41.3	0.49	0					**270** (±168)		1570 (±79)			
2006-D9	70.1	49.66 (±0.37)	2.01 (±0.02)	14.48 (±0.12)	9.75 (±0.37)	0.24 (±0.07)	3.52 (±0.10)	7.17 (±0.17)	4.12 (±0.93)	3.26 (±0.19)	n.d.	n.d.	1.06 (±0.09)	95.27	39.11	0.49	0	0.71 (±0.03)				b.d.l.	**123 (±8)**	1840 (±71)			
2006-E2a	70.2	50.13 (±0.37)	1.85 (±0.09)	15.55 (±0.08)	10.48 (±0.18)	0.23 (±0.15)	3.53 (±0.11)	7.32 (±0.06)	2.72 (±1.23)	2.65 (±0.12)	n.d.	n.d.	0.57 (±0.06)	95.03	37.52	0.47	0	0.87 (±0.10)		500 (±79)		**480** (±110)	444 (±65)	2130 (±50)	88.9	3.42	
2006-E2b	70.2	48.41 (±0.19)	1.91 (±0.06)	14.50 (±0.21)	11.77 (±0.21)	0.32 (±0.12)	4.04 (±0.15)	7.33 (±0.13)	4.06 (±0.16)	2.43 (±0.04)	n.d.	n.d.	0.49 (±0.11)	95.26	37.96	0.51	3.3	1.35 (±0.08)		300 (±40)		**895** (±219)	1004 (±88)	3270 (±156)	57.4	2.24	
2006-F5a	78.0	46.22 (±0.38)	1.65 (±0.13)	14.94 (±0.08)	10.70 (±0.54)	0.13 (±0.08)	5.50 (±0.05)	8.96 (±0.02)	4.64 (±0.06)	2.65 (±0.10)	n.d.	n.d.	0.54	95.93	47.82	0.60	4.4					1387 (±384)		1750 (±613)			
2006-F5b	78.0	47.59	1.67	14.38	10.71	0.21	5.52	7.49	4.82	3.21	n.d.	n.d.	0.95	96.55	47.88	0.52	6.2					520		2170			
2006-F5c	78.0	42.95 (±0.05)	1.63 (±0.13)	16.31 (±0.08)	11.10 (±0.21)	0.24 (±0.06)	5.71 (±0.06)	9.85 (±0.13)	3.85 (±0.10)	1.89 (±0.10)	n.d.	n.d.	0.53	94.06	47.83	0.60	1,0					2167 (±385)		1267 (±158)			
2006-F5d	78.0	45.67 (±0.25)	1.75 (±0.17)	15.47 (±0.04)	10.90 (±0.21)	0.23 (±0.05)	5.62 (±0.06)	8.86 (±0.13)	4.30 (±0.01)	2.17 (±0.05)	n.d.	n.d.	0.52	95.49	47.89	0.57	2.5					1105 (±148)		1495 (±417)			
2006-F5e	78.0	46.28 (±0.17)	1.17 (±0.10)	16.08 (±0.27)	9.87 (±0.29)	0.18 (±0.02)	5.08 (±0.09)	8.04 (±0.11)	4.67 (±0.10)	2.12 (±0.19)	n.d.	n.d.	0.83	94.32	47.85	0.50	1.7					1443 (±140)		1720 (±213)			
2006-F5n	78.0	51.63	1.09	14.66	10.07	0.11	5.19	4.27	4.16	3.47	n.d.	n.d.	1.16	95.81	47.88	0.29	8.0					765		3155			
2006-H2	71.2	49.29 (±0.52)	1.36 (±0.18)	14.64 (±0.33)	10.04 (±0.58)	0.13 (±0.08)	4.08 (±0.08)	6.96 (±0.13)	5.13 (±0.21)	2.60 (±0.14)	n.d.	n.d.	0.53	94.77	42.01	0.48	0					957 (±298)		2960 (±236)			
2006-H4a	71.2	48.71 (±0.12)	1.74 (±0.04)	14.41 (±0.14)	11.37 (±0.09)	0.22 (±0.17)	4.10 (±0.06)	7.58 (±0.15)	4.23 (±0.72)	2.68 (±0.12)	n.d.	n.d.	0.76	95.8	39.13	0.53	1.6					190 (±160)		2177 (±245)			
2006-H4b	71.2	47.99 (±0.20)	1.79 (±0.13)	14.39 (±0.17)	11.45 (±0.14)	0.30 (±0.16)	4.13 (±0.01)	8.68 (±0.03)	3.53 (±0.63)	2.33 (±0.07)	n.d.	n.d.	1.02	95.61	39.13	0.60	1.2					677 (±165)		2163 (±182)			

2006-H4c	71.2	48.46 (±0.30)	1.79 (±0.22)	14.52 (±0.04)	11.92 (±0.05)	0.25 (±0.14)	4.30 (±0.07)	7.89 (±0.03)	3.58 (±0.16)	2.64 (±0.13)	n.d.	n.d.	0.93	96.28	39.14	0.54	3.4					b.d.l.		2210 (±57)			
2006-H7a	69.1	49.65 (±0.61)	1.27 (±0.04)	16.45 (±0.44)	9.15 (±0.87)	0.24 (±0.07)	3.53 (±0.19)	8.30 (±0.30)	4.27 (±0.77)	3.36 (±0.25)	n.d.	n.d.	0.87	97.08	40.78	0.50	0					223 (±152)		1437 (±116)			
2006-H7b	69.1	49.44 (±0.43)	1.86	15.79 (±0.74)	9.55 (±0.34)	0.18 (±0.09)	3.72 (±0.09)	7.43 (±0.01)	3.70 (±1.40)	3.29 (±0.10)	n.d.	n.d.	0.93 (±0.27)	95.89	41.01	0.47	0					165 (±120)		1655 (±78)			
2006-H7c	69.1	48.33 (±0.35)	1.47 (±0.15)	15.40 (±0.23)	10.59 (±0.39)	0.25 (±0.11)	3.83 (±0.04)	9.11 (±0.12)	4.24 (±0.74)	2.91 (±0.06)	n.d.	n.d.	0.90 (±0.09)	97.04	39.22	0.59	0					b.d.l.		1417 (±169)			
2006-18a	70.8	48.71	1.63	14.86	12.41	0.32	4.38	7.72	4.23	2.50	n.d.	n.d.	1.19	97.95	38.62	0.52	3.0					860		2210			
2006-18b	70.8	49.07	1.52	14.71	12.62	0.48	4.45	7.73	4.23	2.29	n.d.	n.d.	1.13	98.23	38.6	0.53	4.1					440		2130			
2006-7 emb	81.1	47.77 (±0.01)	1.87 (±0.07)	16.25 (±0.28)	10.61 (±0.36)	0.25 (±0.02)	3.40 (±0.08)	8.54 (±0.01)	4.35 (±0.17)	3.30 (±0.01)	n.d.	n.d.	0.88 (±0.17)	97.22	36.36	0.50			0.36		b.d.l.	525 (±262)		2240 (±240)	2.4 [a]	2.2	
2006-E2 emb	70.2	49.90	1.97	15.86	10.41	0.19	4.05	7.88	3.26	3.05	n.d.	n.d.	0.85	97.42	40.95	0.50			1.39		b.d.l.	220		1497	30.1 [a]	3.2	
2008/9-1	75.2	48.64 (±0.27)	2.02 (±0.11)	16.60 (±0.20)	9.16 (±0.40)	0.20 (±0.10)	4.06 (±0.05)	8.56 (±0.20)	4.61 (±0.13)	2.76 (±0.17)	n.d.	n.d.	0.93 (±0.19)	97.54	44.14	0.52	2.7	0.13		430 (±64)		b.d.l.	**284** (±6)	2046 (±132)	42.8	1.6	
2008/9-10a	68.7	48.30	1.71	14.65	9.32	0.19	2.99	9.56	5.15	2.46	n.d.	n.d.	0.79	95.12	36.38	0.65	5.5					750		4440			0.02
2008/9-10b	69.5	49.77	1.54	14.67	9.81	0.18	3.26	8.17	5.64	3.04	n.d.	n.d.	1.1	97.18	37.2	0.56	6.7					430		3140			
2008/9-5	76.5	48.47 (±0.77)	1.83 (±0.17)	16.18 (±0.27)	9.34 (±0.64)	0.17 (±0.10)	4.43 (±0.13)	8.74 (±0.48)	4.74 (±0.30)	3.34 (±0.22)	n.d.	n.d.	0.84 (±0.14)	98.08	45.81	0.54	6.4	0.01				461 (±324)		1376 (±193)	160.9	6.2	0.05
2008/9-6a	69.8	55.33 (±0.30)	0.95 (±0.13)	17.98 (±0.26)	7.51 (±0.72)	0.18 (±0.07)	2.53 (±0.02)	7.67 (±0.33)	4.39 (±0.06)	3.45 (±0.13)	n.d.	n.d.	1.15 (±0.20)	101.14	37.52	0.43	4.7					153 (±216)		1897 (±107)			0.01
2008/9-6b	69.8	45.12 (±0.32)	1.74 (±0.08)	16.06 (±0.23)	10.01 (±0.47)	0.17 (±0.12)	3.37 (±0.12)	9.97 (±0.19)	4.95 (±0.06)	3.14 (±0.10)	n.d.	n.d.	0.83 (±0.16)	95.36	37.5	0.62	4.2	0.17		129 (±18)		b.d.l.	**273** (±10)	1394 (±223)	9.0	0.3	
2008/9-7a	69.3	52.49	1.32	17.28	7.50	0.08	2.47	7.73	5.12	3.42	0.03	0.09	1.21	98.62	36.99	0.45	5.0	0.09 (±0.02)		118 (±17)		b.d.l.	**42** (±8)	2410	11.3	0.4	0.03
2008/9-7b	69.3	48.90 (±0.11)	2.27 (±0.07)	16.14 (±0.44)	7.99 (±0.03)	0.21 (±0.11)	2.64 (±0.04)	9.62 (±0.54)	5.41 (±0.22)	4.05 (±0.27)	n.d.	n.d.	1.13	98.36	37.07	0.60	4.5	0.1		87 (±11)		b.d.l.	**46** (±2)	1905 (±106)	5.6	0.2	
2008/9-8	76.9	46.12 (±0.10)	1.43 (±0.21)	14.80 (±0.49)	4.89 (±0.58)	0.14 (±0.13)	2.37 (±0.05)	5.36 (±0.37)	5.34 (±0.09)	4.71 (±0.29)	n.d.	n.d.	0.74 (±0.20)	85.90	46.35	0.36	3.2	0.60 (±0.01)		291 (±41)		**975** (±64)	1107 (±84)	2545 (±488)	23.9	0.9	
2008/9-9b	81.4	44.57 (±0.40)	1.64 (±0.17)	14.58 (±0.40)	11.91 (±0.52)	0.22 (±0.09)	7.60 (±0.86)	8.41 (±0.37)	4.41 (±0.12)	2.88 (±0.11)	n.d.	n.d.	0.60 (±0.10)	96.82	53.22	0.58	11.2	0.03				953 (±256)		1500 (±200)			
2008/9-11	69.4	52.17	1.30	17.36	8.45	0.35	2.79	8.75	4.44	2.69	0.06	0.02	1.07	99.37	37.05	0.50	5.7					690		2580			
2008/9-12a	68.9	56.03	1.27	17.95	5.06	0.11	2.42	5.36	5.07	3.03	0.03	n.d.	n.d.	96.3	45.97	0.30	0					150		2620			

2008/9-12b	68.9	54.77	0.94	17.25	6.71	0.18	2.12	6.71	5.32	2.93	n.d.	n.d.	1.13	98.06	36.03	0.39	3.4					560		2590			0.01
2008/9-16	70.9	52.76	0.90	15.77	9.44	0.24	3.36	7.02	4.65	3.43	n.d.	n.d.	0.84	98.41	38.82	0.45	6.3	0.05				1100		1810			0.01
2008/9-18	78.9	47.49	1.15	15.13	9.92	0.07	5.41	8.96	5.21	3.30	n.d.	n.d.	0.72	97.36	49.29	0.59	8.3	0.22		964 (±37)		240		2130	61.3	2.4	
2008/9-23	69.4	50.47	1.31	14	12.26	0.24	4.05	8.69	3.99	2.70	n.d.	n.d.	0.69	98.4	37.06	0.62	6.8	0.07		675 (±14)		210		2350	79.4	3.06	
2013-1	73.5	49.54 (±0.58)	1.27 (±0.14)	19.31 (±0.32)	6.84 (±0.29)	0.09 (±0.07)	2.77 (±0.05)	7.23 (±0.18)	6.14 (±0.16)	3.65 (±0.13)	n.d.	n.d.	1.26 (±0.26)	98.1	41.92	0.37	3.3	0.11		281 (±47)		**402 (±106)**	508 (±23)	4272 (±257)	17.6	0.68	0.03
2013-2a	77.3	46.95 (±0.70)	1.94 (±0.05)	17.65 (±0.15)	7.66 (±0.02)	0.12 (±0.02)	3.81	10.23 (±0.04)	5.38 (±0.25)	2.57 (±0.15)	n.d.	n.d.	1.10 (±0.24)	97.41	47	0.58	4.5	0.09		339 (±38)		420 (±198**)**		4220 (±226)	25.3	0.98	0.03
2013-2b	77.3	46.74	1.2	19.21	5.99	0.03	2.97	4.95	6.95	4.08	n.d.	n.d.	1.29	93.41	46.92	0.26	4.6	0.04 (±0.01)		543 (±79)		**450**	347 (±117)	n.d.	21.7	0.83	
2013-3a	70.3	50.47 (±0.49)	1.35 (±0.11)	17.25 (±0.27)	8.04 (±0.20)	0.17 (±0.13)	2.77 (±0.03)	7.67 (±0.08)	5.35 (±0.18)	3.48 (±0.11)	n.d.	n.d.	0.97 (±0.29)	97.52	38.05	0.44	3.3	0.01		175 (±17)		147 (±38)		2243 (±136)	14.1	0.54	
2013-3b	70.3	51.06 (±0.46)	1.41 (±0.12)	17.34 (±0.13)	7.74 (±0.46)	0.12 (±0.10)	2.67 (±0.07)	6.66 (±0.10)	5.85 (±0.06)	3.12 (±0.10)	n.d.	n.d.	1.22 (±0.22)	97.19	38.08	0.38	2.6	0.05 (±0.01)		250 (±50)		b.d.l.	**275** (±65)	3760 (±181)	19.4	0.75	
2013-3c	70.3	52.09	1.12	18.27	6.51	0.20	2.24	7.20	5.37	3.85	n.d.	n.d.	1.20	98.05	38.02	0.39	2.5	0.05		426 (±40)		b.d.l.	**364** (±7)	2650	33.4	1.29	
2013-4	73.5	52.14 (±0.40)	1.72 (±0.08)	17.74 (±0.10)	6.48 (±0.22)	0.09 (±0.05)	2.61 (±0.06)	6.84 (±0.11)	5.64 (±0.09)	3.83 (±0.16)	n.d.	n.d.	0.58 (±0.12)	97.67	41.79	0.39	2.1					128 (±45)		1618 (±207)			0.01
2013-6a	70.1	49.16 (±0.30)	1.26 (±0.13)	17.15 (±0.01)	8.64 (±0.34)	0.13 (±0.09)	2.96 (±0.01)	9.28 (±0.07)	5.50 (±0.03)	2.36 (±0.02)	n.d.	n.d.	0.82 (±0.08)	97.26	37.91	0.54	2.1	0.08		243 (±57)		**414 (±142)**	576 (±19)	2928 (±267)	20.6	0.79	
2013-6b	70.1	49.52 (±0.18)	1.12 (±0.07)	17.28 (±0.24)	8.60 (±0.20)	0.16 (±0.06)	2.94 (±0.04)	8.70 (±0.13)	5.65 (±0.07)	2.26 (±0.08)	n.d.	n.d.	0.89 (±0.22)	97.12	37.86	0.50	2.8	0.09		270 (±44)		**310 (±135)**	440 (±19)	3202 (±122)	23.1	0.89	
2013-7a	68.2	53.99 (±0.36)	1.19 (±0.04)	19.40 (±0.22)	5.98 (±0.33)	0.10 (±0.09)	1.98 (±0.04)	3.42 (±0.08)	6.02 (±0.13)	4.26 (±0.18)	n.d.	n.d.	0.38 (±0.20)	96.72	37.12	0.18	3.0					b.d.l.		3627 (±131)			
2013-7b	68.2	51.93 (±0.44)	2.01 (±0.10)	17.47 (±0.03)	7.13 (±0.22)	b.d.l.	2.23 (±0.06)	7.56 (±0.02)	5.41 (±0.09)	3.33 (±0.07)	n.d.	n.d.	1.24 (±0.18)	98.58	35.8	0.43	1.4	0.08		581 (±96)		b.d.l.	**292** (±29)	2607 (±156)	49.8	1.92	
2013-7c	68.2	51.90 (±0.29)	0.83 (±0.16)	17.83 (±0.06)	7.09 (±0.27)	0.09 (±0.07)	2.21 (±0.09)	7.17 (±0.16)	6.49 (±0.13)	3.30 (±0.16)	n.d.	n.d.	1.07 (±0.34)	97.98	35.72	0.40	1.5					375 (±290)		4280 (±255)			
2013-7n	69.6	54.46 (±0.18)	1.21 (±0.08)	19.79 (±0.18)	5.76 (±0.27)	0.10 (±0.01)	1.92 (±0.02)	3.25 (±0.02)	7.59 (±0.03)	3.85 (±0.01)	n.d.	n.d.	0.36 (±0.02)	98.29	37.27	0.16	2.5	0.11		126 (±3)		b.d.l.	**197** (±4)	3740 (±254)	6.3	0.24	0.005
2013-11	80.3	51.72 (±0.21)	1.12 (±0.14)	20.40 (±0.19)	4.30 (±0.23)	0.10 (±0.05)	2.55 (±0.05)	4.21 (±0.07)	6.85 (±0.10)	4.95 (±0.11)	n.d.	n.d.	1.06 (±0.15)	97.26	51.39	0.21	2.0					274 (±14)		3356 (±167)			0.07
2013-12a	71.1	49.91	1.18	17.43	8.26	0.27	2.96	7.96	5.47	3.20	n.d.	n.d.	1.04	97.68	38.98	0.46	4.6	0.16				b.d.l.	**63** (±2)	2400			0.06

2013-12b	71.1	46.72	1.01	16.8	6.53	0.08	2.34	7.57	5.40	3.31	n.d.	n.d.	0.65	90.41	38.98	0.45	4.1					250		2450			0.02
2013-12c	71.1	52.84 (±0.61)	0.702 (±0.09)	18.53 (±0.17)	5.89 (±0.12)	b.d.l.	2.11 (±0.06)	3.92 (±0.08)	6.08 (±0.13)	5.63 (±0.10)	n.d.	n.d.	1.05 (±0.14)	96.84	38.97	0.21	2.9	0.07		139 (±27)		b.d.l.	**180** (±11)	2677 (±40)	6.7	0.26	
2013-12d	71.1	50.15	1.13	17.8	6.66	0.12	2.39	7.89	5.73	3.26	n.d.	n.d.	1.06	96.19	39.01	0.44	3.0					330		2490			0.06
2013-14a	74.2	52.78 (±0.61)	2.07 (±0.09)	18.21 (±0.18)	5.86 (±0.39)	0.12 (±0.09)	2.45 (±0.02)	7.60 (±0.06)	4.73 (±0.08)	3.96 (±0.16)	n.d.	n.d.	1.07 (±0.12)	98.85	42.7	0.42	2.3	0.08		709 (±139)		b.d.l.	**528** (±16)	1749 (±153)	65.7	2.53	0.01
2013-14b	74.2	47.26 (±0.55)	1.96 (±0.06)	17.88 (±0.18)	5.87 (±0.25)	0.14 (±0.09)	2.46 (±0.05)	9.63 (±0.10)	4.27 (±0.06)	3.67 (±0.14)	n.d.	n.d.	0.95 (±0.16)	94.09	42.76	0.54	1.7					284 (±59)		2152 (±85)			
2013-16	76.7	52.34 (±0.24)	2.51 (±0.08)	16.95 (±0.12)	6.35 (±0.19)	b.d.l.	3.05 (±0.02)	5.78 (±0.16)	5.30 (±0.04)	4.79 (±0.16)	n.d.	n.d.	1.03 (±0.14)	98.19	46.13	0.34	3.4	0.07		323 (±59)		b.d.l.	**85** (±4)	1874 (±163)	23.7	0.91	
2013-17a	69.4	50.14 (±0.42)	1.54 (±0.10)	17.69 (±0.17)	7.81 (±0.52)	0.21 (±0.17)	2.58 (±0.04)	7.28 (±0.07)	5.92 (±0.08)	3.09 (±0.16)	n.d.	n.d.	1.14 (±0.21)	97.4	37.06	0.41	1.5	0.09		321 (±43)		332 (±200)	**509** (±20)	4242 (±306)	23.8	0.91	0.01
2013-17b	69.4	48.84 (±0.46)	1.94 (±0.11)	16.91 (±0.20)	7.78 (±0.27)	0.16 (±0.12)	2.57 (±0.05)	7.44 (±0.07)	5.15 (±0.11)	3.27 (±0.07)	n.d.	n.d.	1.29 (±0.13)	95.35	37.06	0.44	1.2	0.09		233 (±31)		308 (±48)	**554** (±24)	2182 (±173)	19.7	0.76	0.02
2013-17c	69.4	51.65	1.88	17.42	7.28	0.06	2.41	6.82	5.15	3.90	n.d.	n.d.	1.11	97.68	37.11	0.39	3.3					190		1540			0.02
2013-17d	69.4	50.39	1.37	19.04	7.04	0.24	2.33	8.19	5.45	2.89	n.d.	n.d.	0.71	97.65	37.11	0.43	2.4	0.03 (±0.01)		545 (±61)		210		2760	45.8	1.76	
2013-19a	73.4	50.55 (±0.33)	2.23 (±0.13)	17.15 (±0.25)	5.99 (±0.41)	0.17 (±0.05)	2.41 (±0.05)	7.84 (±0.16)	5.24 (±0.11)	3.99 (±0.12)	n.d.	n.d.	1.13 (±0.09)	96.7	41.77	0.46	1.8	0.06		1102 (±128)		136 (±41)	**132** (±5)	1228 (±232)	81,2	3.13	0.03
2013-27	77.4	51.98	1.1	20.78	5.05	0.12	2.52	4.26	8.15	4.15			0.84	98.95	47.08	0.21	1.8	0.1		254 (±8)		320	**364** (±8)	2340	9.5	0.37	0.03
2013-30	71.9	45.61 (±2.25)	1.44	18.24 (±0.01)	7.13 (±0.04)	0.15 (±0.11)	2.66 (±0.07)	7.96	5.82 (±0.26)	3.00 (±0.09)	b.d.l.	b.d.l.	0.83 (±0.14)	92.84	39.94	0.44	1.4		0.14		b.d.l.	310		2675	3.7 [a]	0.14	0.11
2013-32	71.5	48.16 (±0.39)	1.69 (±0.14)	16.53 (±0.34)	7.44 (±0.30)	0.18 (±0.09)	2.71 (±0.03)	7.28 (±0.03)	5.75 (±0.02)	3.45 (±0.03)	b.d.l.	b.d.l.	1.11 (±0.23)	94.3	39.37	0.44	1.8		0.15		b.d.l.	b.d.l.		1910 (±353)	3.9 [a]	0.15	0.01
2013-34	71.0	51.47	1.49	19.16	6.23	0.17	2.21	4.98	6.06	3.67	n.d.	n.d.	0.96	96.4	38.74	0.26	2.8		0.13		b.d.l.	270		3350	3.7 [a]	0.14	
2013-36	71.6	52.09 (±1.43)	1.10 (±0.62)	20.08 (±0.63)	5.93 (±1.13)	b.d.l.	2.18 (±0.20)	4.72	7.21 (±0.14)	4.34 (±0.01)	n.d.	n.d.	0.94 (±0.01)	98.64	39.59	0.24	1.8	0.11		483 (±13)		b.d.l.	**320** (±6)	2210 (±170)	21.6	0.83	
2013-37	73.9	50.51	1.75	17.85	6.44	0.23	2.66	7.30	6.80	4.37	n.d.	n.d.	0.73	98.64	42.41	0.41	1.3					b.d.l.		1770			0.32
2013-41	77.7	51.37 (±0.03)	0.87 (±0.05)	20.67 (±0.10)	4.30 (±0.01)	b.d.l.	2.18 (±0.12)	4.00 (±0.06)	7.24 (±0.14)	5.47 (±0.29)	b.d.l.	b.d.l.	0.83 (±0.10)	97.02	47.47	0.19	1.8		0.08		b.d.l.	145		2495 (±78)	2.0 [a]	0.08	0.04

Corrected chemical composition of melt inclusions, uncorrected compositions of glass embayments and matrix glasses and their volatiles contents, from the studied products of Mt Spagnolo (SPA), FS, 2002/2003 South (2002/3S), 2006, 2008/2009 (ET2008/9), and 2013 eruptions. Major elements and H_2O contents are in wt.%, CO_2, S and Cl are in ppm.

Numbers in brackets indicate standard deviations for EMP and FTIR analyses, and acquisitions errors for SIMS analyses.

Fo: forsterite mol.% content of olivine hosting MI. Mg# = 100 x Mg/(Mg+Fe_{tot}). PEC%: estimated amount (wt %) of post-entrapment crystallization. P: minimum entrapment pressure calculated using a H_2O-CO_2 solubility model (Iacono-Marziano et al. 2012). Depth: minimum entrapment depth estimated using a density of 2.65 g cm^{-3} for the basement rocks (Corsaro and Pompilio, 2004b). V_b/V_{MI} : ratio between the volume of vapor bubble (V_b) and the host melt inclusions volume (V_{MI}).

emb = embayment, ext = external glass, sec = secondary melt inclusions. b.d.l. = below detection limit; n.d. = not determined.

a = pressure and relative depth (below crater level) calculated using FTIR data with a CO_2 content fixed at 50 ppm (FT-IR detection limit), considering the estimated CO_2 detection limit (e.g. Cecchetti et al., 2002; Von Aulock et al., 2014).

Figure 1

Click here to download high resolution image

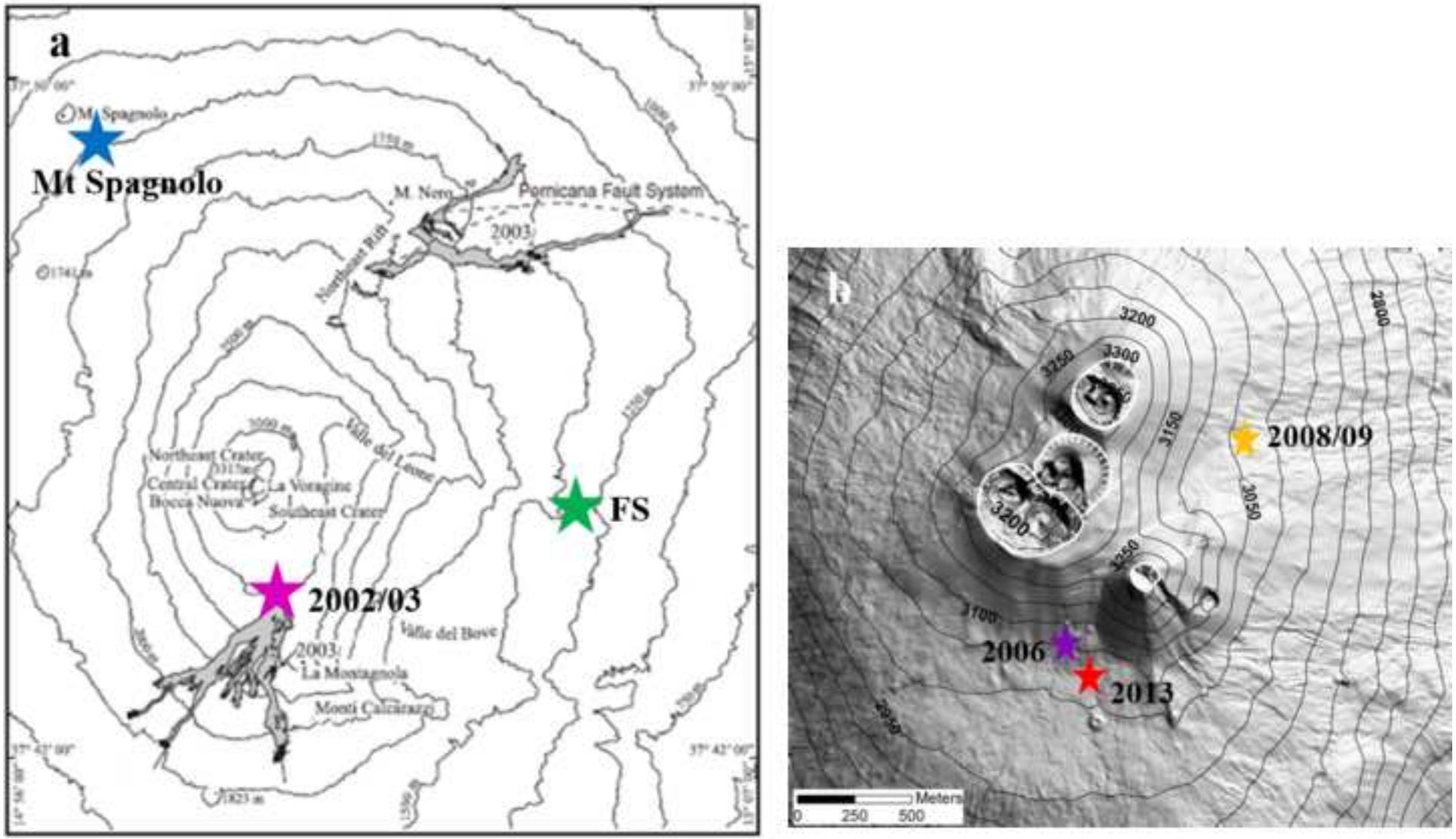

Figure 2

Click here to download high resolution image

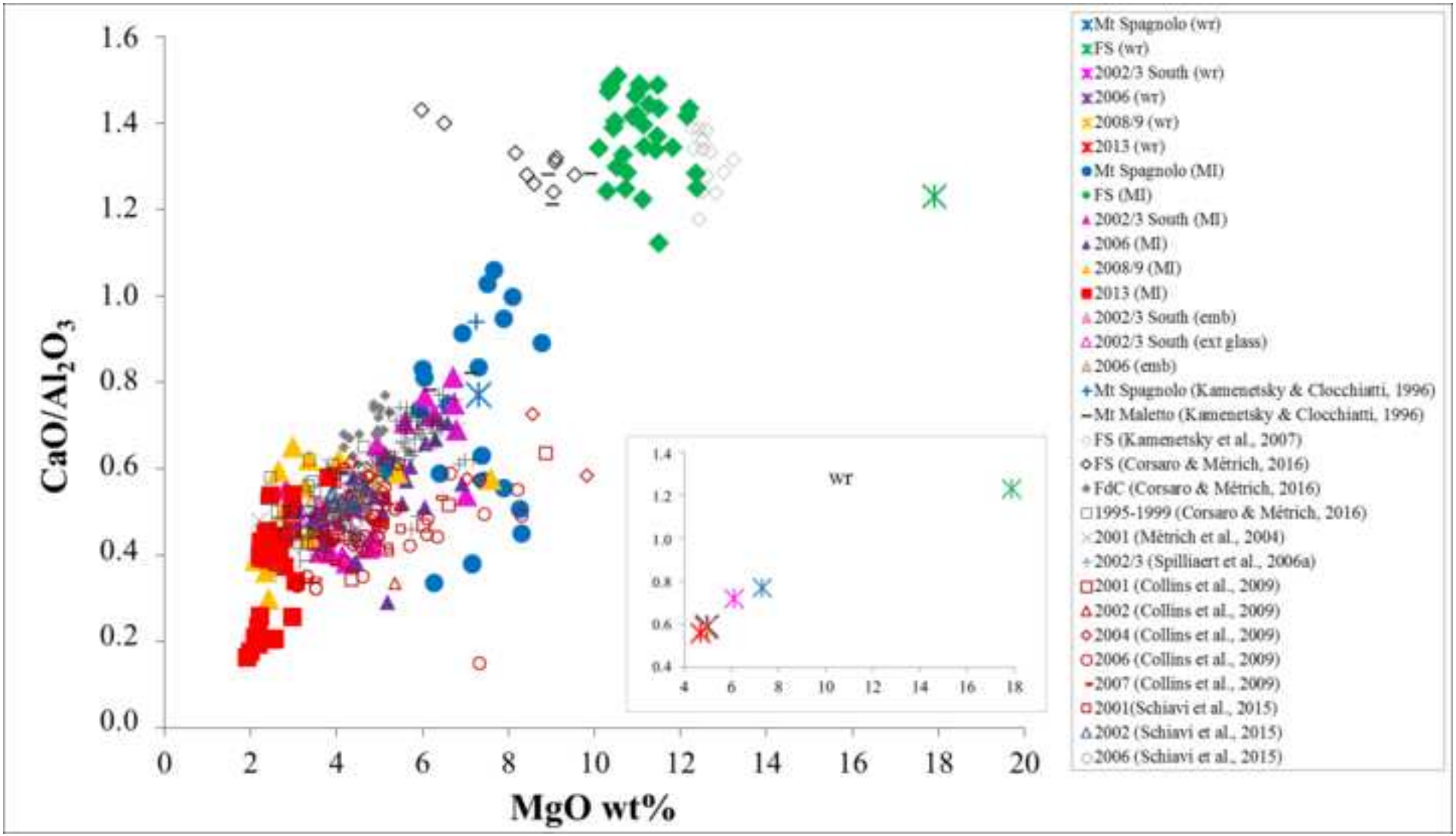

Figure 3

Click here to download high resolution image

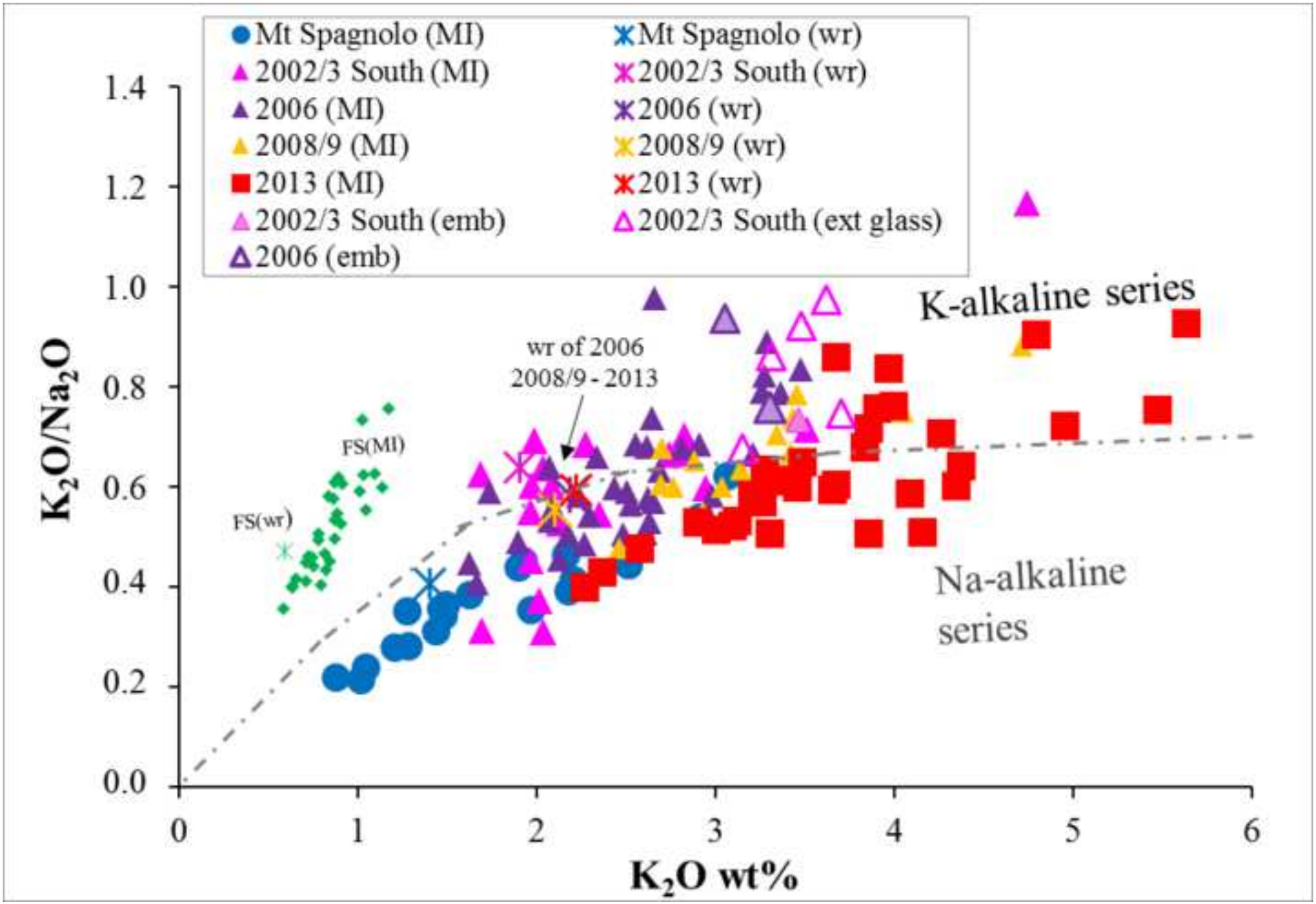

Figure 4

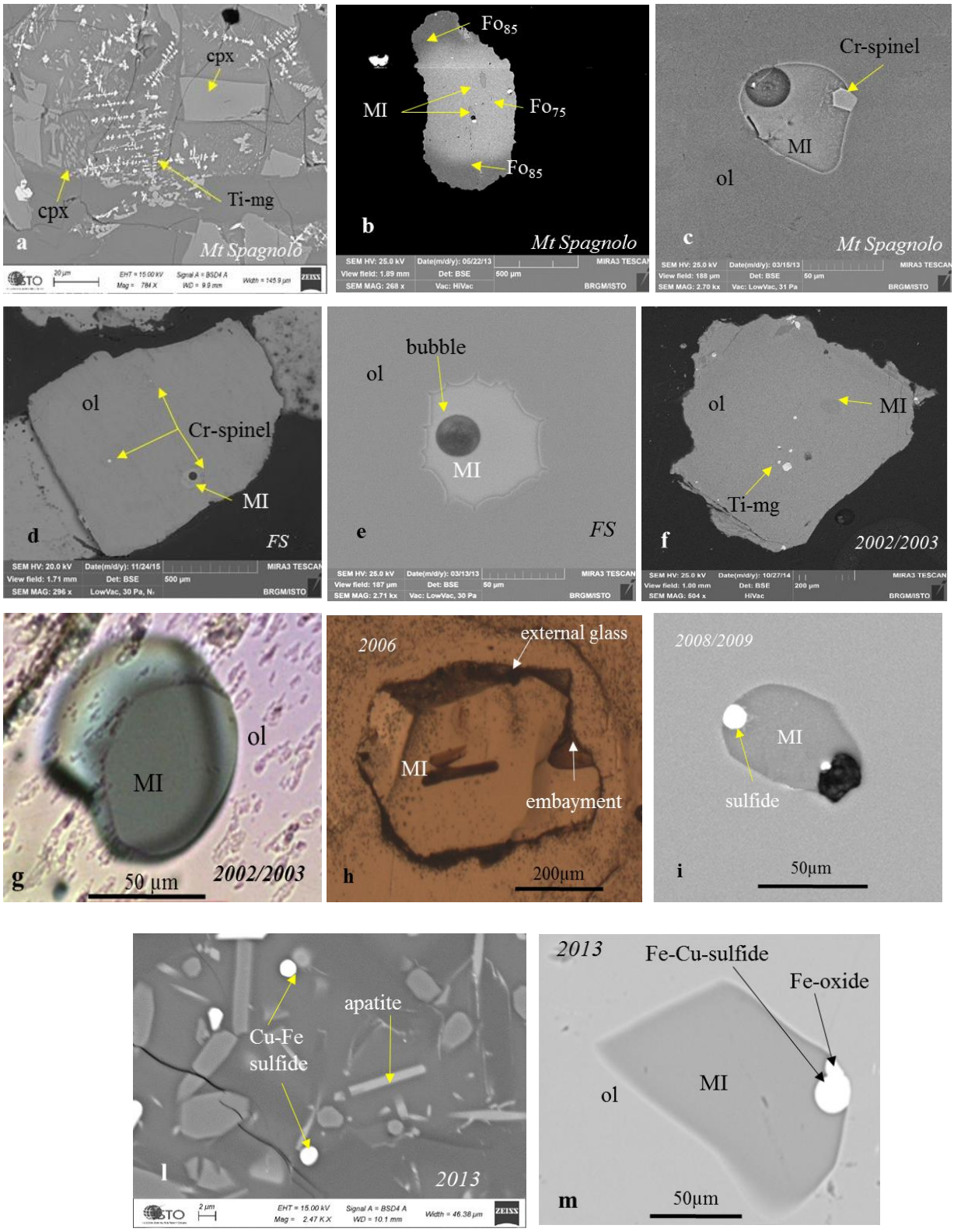
cpx
cpx
Ti-mg
a
Mt Spagnolo
Fo85
MI
Fo75
Fo85
b
Mt Spagnolo
Cr-spinel
MI
ol
c
Mt Spagnolo
ol
Cr-spinel
MI
d
FS
bubble
ol
MI
e
FS
ol
MI
Ti-mg
f
2002/2003
ol
MI
g
50 µm
2002/2003
2006
external glass
MI
embayment
h
200µm
2008/2009
MI
sulfide
i
50µm
Cu-Fe
sulfide
apatite
l
2013
2013
Fe-Cu-sulfide
Fe-oxide
ol
MI
m
50µm

Figure 5

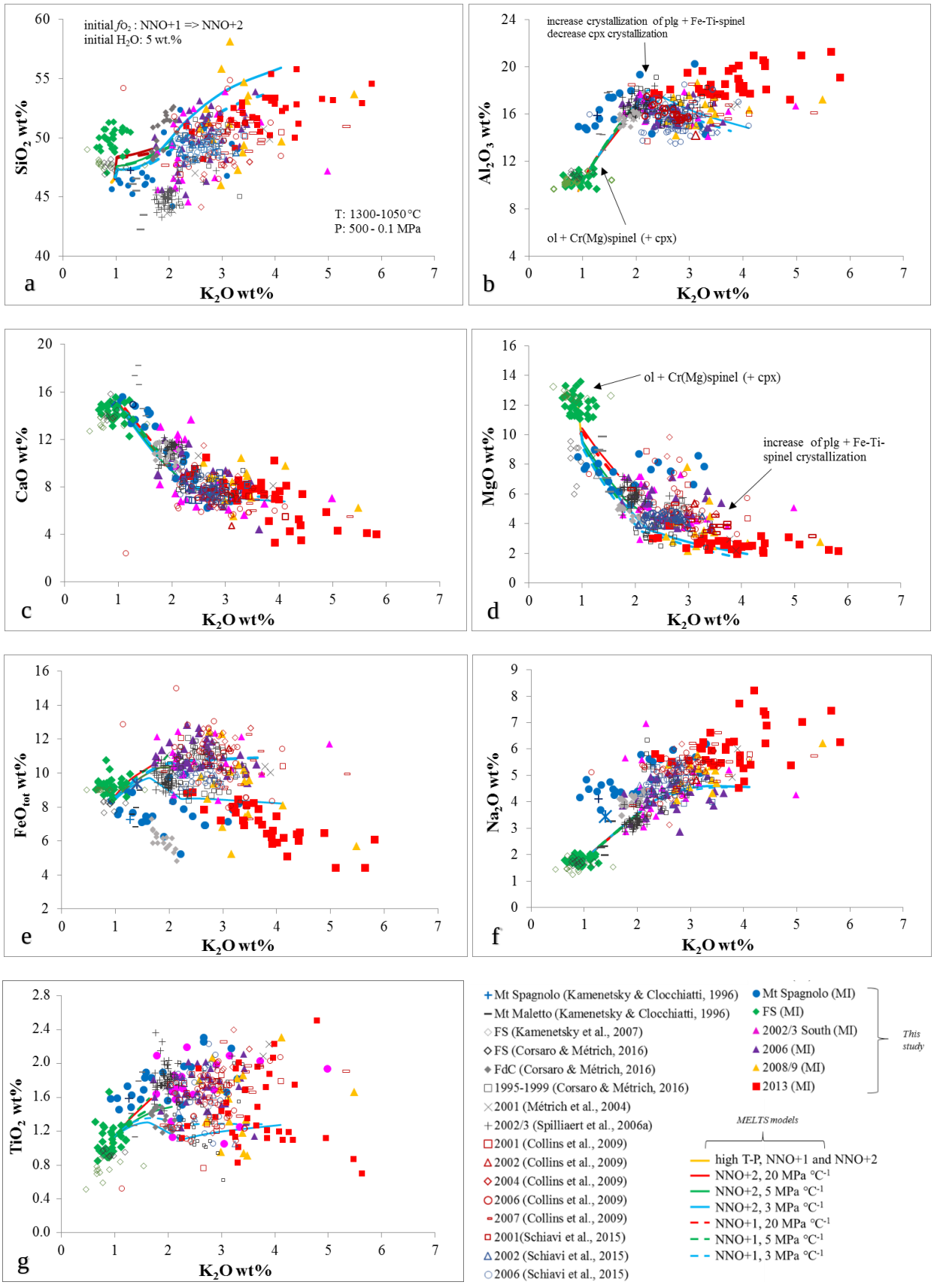
initial fO_2 : NNO+1 => NNO+2
initial H_2O: 5 wt.%
T: 1300-1050 °C
P: 500 - 0.1 MPa
SiO_2 wt%
K_2O wt%
a
increase crystallization of plg + Fe-Ti-spinel
decrease cpx crystallization
ol + Cr(Mg)spinel (+ cpx)
Al_2O_3 wt%
b
CaO wt%
c
MgO wt%
increase of plg + Fe-Ti-spinel crystallization
d
FeO_{tot} wt%
e
Na_2O wt%
f
TiO_2 wt%
g
Mt Spagnolo (Kamenetsky & Clocchiatti, 1996)
Mt Maletto (Kamenetsky & Clocchiatti, 1996)
FS (Kamenetsky et al., 2007)
FS (Corsaro & Métrich, 2016)
FdC (Corsaro & Métrich, 2016)
1995-1999 (Corsaro & Métrich, 2016)
2001 (Métrich et al., 2004)
2002/3 (Spilliaert et al., 2006a)
2001 (Collins et al., 2009)
2002 (Collins et al., 2009)
2004 (Collins et al., 2009)
2006 (Collins et al., 2009)
2007 (Collins et al., 2009)
2001(Schiavi et al., 2015)
2002 (Schiavi et al., 2015)
2006 (Schiavi et al., 2015)
Mt Spagnolo (MI)
FS (MI)
2002/3 South (MI)
2006 (MI)
2008/9 (MI)
2013 (MI)
This study
MELTS models
high T-P, NNO+1 and NNO+2
NNO+2, 20 MPa °C-1
NNO+2, 5 MPa °C-1
NNO+2, 3 MPa °C-1
NNO+1, 20 MPa °C-1
NNO+1, 5 MPa °C-1
NNO+1, 3 MPa °C-1

Figure 6

Click here to download high resolution image

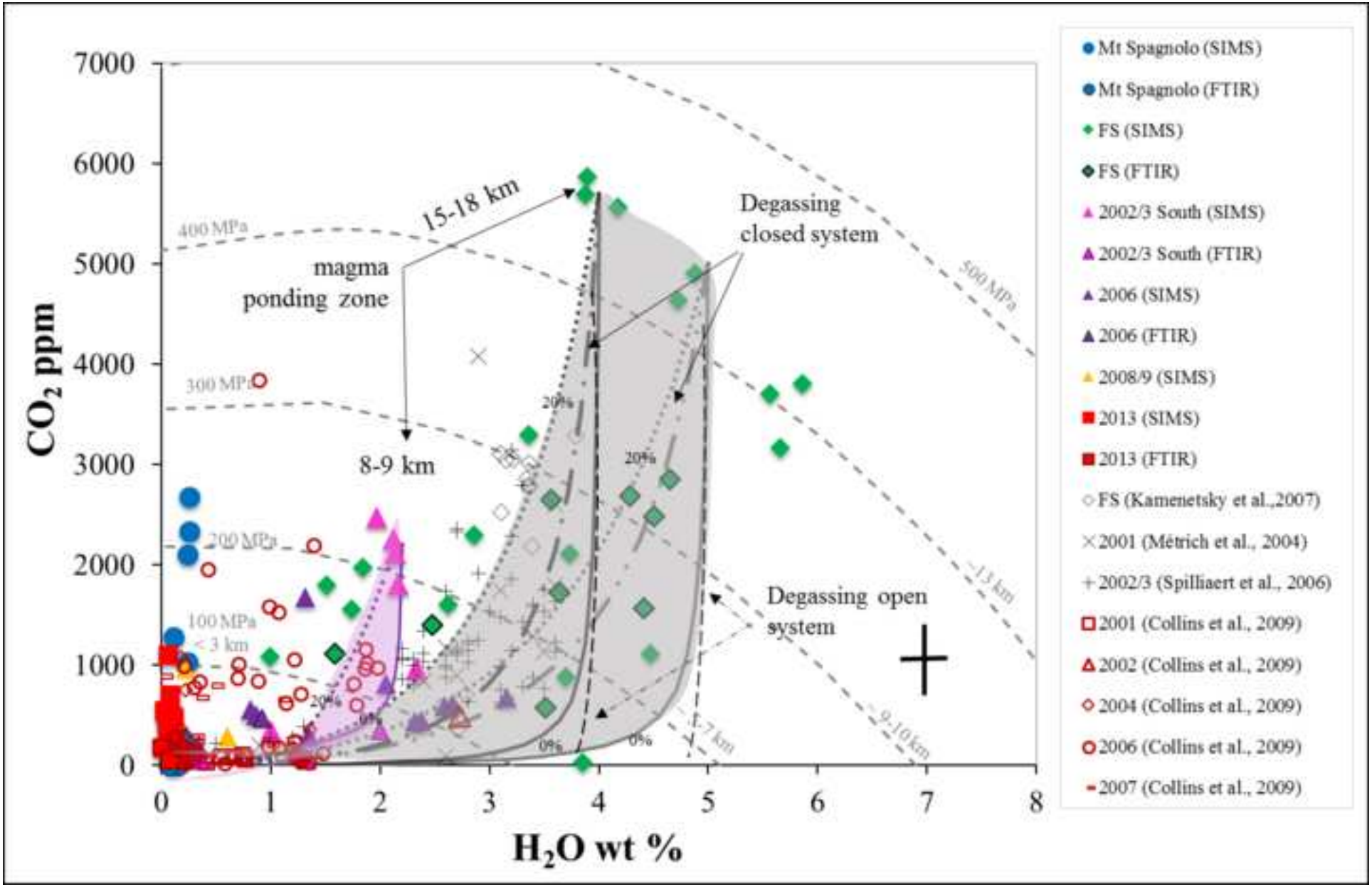

Figure 7

Click here to download high resolution image

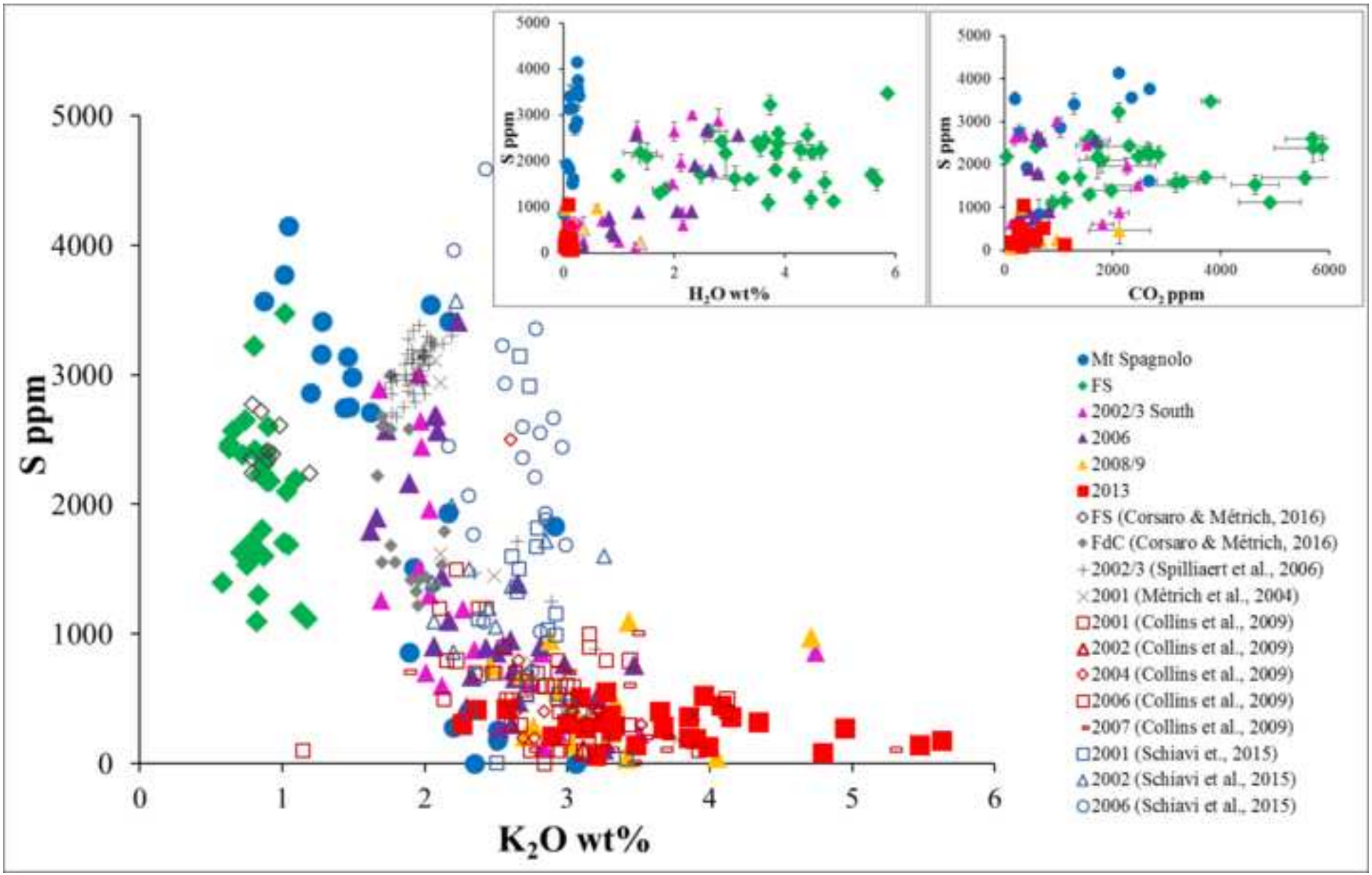

Figure 8
Click here to download high resolution image

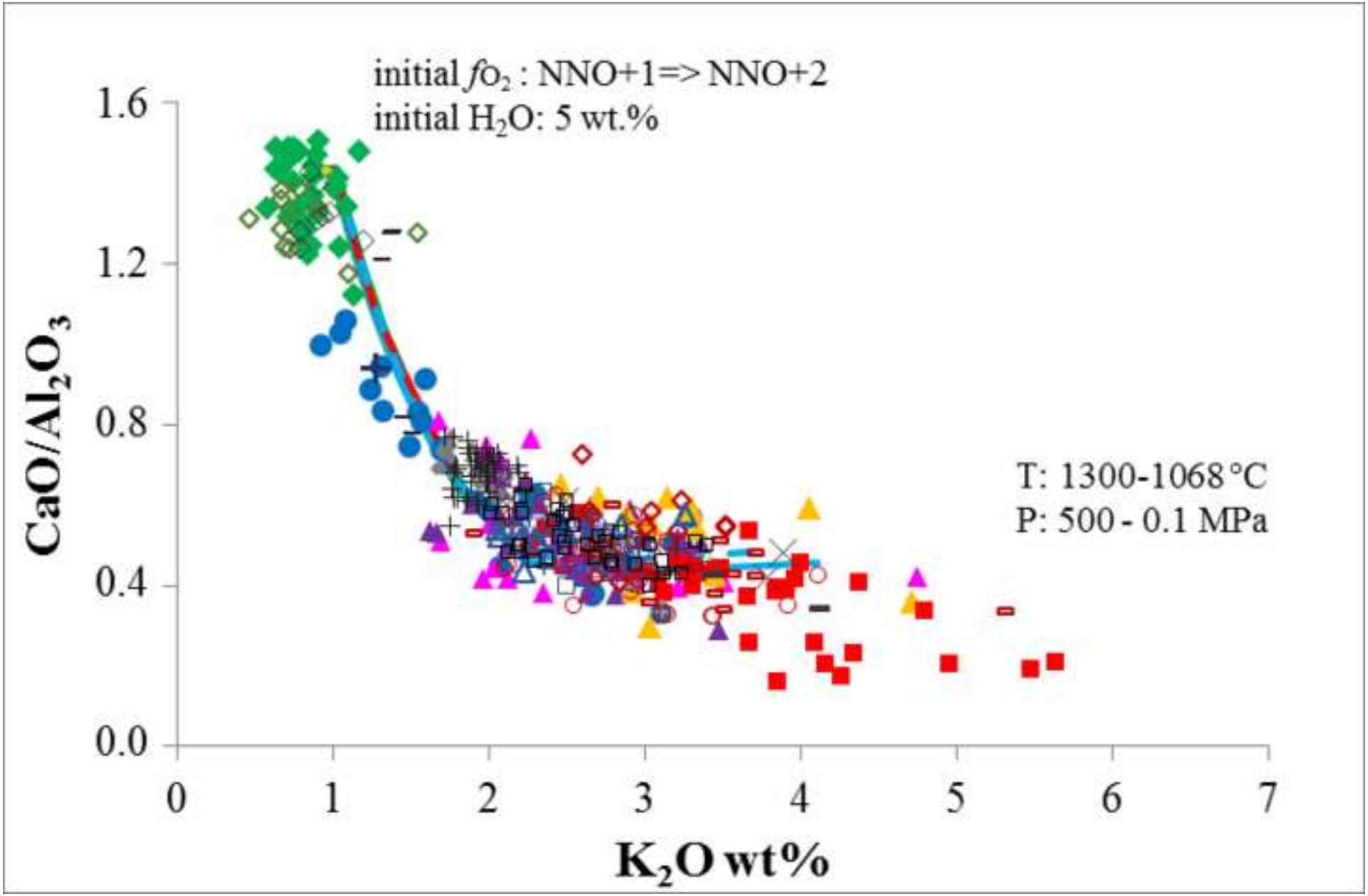

Figure 9

Click here to download high resolution image

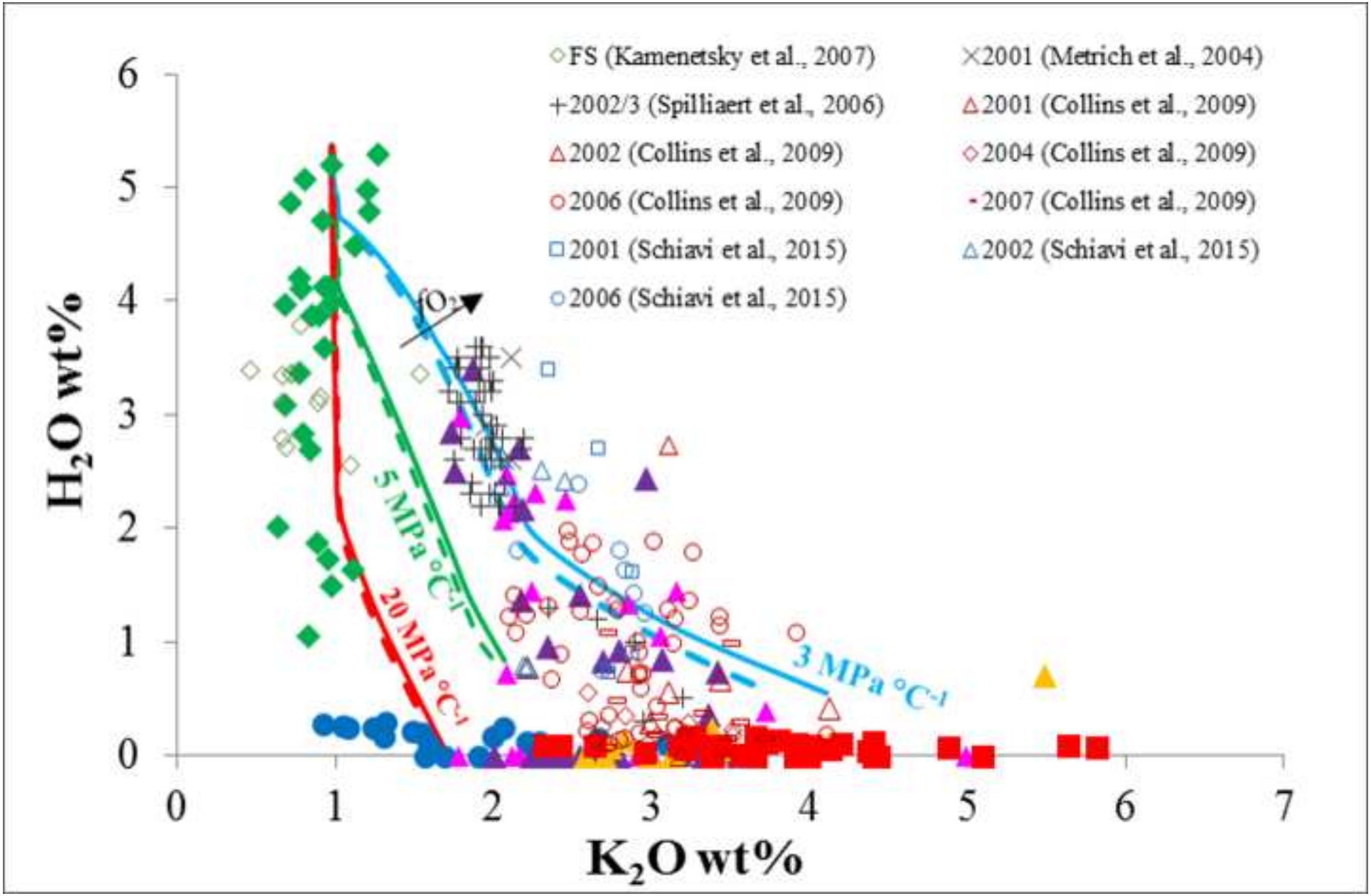

Figure 10

Click here to download high resolution image

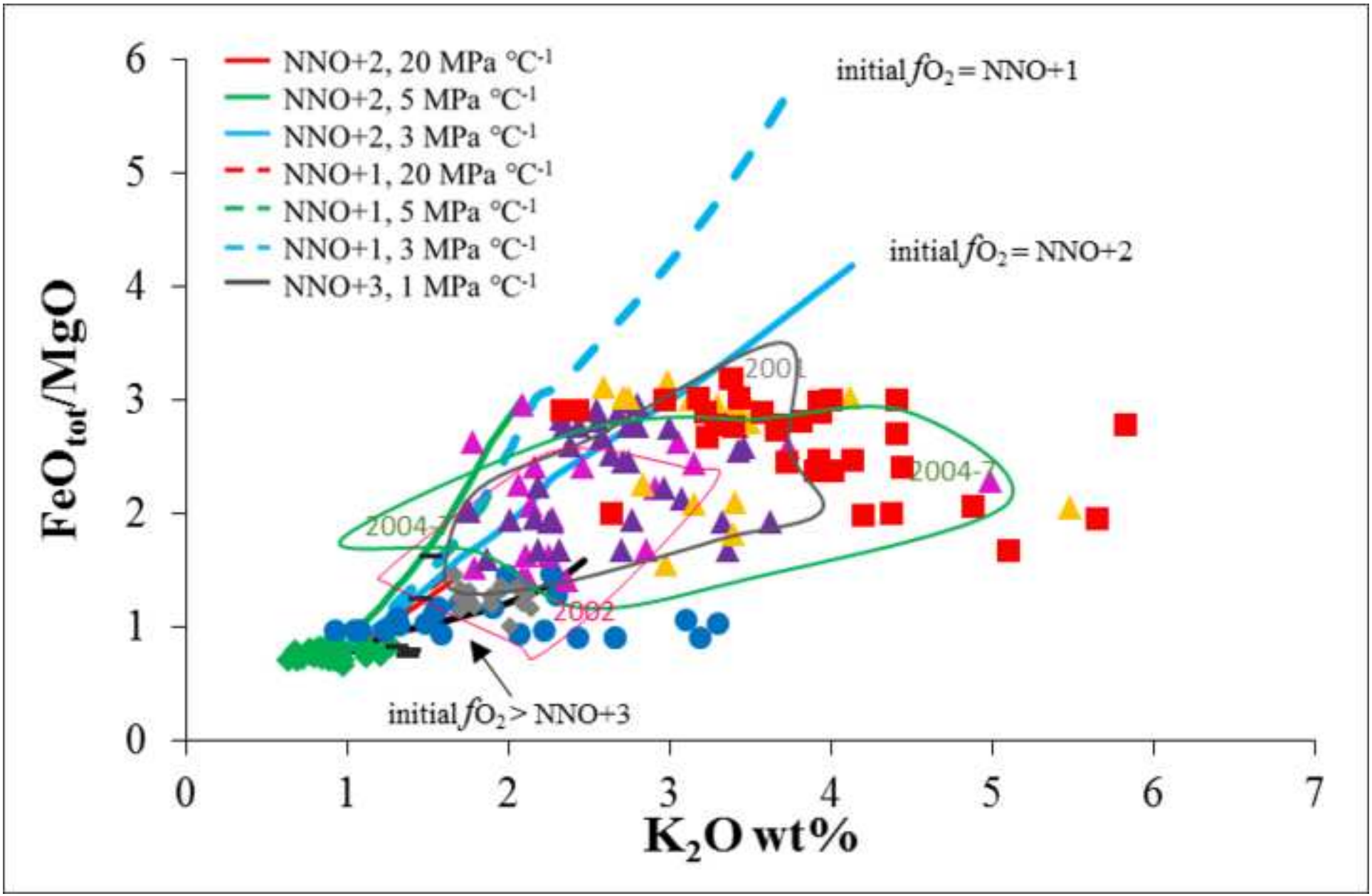

Figure 11

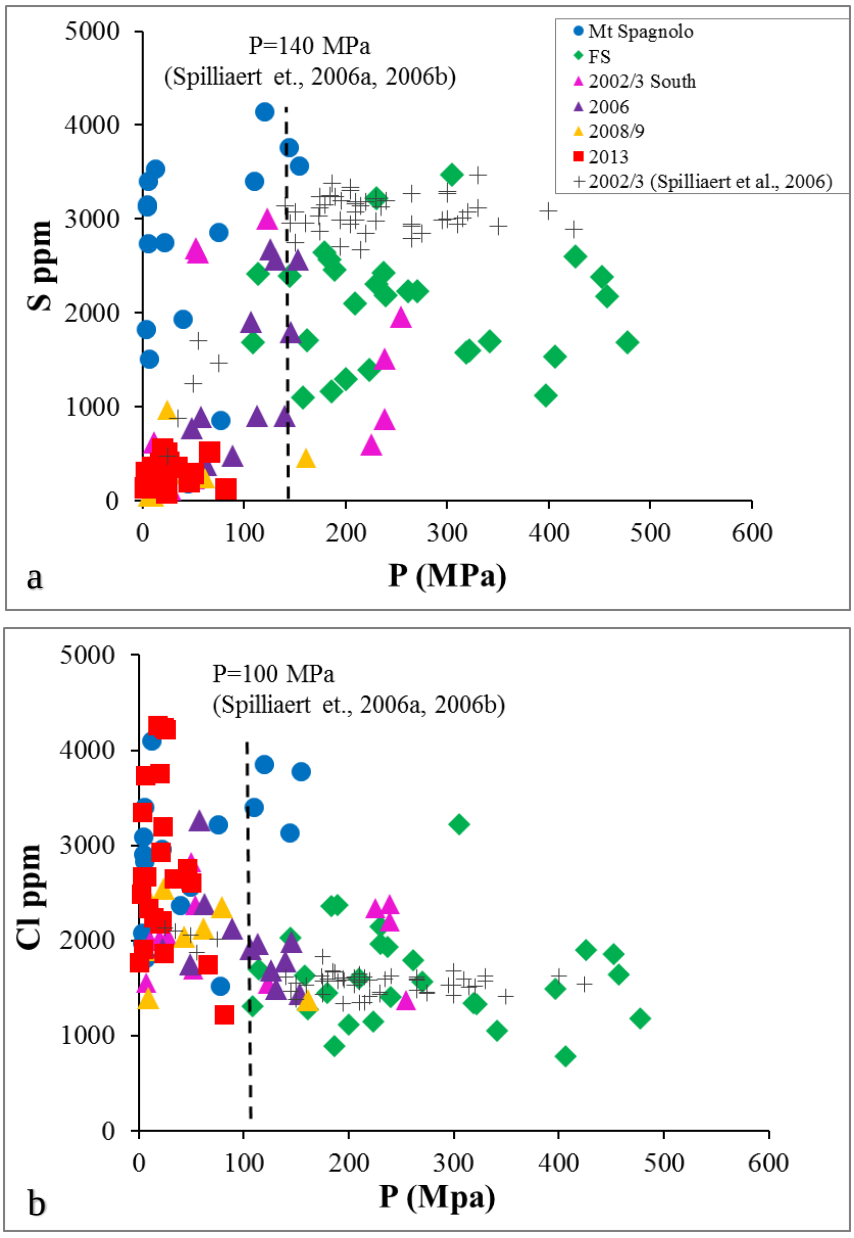
P=140 MPa
(Spilliaert et., 2006a, 2006b)
Mt Spagnolo
FS
2002/3 South
2006
2008/9
2013
2002/3 (Spilliaert et al., 2006)
S ppm
P (MPa)
a
P=100 MPa
(Spilliaert et., 2006a, 2006b)
Cl ppm
P (Mpa)
b

Supplementary data

Click here to download Supplementary Interactive Plot Data (CSV): Gennaro et al - supplementary.docx